Molecular mechanics investigation of conductance regulation in selective K^+ ion channels

Inauguraldissertation

zur

Erlangung der Würde eines Doktors der Philosophie

vorgelegt der

Philosophisch-Naturwissenschaftlichen Fakultät

der Universität Basel

von

Florian Tobias Heer

von Grabs, St. Gallen

Basel, 2018

Genehmigt von der Philosophisch-Naturwissenschaftlichen Fakultät
auf Antrag von

Torsten Schwede, Simon Bernèche und Henning Stahlberg

Basel, 24.05.2016

Prof. Dr. Jörg Schibler
The Dean of Faculty

“Ion channels are involved in every thought, every perception, every movement, every heartbeat.”

- Clay M. Armstrong (Hille et al., 1999)

Acknowledgements

First and foremost I thank Simon Bernèche for the opportunity to work on these exciting projects, the supervision of my work and the trust to let me follow many of my own hypotheses. I thank Torsten Schwede and Henning Stahlberg for the co-supervision of my thesis.

My gratitude goes to our collaborators Brad S. Rothberg and Crina Nimigean and their groups, for their collaboration but also for the exchange of great ideas which had a deep impact in developing hypotheses to push the work forward.

Also many thanks to the group – past members and present ones – for the inspiring environment, many discussions and great working environment. Namely I would like to thank Céline who was mentoring me during my Masters and who placed the cornerstone for my work on KcsA. Wojciech, for the development of iPMF and helping me in performing calculations needed for my work on KcsA. Yanyan as my past long time neighbor and Olivier as my current office neighbor for patiently listen to all my ideas (brilliant and other).

Special gratitude to the administrative staff, especially Rita, Sarah and Yvonne and the whole SciCORE team for all the infrastructure related help. I would like to thank Konstantin, Martin and Pablo in particular.

A special deep thanks to my family, Louise, Beat and Sebastian as well as my dear friends Silvi, Steffi, Angi, Axel, Andreas, Christophe, Camille and Janine for both the moral support and fruitful discussions.

Abstract

Selective ion channels play a crucial role in every aspect of life. The function has been intensively investigated for more than 60 years. Over the years, a clearer picture of the channel functions has emerged. Still many mechanisms are not yet fully understood and some models have to be reevaluated after new insights were gained.

Here I investigated the C-type inactivation mechanism of MthK and its dependence to divalent ions. The effect of the inactivation inducing divalent ion Ca^{2+} was compared with Mg^{2+}, which did not induce inactivation. Binding of Ca^{2+} to the selectivity filter impacts on the binding of K^{+} ions to the selectivity filter and leads to conformational changes putatively associated with inactivation.

A possible mechanism for C-type inactivation was proposed based on KcsA. The conformational changes underlying this mechanism were not observed in other channels, however. We identified inactivation favoring conditions for the channel MthK and a mutant of MthK, which shares a key residue for inactivation in KcsA. Under these conditions, only the mutant inactivated by the described inactivation mechanism, challenging the universality of the mechanism.

Additionally, I investigate the permeation of potassium ions through the selectivity filter of the KcsA channel, which is shown to play a role in the activation process. A closed inner gate lead to a non permeating selectivity filter, in agreement with a pre-activated state with strong ion affinity, increasing the recovery rate from C-type inactivation. Opening of the inner gate reduces the ion binding affinity and increases the channel's conductance. A mutant designed to module steric contact around the selectivity filter is shown to decouple the selectivity filter from the inner gate and to facilitate activation.

Motivation

Recent studies found more than 230 genes encoding for ion channels in humans (Jegla et al., 2009). Ion channels are an essential component of the development of the nervous system. Some even called ion channels the missing piece in evolution. It was somewhat a surprise, when more and more ion channels were found in prokaryotic organisms, and the diversification of ion channels was moved further and further back in the phylogenetic tree. Ion channels raise several very interesting biological questions: When did they develop? What is the function of the different ion channels? How does regulation, activation, inactivation, gating, permeation and selectivity work? Many aspects of these questions were answered during the last few decades. Ion channels are present in all kingdoms of life, yet some organisms with reduced genomes don't have any. I learned three times how K^+ selective channels are selective over Na^+ in my years of study, yet recently it was shown that these explanations cannot be true. Crystal structures of ion channels clarified many aspect of ion channel function, yet the inactivation model based on early structures did not fit with many experiments nor were these findings universal, as revealed by the crystallization of other channels. Permeation on an atomistic scale was tackled with molecular mechanics simulations. Newer investigation of permeation with more modern force fields led to results, which were incompatible with electrophysiological measurements. Altogether, these observations suggest that our understanding of ion channel properties is still incomplete.

Summary

This thesis is focusing on the conductance regulation of selective K^+ ion channels by modulation of activation and (C-type) inactivation. C-type inactivation describes one of the mechanisms by which ion channels stop conducting ions despite the presence of an activation signal. C-type inactivation can be modulated by many different means, one of them are divalent ions on the cytosolic side of the channel. Ca^{2+}, which is the activator of MthK, can promote C-type inactivation, but not Mg^{2+}. Only Ca^{2+} is able to bind to the selectivity filter and displace the K^+ ions in the channel. This leads to the loss of one of the two K^+ ions, which increases the flexibility in the selectivity filter and causes changes in the structure, which are potentially associated with C-type inactivation. In agreement with electrophysiological measurements, the effect increases with stronger applied voltages.

The precise mechanism of inactivation is unknown. X-ray crystallography of the KcsA channel revealed a collapsed and a non conducting conformation of the selectivity filter, which is associated to C-type inactivation. Simulations of KcsA suggest that inactivation happens through the loss of ions, which lead the filter to this conformation. On the other hand, MthK is shown to inactivate but does not loose ions nor does it adopt the collapsed structure observed in KcsA. Inactivation favoring conditions in MthK WT favor the S_1-S_4 occupancy state, which is reminiscent of the observations made in presence of Ca^{2+}. In complete absence of ions the MthK selectivity filter nevertheless adopts the collapsed structure, suggesting that this state might be a later, deeper inactivated state.

In general the computational results obtained in the experiments regarding C-type inactivation agreed well with experimental ones. However, the energy barriers observed between ion states were in general higher than expected. This discrepancy can be either explained by shortcomings in the force fields used for the computational experiments, or missing modulators of activation and inactivation. In the last part, we investigated the influence of the inner gate opening on the conductance of the selectivity filter in KcsA. A closed inner gate leads to a non conducting selectivity filter, whereas a completely open inner gate greatly reduces energy barriers along the permeation pathway and favor ion permeation. These findings show that the inner gate has a strong impact on the gating of the selectivity filter, which thus plays a central role in the channel activation. A small displacement of the P-helix and an increase of flexibility of the selectivity filter was observed upon opening of the inner gate. This allowed us to identify a mutant which facilitates activation of the channel by reducing the coupling between the inner gate and the selectivity filter.

Table of Contents

List of figures

Abbreviations

Kv channel	Voltage gated potassium channel
PDB id	Unique identifier of protein structures in the Protein Data Bank
PMF	Potential of Mean Force
p-helix	Pore forming helix
RCK	Regulator of K^+ conductance
SF	Selectivity filter
S_X	Binding site x of the selectivity filter
TM helix	Transmembrane helix

1 General introduction

Ion channels are essential components of every cell. They allow for the regulation of ion diffusion down their electro-chemical gradient. The ion concentration inside a cell influences, among others, osmotic pressure, cell proliferation, as well as apoptosis (Lang et al., 2007). Ions themselves can act as messenger molecules in multicellular organisms. Ion channels play a crucial role in the nerve system: Nerve impulses results from the combined activity of Na^+ and K^+ channels, muscles use Ca^{2+}-channels to induce muscle contraction, and the pulse from the sinoatrical node is transferred by ion channels between the muscle cells. Epilepsy, migraine, cardiac arrhythmia, kidney failure and blindness are just a few of the pathologies linked to ion channel dysfunction (Jegla et al., 2009).

Selective K^+ ion channels are found in every kingdom of life. Interestingly, mitochondria and chloroplast do not encode their own K^+ channels. Additionally, some obligate intracellular parasitic bacteria from different lineages do not encode K^+ channels (Kuo et al., 2005). Note that these organisms have a heavily reduced genome.

The universal character of ion channels and their role in many essential processes make it unsurprising that ions and ion channels have intrigued scientists for decades and probably will do for many decades to come.

1.1 History of ion channels

The existence of channels was already predicted in the 1840's in connection with osmosis and stayed both in biological and physical circles as a prominent theory. However, these channels were described as pores conducting non specifically water and other small molecules up to the diameter of the pore.

More than a century later, in 1952, Hodgkin and Huxley (Hodgkin and Huxley, 1952) described the potassium and sodium flow along the squid giant axon. (It is worth mentioning that the existence of the nervous system was already described by the famous antique researcher Claudius Galenus (129 AD - ~200 AD).)

This and following experiments led to the theory that ion channels could be responsible for the observed flow of ions (Hodgkin and Keynes, 1955; Hille, 1970). One major challenge with this theory at the time was that the speed of ion permeation through the membrane could be easily described with carrier molecules such as valinomycin, a preferred theory at that time. In 1976, Neher and Sakmann were able to measure single channel activity with the patch clamp method clearly demonstrating the existence of ion channels (Neher and Sakmann, 1976). In 1998 MacKinnon and his lab were able to solve the structure of KcsA, a prokaryotic selective ion channel from *Streptomyces lividans (Doyle et al., 1998)*.

1.2 Structure of selective K^+ channels

Selective K^+ ion channels are homo- or hetero-tetrameric proteins (or mimic the tertiary structure, by forming dimers of two-pore domain subunits, like the K2P channels (Miller and Long, 2012)).

The smallest functional K^+ channel subunit consists of two transmembrane helices (TM helices) separated by a p-segment that includes the p-helix and the selectivity filter (see Fig. 1-1A). *Paramecium bursaria* chlorella virus encodes a functional channel with as little as 94 amino acids per subunit (Kang et al., 2004). Both MthK and KcsA belong to this class of 2 TM channels.

The second common class of K^+ channels has a total of six TM helices, where the first four TMs form an independent domain that is generally a voltage sensor, and the last two TM's form the pore. The Shaker channel from *Drosophila melanogaster* belongs to this class of 6 TM voltage dependent channel (Fig. 1-1B).

1.3 Function of potassium channels

Ion channels are regulated by a variety of signals: transmembrane voltage, pH, concentration of different ions (internally and/ or externally), small ligands like GABA and cyclic-dGMP's, and also mechanical stress.

A simplified gating cycle for K^+ ion channels is shown in Fig. 1-2. A channel in the resting state is characterized by a selectivity filter in a conducting conformation and a closed inner gate, formed by a bundle crossing of the C-terminal helix (TM2 in Fig. 1-2). Upon opening of the inner gate, the conductive state is reached and ions are able to permeate though the channel. The conductance of many channels stops in the presence of an activation signal. A mechanism called C-type inactivation leads to a conformational change in or around the selectivity filter stopping gating of ions. Closure of the inner gate facilitates recovery from the C-type inactivated state.

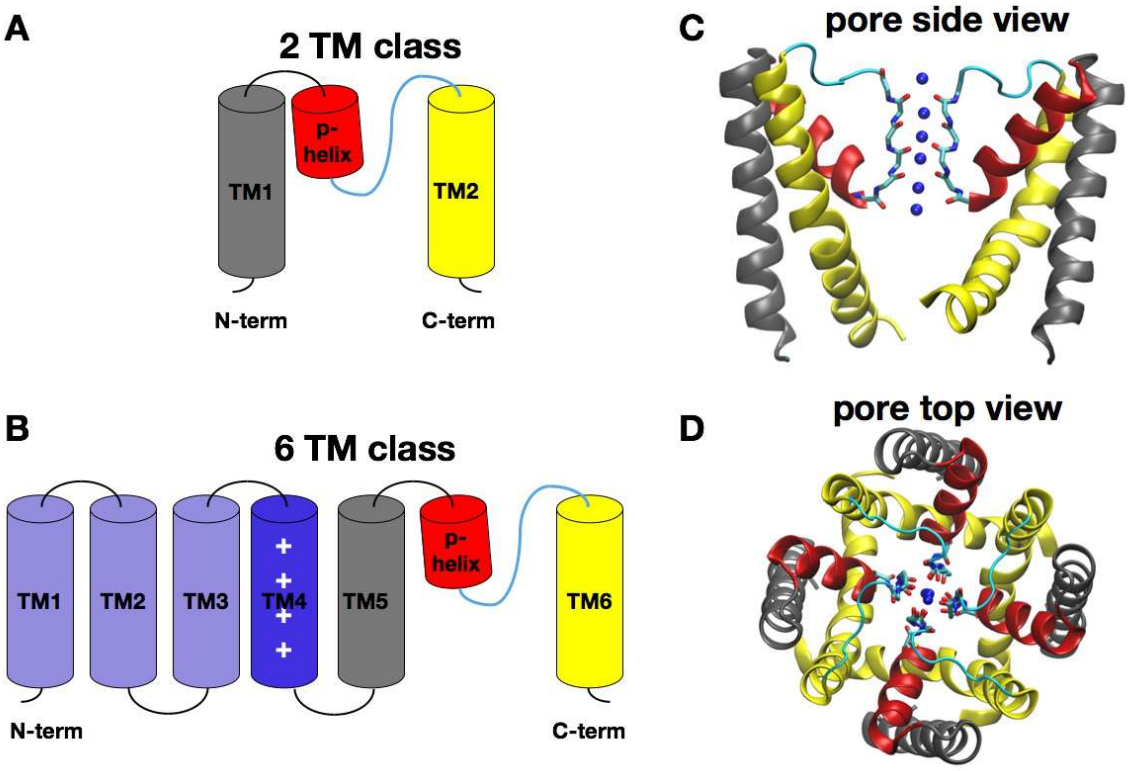

Fig. 1-1 **Structural overview of K^+ ion channel**

(A-B) Structural elements of the 2 TM and 6 TM class of K^+ ion channels. A minimal channel belongs to the 2 TM class and consists of two transmembrane helices (grey and yellow) as well as a pore helix (red) and the selectivity filter and a loop (both cyan). The 6 TM class has four trans-membrane helices (purple/blue) forming a voltage sensor domain at the N-terminal part. Note the labeling shift from TM1 and TM2 to TM5 and TM6 for the pore forming domain. (C) Side view of a 2 TM channel pore domain (the bottom is pointing into the cytoplasm). For clarity, the front and back subunits are not shown. The color scheme is the same as in (A). The selectivity filter backbone is shown in licorice and ion binding sites as blue spheres. (D) Top view on the pore domain. All four subunits are shown. The molecular representations in (C-D) are based on MthK PDB id 3LDC.

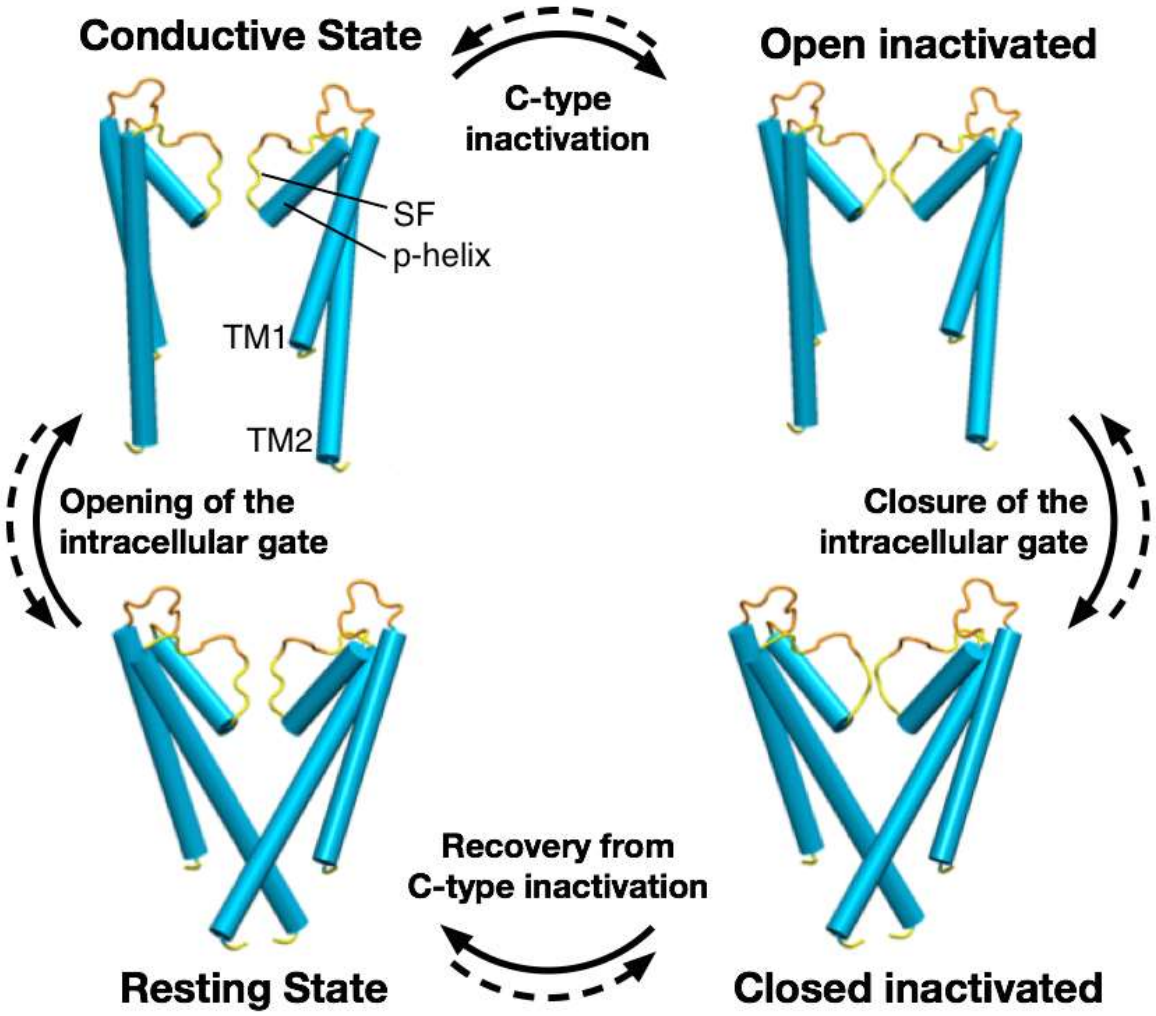

Fig. 1-2 **Gating cycle in K^+ channels**

Generalized model of gating in K^+ ion channels. For clarity the front and back subunit are not shown. Bottom Left: The resting state is characterized by a closed inner gate and a selectivity filter (SF) in a conductive conformation. Top Left: Upon activation of the channel the inner gate formed with the transmembrane 2 (C-terminal) helices opens. Top Right: A conformational change in or around the selectivity filter leads to a ion permeation stop in the presence of an activation signal. Bottom Right: Upon a loss of activation signal the inner gate closes. Modified figure from Céline Boiteux (unpublished)

1.3.1 Ion permeation and selectivity

Many ion channels allow permeation of ions at near diffusion limited rates while being highly selective for a specific ion type over others (Hodgkin and Keynes, 1955; Bezanilla and Armstrong, 1972; Hille, 1973).

The selectivity filter of K^+ channels has four binding sites for potassium ions. Due to its single file arrangement, every ion has to pass every binding site in order to reach the other side. The filter is occupied by two ions on average, with S_1-S_3 and S_2-S_4 states being more stable than S_1-S_4 and S_2-S_3 state. A possible permeation pathway was shown by Bernèche and Roux in 2001 (Bernèche and Roux, 2001) involving a 'knock-on' transition state in which a third ion comes in contact with the ions in the selectivity filter, leading to a three ion state S_1-S_3-S_4,followed by S_0-S_2-S_4. The release of the top ion leaves the channel in the two ion state S_2-S_4.

Potassium channels do not exclusively transport potassium ions, but are highly selective for potassium over other ions. KcsA is about 150 times more likely to transport potassium than sodium (LeMasurier et al., 2001). Selectivity in the K^+ channel is an intrinsic physical property of the selectivity filter forming the binding site (Noskov et al., 2004). It is also clear that the binding of multiple ions in a single file fashion is necessary for selectivity (Nimigean and Allen, 2011). Medovoy et al. showed in a computational study that the selectivity in KcsA can not be explained by the free energy landscape of the Na^+ ion alone, but only in connection with surrounding K^+ ions in the selectivity filter (Medovoy et al., 2016). The channel NaK from *Bacillus cereus* is non selective between Na^+ and K^+ (it is important to mention that selectivity (or the lack of it) is not necessary a property of binding affinity: the single binding sites within the filter of NaK are ~300 times more favorable for K^+ than for Na^+ (Liu and Lockless, 2013; Sauer et al., 2013)). The pore structure of NaK is similar to that of selective K^+ channels, however the selectivity filter shows important differences. Only the two inner binding sites are conserved, while the upper part of the selectivity filter is wider than in K^+ selective channels and forms a cavity open to the extracellular milieu (Alam and Jiang, 2009). K^+ channels are characterized by the filter forming motive TVGYG, which in NaK is replaced by TVGDG. Mutating the selectivity filter motive back only restored one of the two missing binding sites.

This construct with only three binding sites for potassium was not sufficient to obtain a selective channel. An additional mutation in the p-loop region was necessary to obtain a channel with all four binding sites, showing the importance of the interactions with the scaffolding around the selectivity filter for its function (Derebe et al., 2011; Sauer et al., 2011).

Removing the innermost binding site from the K^+ selective NaK mutant channel, as well as from MthK (Thr59Ala mutant), lead to nonselective channels. The same mutation in the Shaker channel however did not lead to a loss of selectivity (Heginbotham et al., 1994). It is worth noting that MthK (and obviously NaK) is able to conduct Na^+ at least in the absence of K^+. KcsA however does not conduct Na^+ and crystal structures solved under low potassium conditions show a collapsed filter, suggesting that stabilization of the selectivity filter by ions plays an additional role in selectivity.

1.3.2 Channel activation

In absence of an activating signal, most channels are in the closed state, where the C-terminal end of helices forming the pore forms a bundle crossing, impermeable for ions. (Liu et al., 1997; Perozo et al., 1999). Upon the application of an activation signal, the helices move apart opening a path toward the cavity below the selectivity filter (Shimizu et al., 2008).

MthK has a cytoplasmic RCK domain which activates the channel upon Ca^{2+} (or Cd^{2+}) binding. This domain consists of a dimer of tetramers where one tetramer is part of the pore forming protein and the second tetramer consists only of the RCK domain part (see also Fig. 1-3).

Voltage gated channels (Kv channels) have a total of six transmembrane helices per subunit (the two C-terminal helices form the functional channel pore domain, while the other four are forming the voltage sensor). Special attention is given to the fourth transmembrane helix which has a positively charged amino acid (arginine or lysine) at every 3rd position and is generally conserved over all voltage gated K^+, Na^+ and Ca^{2+} ion channels (Aggarwal and MacKinnon, 1996). In response to changes in the membrane potential, the equivalent of around 12 electron volts traverse the electric field upon activation of a channel (Schoppa et al., 1992). The precise activation mechanism is not known however. There is currently no known structure of a closed voltage gated channel. Note that channels without the voltage sensing domain may still show voltage dependent gating. This additional voltage sensor is located at the selectivity filter (Posson et al., 2013a) and influences inactivation rates of the channel.

KcsA is a pH gated channel. It consists of the pore forming two helices, but the C-terminal part is prolonged forming a coiled-coil structure with the four helices from all subunits (see Fig. 1-3) The pH sensor consists of the two amino acids, H25 and E118, which are found on TM1 and TM2 respectively, near the intracellular membrane-water interface (Posson et al., 2013b).

1.3.3 N-type inactivation

Many K^+ channels have two different inactivation gates. One is the N-type inactivation gate. It takes its name from a N-terminal amino acid moiety, which consists of about ten neutral charged amino acids (“chain”) followed by a net positively charged head (“ball”), thous often referred to as 'ball and chain'. This motif interacts in the cavity of the channel, where it binds only if the inner gate is open. A typical feature is that the N-terminal domain is competing with internal tetraethyl ammonium (TEA^+).

Such N-terminal motif is found in shaker, as well as several mammalian Kv channels (Hoshi et al., 1990, 1991; Beck et al., 1998). In other mammal Kv channels, it is part of a cytoplasmic ß-subunit (Accili et al., 1997; Morales et al., 1995; Rettig et al., 1994; Sewing et al., 1996).

Channels can have more than one N-type inactivation moiety (one on each N-terminus per subunit) which are either independent (Gomez-Lagunas and Armstrong, 1995) or negatively cooperating (Hashimoto et al., 2000).

1.3.4 C-type inactivation

A second inactivation mechanism is C-type inactivation. Since it is usually much slower than N-type inactivation, it is often called “slow” inactivation. It was originally identified in C-terminal splicing variants of the Shaker channel (Hoshi et al., 1990, 1991). It is now evident that C-type inactivation involves a conformational change in or around the selectivity filter (Baukrowitz and Yellen, 1995, 1996; López-Barneo et al., 1993; Yellen et al., 1994; Liu et al., 1996; Levy and Deutsch, 1996a, 1996b; Loots and Isacoff, 1998; Ray and Deutsch, 2006; Hoshi and Armstrong, 2013). In part, C-type inactivation is inhibited by external potassium ions (Fedida et al., 1999; Hoshi et al., 1990; López-Barneo et al., 1993; Rasmusson et al., 1995; Thomson and Rothberg, 2010).

In stark contrast to N-type inactivation, C-type inactivation is dependent on all subunits, suggesting the formation of a single cooperative gate (Ogielska et al., 1995; Panyi et al., 1995; Wu et al., 2014).

Structural insight on C-type inactivation comes from the 2001 crystal structure of KcsA under low K^+ concentration (Zhou et al., 2001). As argued later, this non-conductive structure might indeed be related to the C-type inactivated state (Cordero-Morales et al., 2007; Yellen, 2001).

It is however an open question, whether this non-conducting state corresponds to the biologically relevant C-type inactivated state for all selective K^+ channels, for a subgroup of channels, or if it corresponds to a defunct state. For instance, a semi-synthetic channel shows inactivation, but is sterically hindered to adopt the observed constricted conformation associated with inactivation (Devaraneni et al., 2013).

When MthK was crystalized under C-type inactivation promoting conditions, no conformational change in the selectivity filter was observed (Ye et al., 2010). However the electron density in the selectivity filter suggests that the channel is occupied by a Na^+ and a K^+ at the same time, and with a preference for state S_1-S_3 over S_2-S_4.

In KcsA, Phe103 was identified as a possible key residue linking the inner gate and the C-type inactivation gate in the selectivity filter (Cuello et al., 2010a). In the structure with a closed inner gate and a selectivity filter in the conductive state, the phenyl ring of Phe103 is interacting with the side-chain of Ile100 of an adjacent subunit. Opening of the inner gate moves the two amino acids towards each other, leading to a rotation of the Phe103 side-chain which favor an interaction with the selectivity filter at the level of Thr75. The interaction with the selectivity filter favors inactivation. Mutating Phe103 to an amino acid with a smaller side-chain like alanine or cysteine decreases inactivation, while a tryptophan had similar properties as WT.

1.3.5 Recovery from C-type inactivation

Recovery of conductance after inactivation is a slow process. Recovery is promoted or enhanced by the closing of the inner gate of the channel.

Ostmeyer et al. showed that the collapsed state is stabilized by water molecules behind the selectivity filter (Ostmeyer et al., 2013). As long as these water molecules are in place, the selectivity filter cannot adopt the conductive state since the filter would clash with the water molecules. During their 17 µs simulation, no ion entered into the selectivity filter, which remained unchanged. Upon removal of the buried water molecules behind the selectivity filter, ions are recruited into the channel and the structure changes to a conductive state within 2 ns of simulation.

It is worth noting that recovery from inactivation did not occur in the absence of ion, in agreement with experimental data showing that potassium concentration influences recovery time.

1.4 The model channels KcsA and MthK

The basis for every molecular dynamic simulation is the starting structure and the most common source are structures solved by X-ray crystallography. While the structures can already give great insight into the functionality of a protein, all dynamic dependent mechanisms remain hidden. The observations made with molecular dynamic simulations are on the atomic level, while electrophysiological measurements are among the most efficient tools of gaining insights into the macroscopic behavior of ion channels. Ideal channels for studying processes such as modulation of activation and inactivation thus have high-resolution structures and are well established in the experimental community.

The two prokaryotic model channels KcsA from *Streptomyces lividans* and MthK from *Methanobacterium thermoautotrophicum* both fulfill these criteria.

In 1998 Doyle et al. solved the first crystal structure of a selective ion channel, it was KcsA from the bacterium *Streptomyces lividans* at a resolution of 3.2 Å (Doyle et al., 1998). This structure answered many questions in the field. It notably showed that ions are de-solvated in the selectivity filter (see Fig. 1-1C, the ions are interacting directly with the selectivity filter).

The structure of KcsA was solved again three years later at 2 Å resolution using Fab-antibodies (Zhou et al., 2001). The structure was solved under two different ion concentrations. In the crystal soaked in the so called high K^+ solution with 200 mM KCl concentration, the selectivity filter revealed four peaks at the ion binding sites corresponding to roughly 1/2 K^+ (and 1/2 water) each, which fits well with the presumed occupancy of 2 ions on average in the selectivity filter. In the presence of the lower K^+ concentration (3 mM), the selectivity filter changed its conformation. More precisely, no electron density peaks at the positions S_2 and S_3 were detected and the backbone of amino acids Val76 and Gly77 rearranged. The carbonyl oxygen of Val76 is rotated out of the filter, making a H-bond with a water molecule between the selectivity filter and the p-helix. This water molecule forms an additional H-bond with Gly77 of a neighboring subunit. The alpha carbon of Gly77 is shifted towards the center of the pore and prevents ion binding at site S_2. This state was later proposed as the inactivated state of the channel (Cordero-Morales et al., 2007; Yellen, 2001). All three KcsA structures mentioned here have a closed inner gate and are truncated.

One year later, in 2002, Jiang et al. solved the structure of the calcium-gated K^+ ion channel MthK from the archon *Methanobacterium thermoautotrophicum* (Jiang et al., 2002). MthK has a Ca^{2+} binding domain, or RCK (regulator of K^+ conductance) domain. It consists of eight subunits, four expressed as C-terminus of the protein and four additional originate from a second start codon excluding the pore forming part of the protein (see Fig. 1-3). In this MthK structure, the inner gate is open and the selectivity filter resembles the open conductive state revealed by the KcsA high K^+ structure. This structure was used to model the open active state of KcsA, which like MthK opens via a hinge (Kelly and Gross, 2003). In 2010, the structure of the isolated pore domain of MthK channel was solved (Ye et al., 2010). Removing the RCK domain did not lead to a significant change in the structure (RMSD of the alpha carbon atoms of the tetrameric pore is 1.6 Å compared to the pore domain of the structure crystalized by Jiang et al.) and allowed to solve the structure up to a resolution of 1.45 Å. Similar to the approach taken by Zhou et al.(Zhou et al., 2001), different ion concentrations were used to identify a possible inactivated structure. The results were however strikingly distinct. Under high potassium concentrations the selectivity filter had four equally occupied binding sites and the selectivity filter was in the conductive state with an open inner gate. Lowering the K^+ concentration had no effect on the selectivity filter. The sites S_2 and S_4 however were less occupied than S_1 and S_3. Additionally, occupancy of these sites by one K^+ and one Na^+ was proposed.

In 2010, Cuello et al. (Cuello et al., 2010b) crystalized the KcsA channel in different opening states of the inner gate. A key aspect of these structures is that the selectivity filter changes its conformation towards a nonconductive state when the inner gate opens (while still keeping the K^+ concentration high in all crystals), underscoring the dependence between the selectivity filter and the inner gate.

With this last series of ion channels, a molecular representation exists for all states of the gating cycle, as shown in Fig. 1-2: The 2001 crystal structure of KcsA (Zhou et al., 2001) is in the resting state (PDB id 1K4C) and closed inactivated state (PDB id 1K4D). The open inactivated state is represented by (PDB id 3F5W) (Cuello et al., 2010a). A Structure associated with the conductive state was only crystallized for MthK (PDB id 3LDC) (Zhou et al., 2001). Note a KcsA structure in the Conductive state was solved recently by Luis Cuello, but is not yet published (Medovoy et al., 2016).

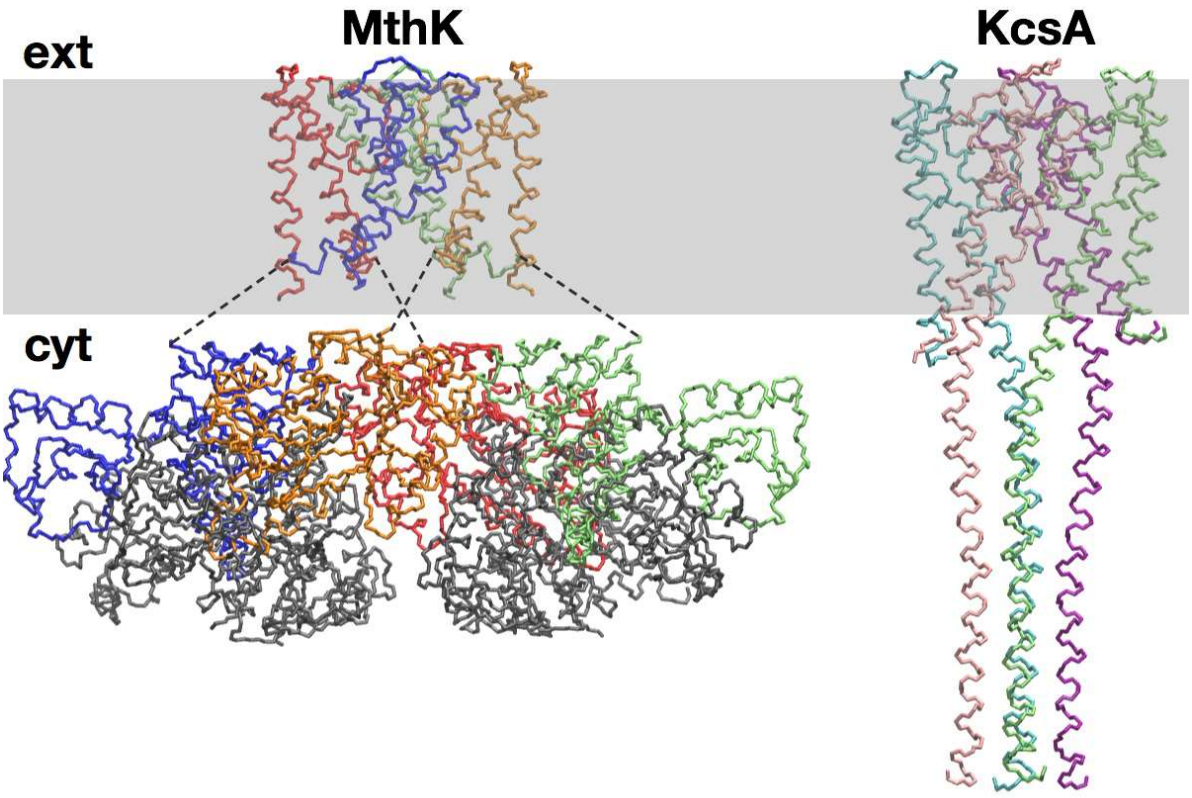

Fig. 1-3 **Structure of MthK and KcsA**

Biologically functional unit of the crystal structures of MthK, left (PDB id 1LNQ) and KcsA, right (PDB id 3PJS). The approximated position of the membrane is marked with a grey box. Each subunit is represented in a different color. MthK has an octameric RCK domain in the cytoplasm. The top ring is linked to the pore domain, the linker is however not resolved in the crystal structure and is represented by a dotted line. The bottom ring, shown in grey, is formed with four additional subunits of the RCK domain. In the crystal structure they are linked to a pore domain (not shown). KcsA has prolonged C-terminal helices, which form the pH sensor. Most other KcsA structures have a truncated C-terminal domain and thus lack this cytosolic elongation.

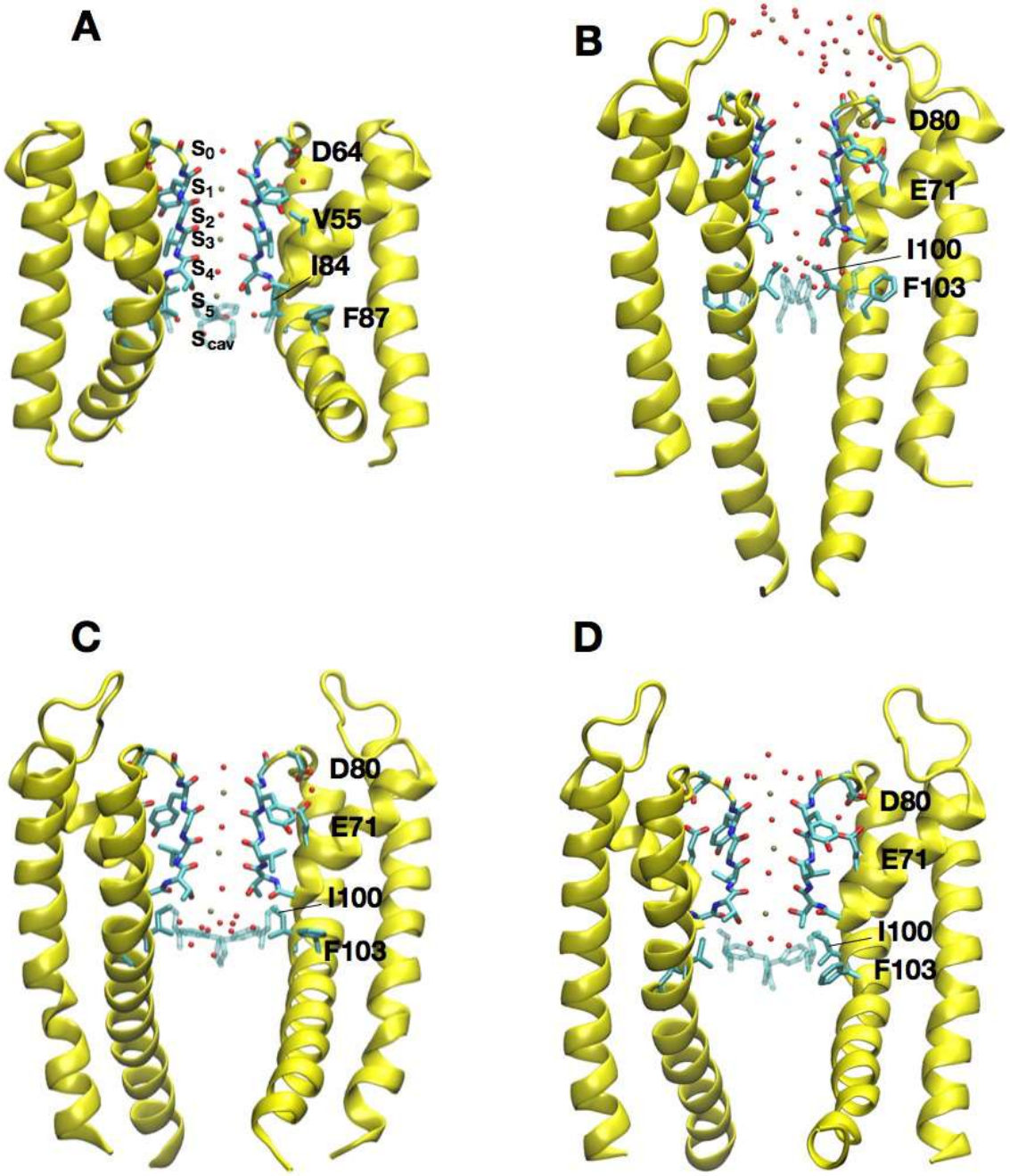

Fig. 1-4 **Opening grade of the inner gates**

(A) Molecular representations of the MthK channel with an open inner gate (PDB id 3LDC). (B-D) Molecular representation of the KcsA channel with the inner gate in the closed state (PDB id 1K4D) (B), in the partially open state (PDB id 3F7V) (C), and the open state (model based on PDB id 3F5W)(D). The TM helices and p-helices are shown in yellow cartoon. The selectivity filter is depicted in licorice with the usual atom type colors (oxygen in red, nitrogen in blue and carbon in cyan, hydrogens are not shown). The side-chains of E71 (V55) and D80 (D64) as well as I100 (I84) and F103 (F87) are shown. The latter two are shown in transparent for the other two sub units. The labeling of the binding sites is shown in (A). For clarity only two adjacent subunits are shown.

The structures presented in Fig. 1-4C-D deviate from the selectivity filter conformation in the crystal structures (see Methods in chapter 4.6.1).

1.5 Aim of the thesis

The aim of this thesis is to determine quantitative, predictive models for the regulation of permeation and inactivation at the selectivity filter of K^+ ion channels.

There is some understanding of permeation through the selectivity filter, however we do not know how the conductance is regulated, and more importantly, why (and how) it differs from channel to channel. In a series of crystal structures, it was shown that opening of the inner gate changes the structure of the selectivity filter toward a non-conducting state in KcsA. These structures can serve as basis to build models that can then be used to investigate conductance regulation.

A model for inactivation based on a crystal structure of KcsA was proposed, but a similar conformation was never observed in other channels, nor was the mechanism described with computational methods in those channels. The aim here is two-fold: On one hand an inactivation mechanism has to be identified in MthK (no non-conductive structure was found), on the other hand the existing (and challenged) inactivation mechanism has to be complemented or a new one proposed.

1.6 References

Accili, E.A., Kiehn, J., Yang, Q., Wang, Z., Brown, A.M., Wible, B.A., 1997. Separable Kvbeta subunit domains alter expression and gating of potassium channels. J. Biol. Chem. 272, 25824–25831.

Aggarwal, S.K., MacKinnon, R., 1996. Contribution of the S4 segment to gating charge in the Shaker K+ channel. Neuron 16, 1169–1177.

Alam, A., Jiang, Y., 2009. Structural analysis of ion selectivity in the NaK channel. Nat. Struct. Mol. Biol. 16, 35–41. doi:10.1038/nsmb.1537

Baukrowitz, T., Yellen, G., 1996. Use-dependent blockers and exit rate of the last ion from the multi-ion pore of a K+ channel. Science 271, 653–656.

Baukrowitz, T., Yellen, G., 1995. Modulation of K+ current by frequency and external [K+]: a tale of two inactivation mechanisms. Neuron 15, 951–960.

Beck, E.J., Sorensen, R.G., Slater, S.J., Covarrubias, M., 1998. Interactions between multiple phosphorylation sites in the inactivation particle of a K+ channel. Insights into the molecular mechanism of protein kinase C action. J. Gen. Physiol. 112, 71–84.

Bernèche, S., Roux, B., 2001. Energetics of ion conduction through the K+ channel. Nature 414, 73–77. doi:10.1038/35102067

Bezanilla, F., Armstrong, C.M., 1972. Negative conductance caused by entry of sodium and cesium ions into the potassium channels of squid axons. J. Gen. Physiol. 60, 588–608.

Cordero-Morales, J.F., Jogini, V., Lewis, A., Vásquez, V., Cortes, D.M., Roux, B., Perozo, E., 2007. Molecular driving forces determining potassium channel slow inactivation. Nat. Struct. Mol. Biol. 14, 1062–1069. doi:10.1038/nsmb1309

Cuello, L.G., Jogini, V., Cortes, D.M., Pan, A.C., Gagnon, D.G., Dalmas, O., Cordero-Morales, J.F., Chakrapani, S., Roux, B., Perozo, E., 2010a. Structural basis for the coupling between activation and inactivation gates in K(+) channels. Nature 466, 272–275. doi:10.1038/nature09136

Cuello, L.G., Jogini, V., Cortes, D.M., Perozo, E., 2010b. Structural mechanism of C-type inactivation in K(+) channels. Nature 466, 203–208. doi:10.1038/nature09153

Derebe, M.G., Sauer, D.B., Zeng, W., Alam, A., Shi, N., Jiang, Y., 2011. Tuning the ion selectivity of tetrameric cation channels by changing the number of ion binding sites. Proc. Natl. Acad. Sci. U. S. A. 108, 598–602. doi:10.1073/pnas.1013636108

Devaraneni, P.K., Komarov, A.G., Costantino, C.A., Devereaux, J.J., Matulef, K., Valiyaveetil, F.I., 2013. Semisynthetic K+ channels show that the constricted conformation of the selectivity filter is not the C-type inactivated state. Proc. Natl. Acad. Sci. U. S. A. 110, 15698–15703. doi:10.1073/pnas.1308699110

Doyle, D.A., Morais Cabral, J., Pfuetzner, R.A., Kuo, A., Gulbis, J.M., Cohen, S.L., Chait, B.T., MacKinnon, R., 1998. The structure of the potassium channel: molecular basis of K+ conduction and selectivity. Science 280, 69–77.

Fedida, D., Maruoka, N.D., Lin, S., 1999. Modulation of slow inactivation in human cardiac Kv1.5 channels by extra- and intracellular permeant cations. J. Physiol. 515 (Pt 2), 315–329.

Gomez-Lagunas, F., Armstrong, C.M., 1995. Inactivation in ShakerB K+ channels: a test for the number of inactivating particles on each channel. Biophys. J. 68, 89–95. doi:10.1016/S0006-3495(95)80162-1

Hashimoto, Y., Nunoki, K., Kudo, H., Ishii, K., Taira, N., Yanagisawa, T., 2000. Changes in the inactivation of rat Kv1.4 K(+) channels induced by varying the number of inactivation particles. J. Biol. Chem. 275, 9358–9362.

Heginbotham, L., Lu, Z., Abramson, T., MacKinnon, R., 1994. Mutations in the K+ channel signature sequence. Biophys. J. 66, 1061–1067. doi:10.1016/S0006-3495(94)80887-2

Hille, B., 1973. Potassium channels in myelinated nerve. Selective permeability to small cations. J. Gen. Physiol. 61, 669–686.

Hille, B., 1970. Ionic channels in nerve membranes. Prog. Biophys. Mol. Biol. 21, 1–32.

Hille, B., Armstrong, C.M., MacKinnon, R., 1999. Ion channels: from idea to reality. Nat. Med. 5, 1105–1109. doi:10.1038/13415

Hodgkin, A.L., Huxley, A.F., 1952. A quantitative description of membrane current and its application to conduction and excitation in nerve. J. Physiol. 117, 500–544.

Hodgkin, A.L., Keynes, R.D., 1955. The potassium permeability of a giant nerve fibre. J. Physiol. 128, 61–88.

Hoshi, T., Armstrong, C.M., 2013. C-type inactivation of voltage-gated K+ channels: pore constriction or dilation? J. Gen. Physiol. 141, 151–160. doi:10.1085/jgp.201210888

Hoshi, T., Zagotta, W.N., Aldrich, R.W., 1991. Two types of inactivation in Shaker K+ channels: Effects of alterations in the carboxy-terminal region. Neuron 7, 547–556. doi:10.1016/0896-6273(91)90367-9

Hoshi, T., Zagotta, W.N., Aldrich, R.W., 1990. Biophysical and molecular mechanisms of Shaker potassium channel inactivation. Science 250, 533–538.

Jegla, T.J., Zmasek, C.M., Batalov, S., Nayak, S.K., 2009. Evolution of the human ion channel set. Comb. Chem. High Throughput Screen. 12, 2–23.

Jiang, Y., Lee, A., Chen, J., Cadene, M., Chait, B.T., MacKinnon, R., 2002. Crystal structure and mechanism of a calcium-gated potassium channel. Nature 417, 515–522. doi:10.1038/417515a

Kang, M., Moroni, A., Gazzarrini, S., DiFrancesco, D., Thiel, G., Severino, M., Van Etten, J.L., 2004. Small potassium ion channel proteins encoded by chlorella viruses. Proc. Natl. Acad. Sci. U. S. A. 101, 5318–5324. doi:10.1073/pnas.0307824100

Kelly, B.L., Gross, A., 2003. Potassium channel gating observed with site-directed mass tagging. Nat. Struct. Biol. 10, 280–284. doi:10.1038/nsb908

Kuo, M.M.-C., Haynes, W.J., Loukin, S.H., Kung, C., Saimi, Y., 2005. Prokaryotic K(+) channels: from crystal structures to diversity. FEMS Microbiol. Rev. 29, 961–985. doi:10.1016/j.femsre.2005.03.003

Lang, F., Föller, M., Lang, K., Lang, P., Ritter, M., Vereninov, A., Szabo, I., Huber, S.M., Gulbins, E., 2007. Cell volume regulatory ion channels in cell proliferation and cell death. Methods Enzymol. 428, 209–225. doi:10.1016/S0076-6879(07)28011-5

LeMasurier, M., Heginbotham, L., Miller, C., 2001. Kcsa. J. Gen. Physiol. 118, 303–314.

Levy, D.I., Deutsch, C., 1996a. A voltage-dependent role for K+ in recovery from C-type inactivation. Biophys. J. 71, 3157–3166. doi:10.1016/S0006-3495(96)79509-7

Levy, D.I., Deutsch, C., 1996b. Recovery from C-type inactivation is modulated by extracellular potassium. Biophys. J. 70, 798–805. doi:10.1016/S0006-3495(96)79619-4

Liu, S., Lockless, S.W., 2013. Equilibrium selectivity alone does not create K+-selective ion conduction in K+ channels. Nat. Commun. 4, 2746. doi:10.1038/ncomms3746

Liu, Y., Holmgren, M., Jurman, M.E., Yellen, G., 1997. Gated access to the pore of a voltage-dependent K+ channel. Neuron 19, 175–184.

Liu, Y., Jurman, M.E., Yellen, G., 1996. Dynamic rearrangement of the outer mouth of a K+ channel during gating. Neuron 16, 859–867.

Loots, E., Isacoff, E.Y., 1998. Protein rearrangements underlying slow inactivation of the Shaker K+ channel. J. Gen. Physiol. 112, 377–389.

López-Barneo, J., Hoshi, T., Heinemann, S.H., Aldrich, R.W., 1993. Effects of external cations and mutations in the pore region on C-type inactivation of Shaker potassium channels. Receptors Channels 1, 61–71.

Medovoy, D., Perozo, E., Roux, B., 2016. Multi-ion free energy landscapes underscore the microscopic mechanism of ion selectivity in the KcsA channel. Biochim. Biophys. Acta. doi:10.1016/j.bbamem.2016.02.019

Miller, A.N., Long, S.B., 2012. Crystal structure of the human two-pore domain potassium channel K2P1. Science 335, 432–436. doi:10.1126/science.1213274

Morales, M.J., Castellino, R.C., Crews, A.L., Rasmusson, R.L., Strauss, H.C., 1995. A novel beta subunit increases rate of inactivation of specific voltage-gated potassium channel alpha subunits. J. Biol. Chem. 270, 6272–6277.

Neher, E., Sakmann, B., 1976. Single-channel currents recorded from membrane of denervated frog muscle fibres. Nature 260, 799–802.

Nimigean, C.M., Allen, T.W., 2011. Origins of ion selectivity in potassium channels from the perspective of channel block. J. Gen. Physiol. 137, 405–413. doi:10.1085/jgp.201010551

Noskov, S.Y., Bernèche, S., Roux, B., 2004. Control of ion selectivity in potassium channels by electrostatic and dynamic properties of carbonyl ligands. Nature 431, 830–834. doi:10.1038/nature02943

Ogielska, E.M., Zagotta, W.N., Hoshi, T., Heinemann, S.H., Haab, J., Aldrich, R.W., 1995. Cooperative subunit interactions in C-type inactivation of K channels. Biophys. J. 69, 2449–2457. doi:10.1016/S0006-3495(95)80114-1

Ostmeyer, J., Chakrapani, S., Pan, A.C., Perozo, E., Roux, B., 2013. Recovery from slow inactivation in K+ channels is controlled by water molecules. Nature 501, 121–124. doi:10.1038/nature12395

Panyi, G., Sheng, Z., Deutsch, C., 1995. C-type inactivation of a voltage-gated K+ channel occurs by a cooperative mechanism. Biophys. J. 69, 896–903. doi:10.1016/S0006-3495(95)79963-5

Perozo, E., Cortes, D.M., Cuello, L.G., 1999. Structural rearrangements underlying K+-channel activation gating. Science 285, 73–78.

Posson, D.J., McCoy, J.G., Nimigean, C.M., 2013a. The voltage-dependent gate in MthK potassium channels is located at the selectivity filter. Nat. Struct. Mol. Biol. 20, 159–166. doi:10.1038/nsmb.2473

Posson, D.J., Thompson, A.N., McCoy, J.G., Nimigean, C.M., 2013b. Molecular interactions involved in proton-dependent gating in KcsA potassium channels. J. Gen. Physiol. 142, 613–624. doi:10.1085/jgp.201311057

Poveda, J.A., Giudici, A.M., Renart, M.L., Molina, M.L., Montoya, E., Fernández-Carvajal, A., Fernández-Ballester, G., Encinar, J.A., González-Ros, J.M., 2014. Lipid modulation of ion channels through specific binding sites. Biochim. Biophys. Acta 1838, 1560–1567. doi:10.1016/j.bbamem.2013.10.023

Rasmusson, R.L., Morales, M.J., Castellino, R.C., Zhang, Y., Campbell, D.L., Strauss, H.C., 1995. C-type inactivation controls recovery in a fast inactivating cardiac K+ channel (Kv1.4) expressed in Xenopus oocytes. J. Physiol. 489 (Pt 3), 709–721.

Ray, E.C., Deutsch, C., 2006. A trapped intracellular cation modulates K+ channel recovery from slow inactivation. J. Gen. Physiol. 128, 203–217. doi:10.1085/jgp.200609561

Rettig, J., Heinemann, S.H., Wunder, F., Lorra, C., Parcej, D.N., Dolly, J.O., Pongs, O., 1994. Inactivation properties of voltage-gated K+ channels altered by presence of beta-subunit. Nature 369, 289–294. doi:10.1038/369289a0

Sauer, D.B., Zeng, W., Canty, J., Lam, Y., Jiang, Y., 2013. Sodium and potassium competition in potassium-selective and non-selective channels. Nat. Commun. 4, 2721. doi:10.1038/ncomms3721

Sauer, D.B., Zeng, W., Raghunathan, S., Jiang, Y., 2011. Protein interactions central to stabilizing the K+ channel selectivity filter in a four-sited configuration for selective K+ permeation. Proc. Natl. Acad. Sci. U. S. A. 108, 16634–16639. doi:10.1073/pnas.1111688108

Schoppa, N.E., McCormack, K., Tanouye, M.A., Sigworth, F.J., 1992. The size of gating charge in wild-type and mutant Shaker potassium channels. Science 255, 1712–1715.

Sewing, S., Roeper, J., Pongs, O., 1996. Kvβ1 subunit binding specific for Shaker-related potassium channel αsSubunits. Neuron 16, 455–463. doi:10.1016/S0896-6273(00)80063-X

Shimizu, H., Iwamoto, M., Konno, T., Nihei, A., Sasaki, Y.C., Oiki, S., 2008. Global twisting motion of single molecular KcsA potassium channel upon gating. Cell 132, 67–78. doi:10.1016/j.cell.2007.11.040

Thomson, A.S., Rothberg, B.S., 2010. Voltage-dependent inactivation gating at the selectivity filter of the MthK K+ channel. J. Gen. Physiol. 136, 569–579. doi:10.1085/jgp.201010507

Wu, W., Gardner, A., Sanguinetti, M.C., 2014. Cooperative subunit interactions mediate fast C-type inactivation of hERG1 K+ channels. J. Physiol. 592, 4465–4480. doi:10.1113/jphysiol.2014.277483

Yellen, G., 2001. Keeping K+ completely comfortable. Nat. Struct. Biol. 8, 1011–1013. doi:10.1038/nsb1201-1011

Yellen, G., Sodickson, D., Chen, T.Y., Jurman, M.E., 1994. An engineered cysteine in the external mouth of a K+ channel allows inactivation to be modulated by metal binding. Biophys. J. 66, 1068–1075. doi:10.1016/S0006-3495(94)80888-4

Ye, S., Li, Y., Jiang, Y., 2010. Novel insights into K+ selectivity from high-resolution structures of an open K+ channel pore. Nat. Struct. Mol. Biol. 17, 1019–1023. doi:10.1038/nsmb.1865

Zhou, Y., Morais-Cabral, J.H., Kaufman, A., MacKinnon, R., 2001. Chemistry of ion coordination and hydration revealed by a K+ channel-Fab complex at 2.0 A resolution. Nature 414, 43–48. doi:10.1038/35102009

2 Initial steps of inactivation at the K^+ channel selectivity filter

Andrew S. Thomson[a,1,2], Florian T. Heer[b,2], Frank J. Smith[a,1], Eunan Hendrona,

Simon Bernèche[b,3], and Brad S. Rothberg[a,3]

[a]Department of Biochemistry, Temple University School of Medicine, Philadelphia, PA 19140;

[b]Swiss Institute of Bioinformatics and Biozentrum, University of Basel, CH-4056 Basel, Switzerland

Edited by Richard W. Aldrich, The University of Texas at Austin, Austin, TX, and approved March 21, 2014 (received for review September 17, 2013)

Author contributions: S.B. and B.S.R. designed research; A.S.T., F.T.H., F.J.S., and E.H. performed research; A.S.T., F.T.H., F.J.S., E.H., S.B., and B.S.R. analyzed data; and A.S.T., F.T.H., S.B., and B.S.R. wrote the paper.

The authors declare no conflict of interest.

This article is a PNAS Direct Submission.

[1]Present address: Department of Physiology, University of Pennsylvania Perelman School of Medicine, Philadelphia, PA 19104.

[2]A.S.T. and F.T.H. contributed equally to this work.

[3]To whom correspondence may be addressed. E-mail: simon.berneche@unibas.ch or rothberg@temple.edu.

Published in Proceedings of the National Academy of Sciences USA (*Proc. Natl. Acad. Sci. U. S. A.* **111,** E1713–1722 (2014))

2.1 Statement of own contribution

This publication was reformatted to fit the stile of the thesis. My own data is represented in Fig. 2-4, Fig. 2-5, Fig. 2-6, Fig. 2-7, Fig. 2-8 ,Fig. 2-10, Fig. 2-11, Fig. 2-12 and Fig. 2-13. I performed all simulations and analyses (represented in the figures mentioned above), which I co-designed with S. Bernèche.

2.2 Abstract

K^+ efflux through K^+ channels can be controlled by C-type inactivation, which is thought to arise from a conformational change near the channel's selectivity filter. Inactivation is modulated by ion binding near the selectivity filter; however, the molecular forces that initiate inactivation remain unclear. We probe these driving forces by electrophysiology and molecular simulation of MthK, a prototypical K^+ channel. Either Mg^{2+} or Ca^{2+} can reduce K^+ efflux through MthK channels. However, Ca^{2+}, but not Mg^{2+}, can enhance entry to the inactivated state. Molecular simulations illustrate that, in the MthK pore, Ca^{2+} ions can partially dehydrate, enabling selective accessibility of Ca^{2+} to a site at the entry to the selectivity filter. Ca^{2+} binding at the site interacts with K^+ ions in the selectivity filter, facilitating a conformational change within the filter and subsequent inactivation. These results support an ionic mechanism that precedes changes in channel conformation to initiate inactivation.

2.3 Significance

C-type inactivation represents a key process that governs cellular K^+ channel activity. Although C-type inactivation seems to be inextricably linked with dissociation of K^+ from the channel's pore, the structural connection between K^+ dissociation and initiation of C-type inactivation has been unclear. Here, we combine electrophysiology and molecular simulation of MthK, a prototypical K^+ channel of known structure, to determine relations between K^+ dissociation and entry into the inactivated state. We find that Ca^{2+} can bind to a site in the pore favored by outward movement of K^+. K^+ subsequently dissociates, favoring a conformational change to the inactivated state. This study, thus, establishes a direct link between K^+ dissociation and initiation of C-type inactivation.

2.4 Introduction

Potassium (K^+) channels are activated and opened by a variety of stimuli, including ligand binding and transmembrane voltage, to enable K^+ efflux and thus, modulate physiological processes related to electrical excitability, such as regulation of action potential firing, smooth muscle contraction, and hormone secretion (1). In addition, many K^+ channels are further controlled by a gating phenomenon known as C-type inactivation, in which K^+ conduction is stopped, despite the continued presence of an activating stimulus (2). The mechanisms underlying C-type inactivation in voltage-gated K^+ channels (Kv channels) are linked to both intracellular and extracellular permeant ion concentrations, and several lines of evidence have suggested that C-type inactivation is associated with a conformational change near the external mouth of the K^+ channel pore (i.e., at the canonical K^+ channel selectivity filter) (3–11).

In Shaker Kv channels, C-type inactivation is known to be enhanced and recovery from inactivation is slowed by impermeant cations accessing the cytoplasmic side of the channel (5, 6, 10). Enhancement of inactivation by these cations suggests a working hypothesis, in which the impermeant ion prevents refilling of the selectivity filter with K^+ (6). Thus, K^+ presumably dissociates from the filter to the external solution, and this vacancy leaves the filter susceptible to a conformational change that underlies the nonconducting, inactivated state. However, the physical basis for the relation between ion movements and C-type inactivation as well as the structural underpinnings of the mechanism remain unclear.

Here, we use divalent metal cations (Mg^{2+}, Ca^{2+}, and Sr^{2+}) as probes of inactivation mechanisms in MthK, a model K^+ channel of known structure (Fig. 2-9) (12–14). Specifically, we analyze conduction and gating of single MthK channels by electrophysiology combined with analysis of ion and protein movements by molecular simulation. Our electrophysiological experiments indicate that, although each of these divalent metal ions can reduce the size of single channel currents, only Ca^{2+} and Sr^{2+} can enhance inactivation, whereas Mg^{2+} does not. Using molecular simulation and potential of mean force (PMF) calculations, we find that Ca^{2+}, but not Mg^{2+}, can shed its hydration shell waters to access a site, termed S_5, at the entry to the channel's selectivity filter (Fig. 2-9C) after displacement of K^+ ions to the extracellular side of the channel. Subsequent dissociation of a K^+ ion from the filter, in turn, favors a conformational change within the selectivity filter, contributing to enhanced inactivation. These results support a working hypothesis that directly relates dissociation of K^+ with a structural change in the selectivity filter to initiate inactivation of K^+ channels.

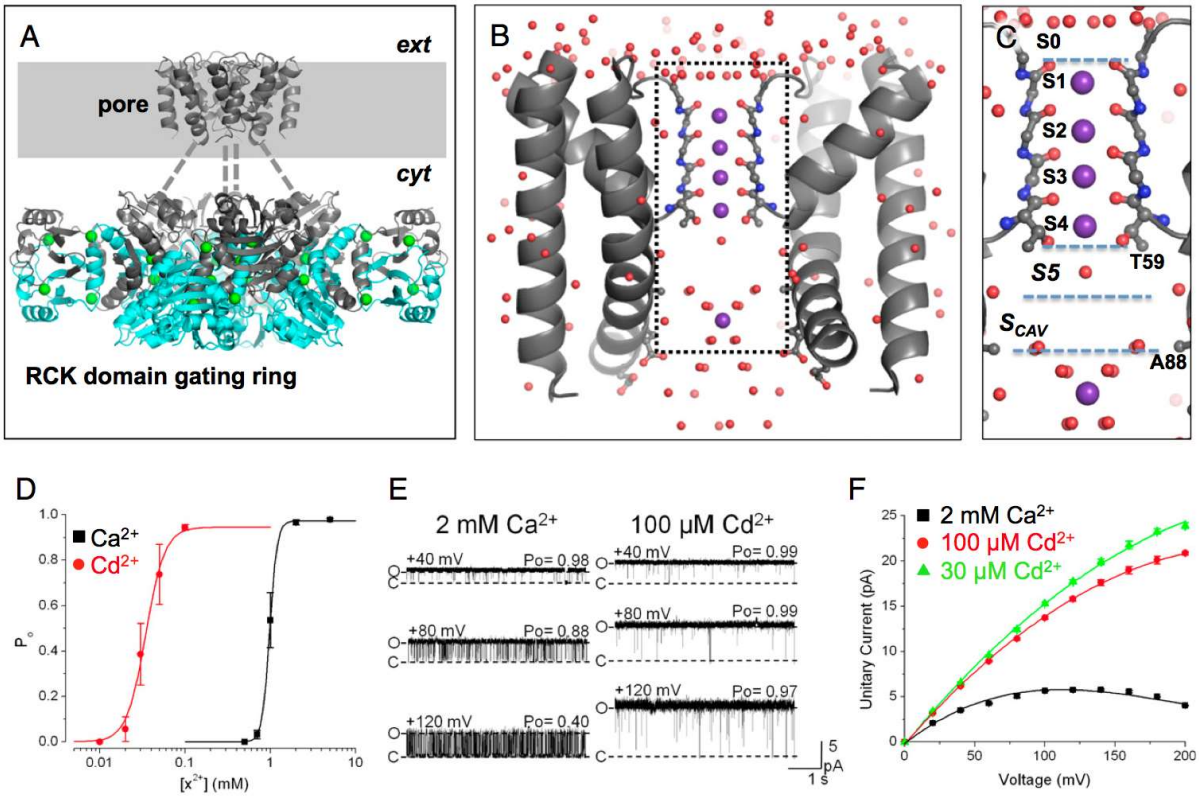

Fig. 2-1 Structure and activation properties of MthK

(A) Presumed biological structure of MthK shown as a Cα-trace [Protein Data Bank (PDB) ID code 3RBZ]. The channel consists of a transmembrane pore domain tethered to a ring of RCK domains, which mediate channel activation by cytoplasmic Ca^{2+} (green spheres). The gray-shaded region represents the presumed plasma membrane; dashed lines represent the linker region between the pore and RCK gating ring that is unresolved in the crystal structure. (B) High-resolution structure of the MthK pore domain, with the selectivity filter shown in ball and stick representation (PDB ID code 3LDC). Subunits in the front and back have been removed for clear visualization of the conduction pathway (inside dashed rectangle), with K^+ ions shown as purple spheres and ordered water molecules shown as red spheres. (C) Magnified view of the MthK conduction pathway (boxed region in B) with potential ion binding sites (S_0–S_{cav}) indicated. (D) *Po* vs. [Ca^{2+}] (black symbols) and [Cd^{2+}] (red symbols) from currents recorded at −100 mV. MthK activation requires ~20-fold lower [Cd^{2+}] compared with [Ca^{2+}]. Curves represent fits with a Hill equation with the following parameters: EC50 = 1.0 mM and n_H = 9.5 for Ca^{2+}; EC50 = 49 µM and n_H = 8.4 for Cd^{2+}. (E) Representative single channel currents from reconstituted MthK at depolarized voltages with 200 mM KCl at both sides of the membrane and Ca^{2+} or Cd^{2+} at the cytoplasmic side of the channel as indicated. Cd^{2+} can fully activate MthK at concentrations that produce much less fast blockade than Ca^{2+}. O and C indicate open and closed current levels, respectively. (F) Unitary current vs. voltage for MthK channels activated with 30 and 100 µM Cd^{2+} (green and red, respectively) and 2 mM Ca^{2+} (black). Smooth curves are drawn for display only; 100 µM Cd^{2+} results in nominal levels of fast blockade, yielding large outward current.

2.5 Results

2.5.1 Rapid blockade of MthK channels by cytoplasmic divalent cations

MthK channels can be activated through binding of Ca^{2+} to the channel's cytoplasmic domain (Fig. 2-9). However, Ca^{2+} can also apparently enter the pore of the channel to produce a rapid blockade of outward K^+ current (12, 14–18). To avoid potential confounds arising from blocking effects of Ca^{2+}, we used Cd^{2+} as an alternative agonist to activate MthK channels in our experiments (19–21). Fig. 2-9D and E illustrates that, under the conditions of our experiments, 100 µM Cd^{2+} was sufficient to activate MthK channels to a mean *Po* > 0.95 (measured at −100 mV), which is equivalent to the mean *Po* with 2 mM Ca^{2+}. In contrast, 100 µM Cd^{2+} yielded much less reduction in outward current than 2 mM Ca^{2+} (Fig. 2-9E and F). For example, outward K^+ current measured at +100 mV with 100 µM Cd^{2+} was 13.7 ± 0.2 pA compared with 5.7 ± 0.1 pA with 2 mM Ca^{2+}.

Using 100 µM Cd^{2+} to fully activate MthK channels, we observe that Mg^{2+}, Ca^{2+}, and Sr^{2+}, applied to the cytoplasmic side of the channel, reduced outward current in a voltage-dependent manner (Fig. 2-13). We quantified current blockade by Mg^{2+}, Ca^{2+}, and Sr^{2+} using the Woodhull equilibrium block model, which yields estimates of zδ (the effective fraction of the transmembrane electric field traversed by the charged blocker) and $K_{app}(0)$ (the apparent 0 mV dissociation constant of the blocking ion) (22). Interestingly, the estimated zδ-values were similar for each of the blocking ions (zδ = 0.43 ± 0.03, 0.45 ± 0.03, and 0.45 ± 0.02 e_0 for Mg^{2+}, Ca^{2+}, and Sr^{2+}, respectively) (Fig. 2-13C). If we assume that each of these divalent cations elicits fast blockade of the outward K^+ current by acting at one site, then these similar zδ-values are consistent with Mg^{2+}, Ca^{2+}, and Sr^{2+} blocking at the same site within the MthK pore. In contrast to their similar estimated zδ-values, the $K_{app}(0)$ for each ion followed the sequence $Mg^{2+} < Ca^{2+} < Sr^{2+}$ [$K_{app}(0)$ = 1.9 ± 0.1, 7.6 ± 0.4, and 9.4 ± 0.7 mM for Mg^{2+}, Ca^{2+}, and Sr^{2+}, respectively] (Fig. 2-13C). Thus, if these ions block at a single common site, then Mg^{2+} seems to bind to the site with a greater affinity than the larger divalent ions Ca^{2+} and Sr^{2+}.

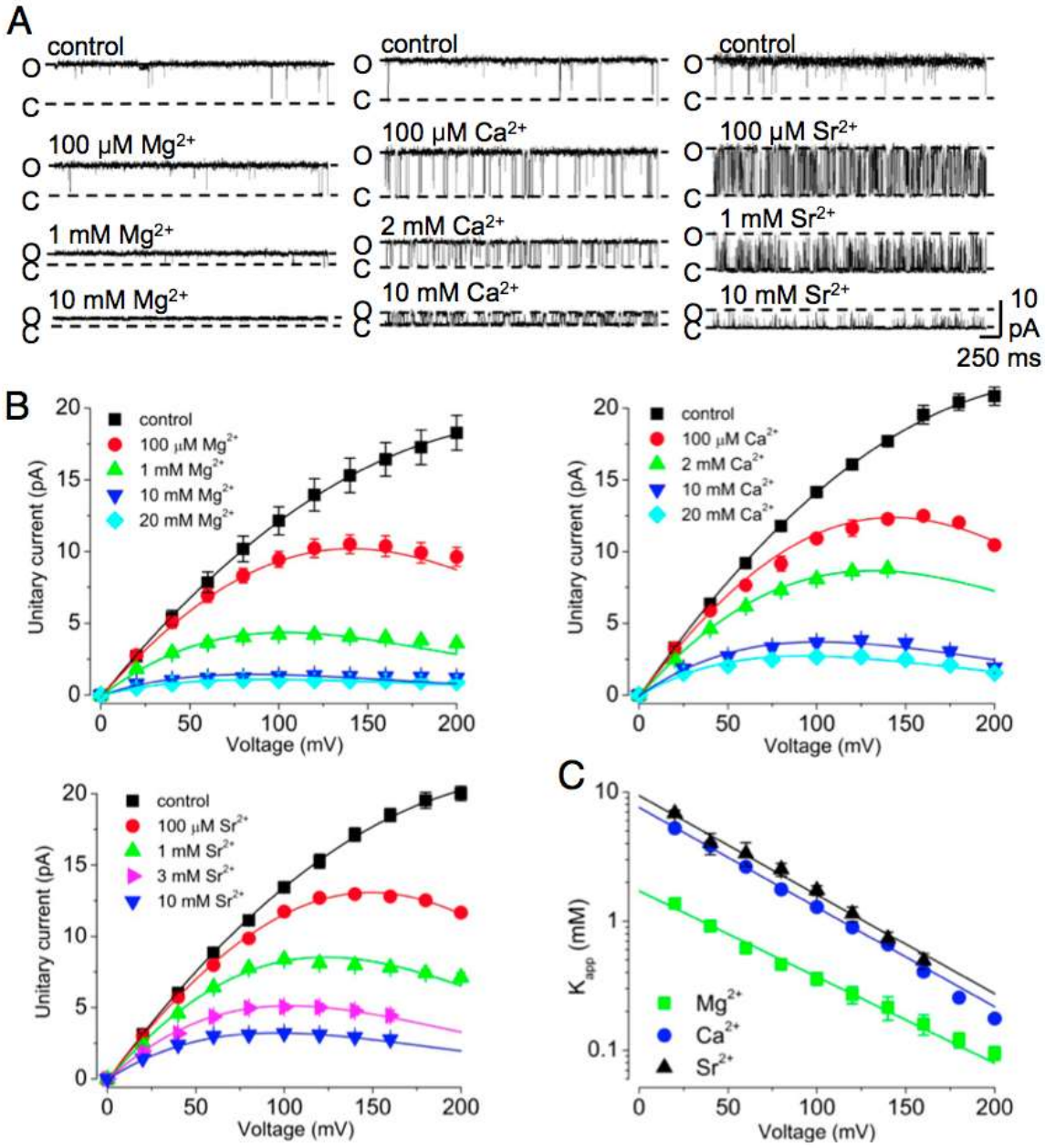

Fig. 2-2 **Rapid blockade of MthK channels by cytoplasmic divalent cations**

(A) Representative currents at 120 mV with the indicated concentrations of divalent cation. In these experiments and subsequent experiments, channels are activated using 100 μM Cd^{2+}, and control indicates recordings and results obtained without the addition of Mg^{2+}, Ca^{2+}, or Sr2+. (B) Unitary current amplitude vs. voltage over a range of $[Mg^{2+}]$, $[Ca^{2+}]$, and $[Sr^{2+}]$ as indicated. Smooth curves are drawn for display only. (C) $K_{app}(V)$ vs. voltage for experiments with Mg^{2+}, Ca^{2+}, and Sr^{2+}. Fractional current (relative to amplitude without added divalent) was measured over a range of depolarized voltages and fitted with Hill equations to estimate $K_{app}(V)$. $K_{app}(V)$ vs. voltage relations values were fit with an equilibrium block model, $K_{app}(V) = K_{app}(0)*\exp^{(-z\delta VF/RT)}$, to estimate $K_{app}(0)$ and zδ. The similar zδ-values of ~0.45 e_0 for $[Mg^{2+}]_i$, $[Ca^{2+}]_i$, and $[Sr^{2+}]_i$ suggest that the fast blocking site for these ions is at the same location in the conduction pathway, whereas the estimated $K_{app}(0)$ values are consistent with a lower apparent affinity of Sr^{2+} and Ca^{2+} compared with Mg^{2+}.

2.5.2 Ca^{2+} and Sr^{2+}, but not Mg^{2+}, enhance gating into an inactivated state

In previous experiments, MthK channels activated by Ca^{2+} were found to spend increased time in a nonconducting or inactivated state with increasing depolarization (18, 23). However, with Cd^{2+} activation, entry into the inactivated state occurs at more depolarizing voltages compared with gating in the presence of Ca^{2+} (Fig. 2-9E).

Because Ca^{2+} both facilitates inactivation and leads to fast blockade of MthK, we wondered whether inactivation and fast blockade occur through Ca^{2+} binding at a single inactivation/ blocking site. If inactivation and fast blockade occur through a single site, then based on the observation that Mg^{2+} is a more potent fast blocker than Ca^{2+} (Fig. 2-13), one might predict that Mg^{2+} would facilitate inactivation even more potently than Ca^{2+}. To test this possibility, we measured *Po* in the presence of Mg^{2+} over a range of voltages (Fig. 2-10A, Left). In contrast to the effects of Ca^{2+}, we observe that inactivation was not enhanced with increasing [Mg^{2+}] over the range of 100 μM to 1 mM (Fig. 2-10B, Left). However, inactivation was enhanced with increasing [Sr^{2+}] (even more potently than Ca^{2+}) (Fig. 2-10B, Center and Right). Because increasing [Mg^{2+}] does not facilitate entry into the inactivated state as observed with Ca^{2+} and Sr^{2+}, these results indicate clearly that fast blockade on its own is not correlated with inactivation and that inactivation does not occur by divalent cations binding to the fast blocking site. The results further suggest that inactivation can occur at strongly depolarized voltages without the addition of either Ca^{2+} or Sr^{2+} (Fig. 2-10B, Left).

The observation that inactivation occurs in strongly depolarized MthK channels without added Ca^{2+} or Sr^{2+} (Fig. 2-10) suggests that inactivation does not correspond to discrete events of Ca^{2+} blockade (18, 23). However, it could also be argued that low levels of Ca^{2+} present in these solutions might lead to discrete events of Ca^{2+} blockade, which become more frequent at depolarized voltages. We tested this possibility in two ways. First, we performed experiments using recording solutions, in which contaminating divalents were first sequestered using Chelex-100 resin (details are provided in Methods 2.7.2). Briefly, the Chelex-100 resin is expected to reduce the low levels of contaminating Ca^{2+} in our 200 mM KCl-based solutions to <0.5 μM (24); after removal of the Chelex-100 resin by filtration, 100 μM $CdCl_2$ is added to the solution. Second, we performed experiments in bath solutions using KF substituted for KCl. Because CaF_2 forms a tight complex that is very poorly soluble in water (K_{sp} for CaF_2 = 3.5 × 10^{-11}), F^- greatly lowers free [Ca^{2+}] in these solutions, such that the effective free [Ca^{2+}] can be considered <20 nM; Cd^{2+}, however, does not form an insoluble complex with F^- (K_{sp} for CdF_2 = 6.4 × 10^{-3}) and is free to bind and activate the channel (25, 26).

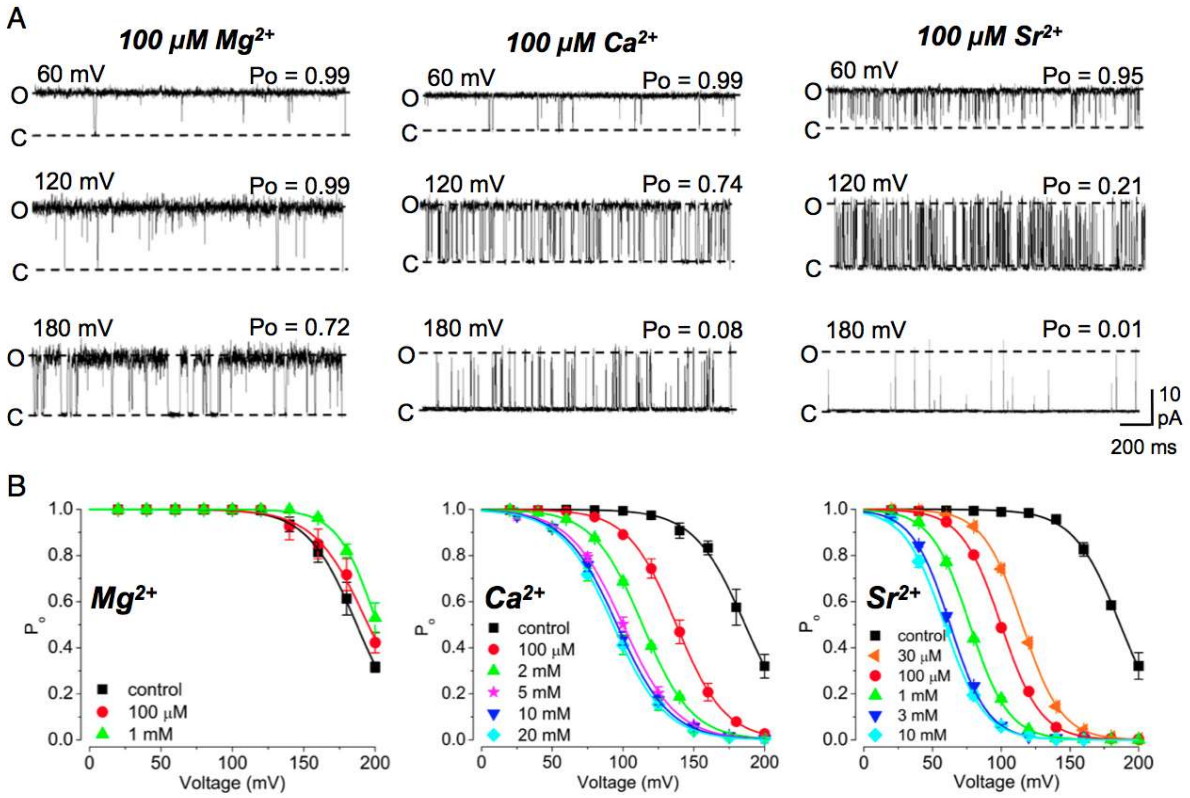

Fig. 2-3 **Effects of divalent ions on inactivation in MthK**

(A) Representative currents with 100 μM Mg^{2+}, Ca^{2+}, and Sr^{2+} over a range of voltages. Ca^{2+} and Sr^{2+} facilitate entry to an inactivated state at depolarized voltages. (B) Po vs. voltage in the presence of Mg^{2+}, Ca^{2+}, or Sr^{2+} at the indicated concentrations; curves represent fits with a Boltzmann equation. Increasing [Mg^{2+}] has nominal effects on *Po* compared with increasing [Ca^{2+}] or [Sr^{2+}], consistent with the idea that Ca^{2+} and Sr^{2+} enhance entry to an inactivated state by acting at a site that is inaccessible to Mg^{2+}.

We observed that channels entered the inactivated state in either the Chelex-100–treated 200 mM KCl solutions or KF-based solutions (Fig. 2-2A). In addition, we observed that, with nominal Ca^{2+}, KF-based solutions lowering [K^+] at the external side of the channel from 200 to 5 mM resulted in an ~70 mV leftward shift in the $V_{1/2}$ for steady-state inactivation ($V_{1/2}$ = 170 ± 2.1 mV with 200 mM K^+_{ext}; 96 ± 3.5 mV with 5 mM K^+_{ext}), which was observed previously in MthK channels using KCl-based solutions (18). Together, these results suggest that entry into the inactivated state arises from a gating mechanism that does not strictly require Ca^{2+} and responds to lowering external [K^+] similar to slow inactivation observed in Shaker Kv channels (3, 9).

To rule out the possibility that entry into the nonconducting, inactivated state arises from Cd^{2+}, we reasoned that if 100 μM Cd^{2+} promoted gating into the inactivated state, then reducing [Cd^{2+}] to 30 μM should lead to higher *Po* at 200 mV compared with that observed with 100 μM Cd^{2+}. In contrast, we observe that lowering the [Cd^{2+}] to 30 μM leads to overall lower *Po* compared with 100 μM Cd^{2+} (Fig. 2-2B). Together with the results obtained in nominally Ca^{2+}-free solutions, these experiments suggest that gating in the inactivated state does not strictly arise from either Cd^{2+} or from levels of contaminant Ca^{2+}.

2.5.3 Molecular simulations at 0 mV suggest the locations of ion binding sites in the pore

We next sought to determine why inactivation at depolarized voltages might be effectively enhanced by Ca^{2+} but immune to Mg^{2+}. To examine this mechanism further, we performed atomistic simulations of the MthK pore containing two K^+ ions at defined positions in the selectivity filter (either S_1 and S_3 or S_2 and S_4) and a cation (K^+, Mg^{2+}, or Ca^{2+}) initially in the cavity of the pore. The free energies of each ion at positions along the length of the cavity were estimated through calculation of the PMF; thus, the positions of energy minima (i.e., wells) would correspond to potential binding pockets for ions, and energy maxima correspond to barriers impeding ion access.

Initially, we performed simulations with a transmembrane voltage of 0 mV, reasoning that these simulations should reveal the positions of energy wells and barriers attributable to interactions between the channel protein, ions, and water, whereas additional experiments (see below) might further reveal effects of depolarizing voltage on free energy profiles. In simulations at 0 mV with K^+ ions in the S_1-S_3 positions, an additional K^+ ion in the cavity can occupy one of two largely overlapping energy wells that correspond to two microscopically adjacent sites on either side of the threshold of the selectivity filter (Fig. 4 A and B, solid curve). At one site, termed S_5 (located at approximately z = −7.5 Å), a partially hydrated K^+ ion is coordinated by the oxygen atoms from the side chain hydroxyl groups of T59 (in each subunit); this Thr residue forms part of the highly conserved K^+ channel signature sequence (TVGYG) (27). The adjacent energy well, appearing as a shoulder to the right of the S_5 energy well, is located at the S_4 site within the selectivity filter (approximately z = −5.5 Å). The relatively small (1–2 kcal/mol) energy barrier for K^+ movement from S_5 to S_4 under these conditions is consistent with a permeation mechanism in which a K^+ ion moves from the cavity region to S_4, where it may subsequently drive outward movement of K^+ ions at S_3 and S_1, similar to the knock-on permeation mechanism suggested for the K^+ channel KcsA (28, 29). In contrast, with K^+ ions in the S_2-S_4 positions (Fig. 2-5B, dashed curve), a K^+ ion in the cavity occupies no substantial energy well and encounters a steep energy barrier impeding access to the S_5 site. This result implies that the S_2-S_4 K^+ ions can destabilize ion binding in the MthK cavity and are obliged to translocate (i.e., to S_1-S_3) as a new ion approaches the selectivity filter.

In contrast to K^+, Mg^{2+} can occupy an energy well within the cavity of the pore (z = −10 Å), termed S_{cav}, and encounters a strong energy barrier (>10 kcal/mol) impeding its movement to the S_5 position, with K^+ ions at S_1-S_3 (Fig. 2-5C, solid green curve). With K^+ ions at S_2-S_4, Mg^{2+} encounters a steep energy barrier, impeding its approach to either S_{cav} or S_5. These observations are consistent with the idea that, when in the cavity, Mg^{2+} interacts with K^+ ions in the selectivity filter but is unlikely to either occupy a binding site at S_5 or enter the filter. In contrast, a Ca^{2+} ion can occupy the energy well corresponding to S_{cav} and could also potentially move beyond S_{cav} to the S_5 position, encountering a moderate energy barrier of ~4 kcal/mol under the conditions of this simulation, with K^+ ions in S_1-S_3 (Fig. 2-5D).

Because both Ca^{2+} and Mg^{2+} can produce a fast blockade of outward K^+ current (i.e., reduced conductance) that displays a relatively weak voltage dependence (Fig. 2-13), these simulations seem consistent with the idea that the S_{cav} site, which corresponds to an energy well common to both Ca^{2+} and Mg^{2+}, underlies fast blockade (Discussion, chapter 2.6). However, movement to the S_5 site seems possible for Ca^{2+} but not Mg^{2+}. This difference may begin to explain the differential effects of Ca^{2+} vs. Mg^{2+} on entry to the inactivated state.

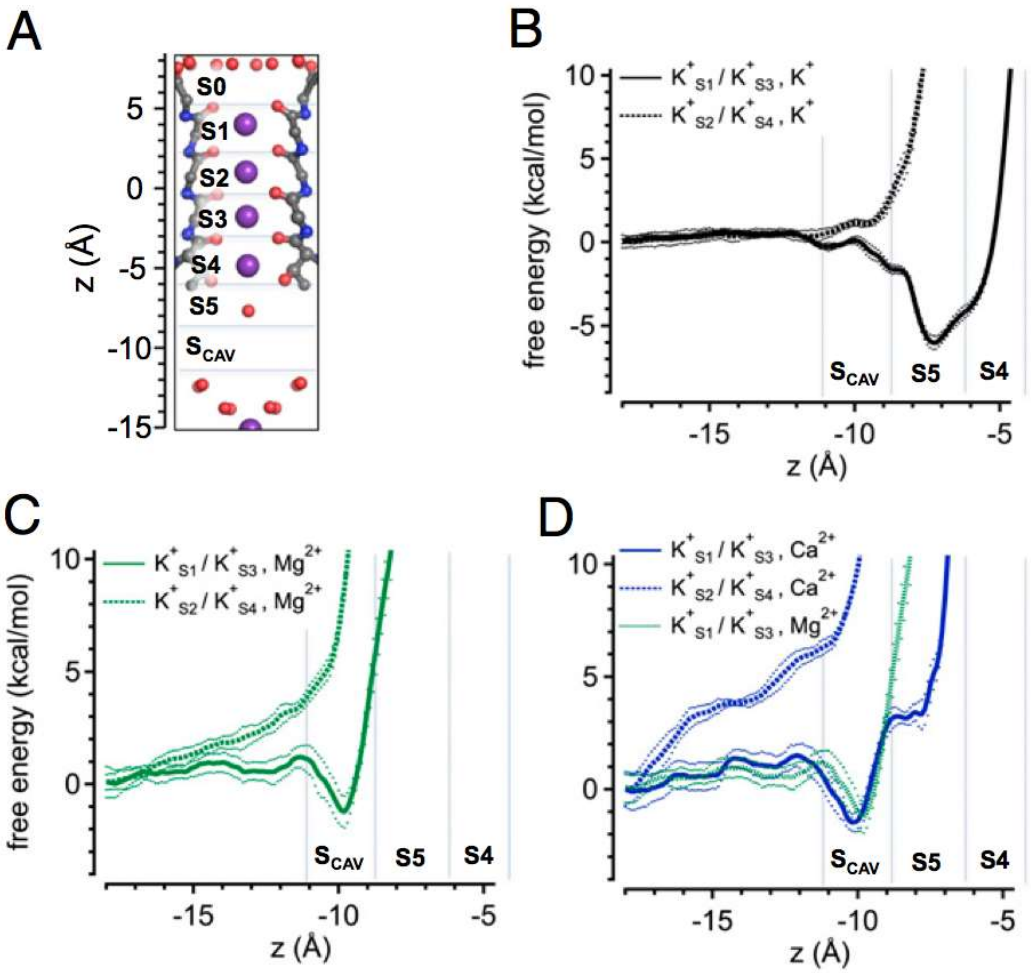

Fig. 2-4 **Free energies of ions in the MthK pore based on PMF calculations**

(A) Structure of the MthK selectivity filter (PDB ID code 3LDC) with potential ion binding sites S_0–S_{cav} indicated. The axis at the left indicates distance (z) relative to the center of mass of the selectivity filter. (B–D) Free energies for K^+, Mg^{2+}, and Ca^{2+} ions in the cavity region, respectively, plotted as a function of ion position along the central axis of the pore. Vertical dashed lines indicate approximate boundaries of potential ion binding sites. Simulations were performed with K^+ ions at S_1 and S_3 (solid curves) or S_2 and S_4 (dashed curves) at 0 mV. These results suggest that either Mg^{2+} or Ca^{2+} can occupy an energy well near −10 Å (S_{cav}), whereas Ca^{2+} may further access the S_5 position (near −7.5 Å) at the entrance to the filter. Dotted curves indicate ± SD (Methods chapter 2.7.4).

2.5.4 Voltage-driven outward movement of K^+ ions can stabilize Ca^{2+} binding at the threshold of the selectivity filter

The PMF calculations in Fig. 2-5 illustrate the free energies of Mg^{2+} and Ca^{2+} ions with K^+ ions at fixed positions in the filter. To further explore the energetic relations among these ion configurations, we performed 2D PMF calculations, which provide information on the energy landscape as a function of K^+ and divalent ion locations along the pore axis. In the 2D PMF contour plots (Fig. 2-6), the combined reaction coordinate z_{12} represents the positions of K^+ ions in the filter (calculated as the center of mass of pairs of K^+ ions relative to the center of mass of the selectivity filter backbone) (29), and z_3 represents the position of the Ca^{2+} or Mg^{2+} ion as indicated.

Fig. 2-6A indicates that, at 0 mV, Mg^{2+} (Fig. 2-6A, Left) does not occupy an energy well beyond z = −10 Å (corresponding to the S_{cav} position in Fig. 2-5A) and that occupancy of Mg^{2+} at the S_{cav} position leads to relative stabilization of K^+ ions centered on the S_1-S_3 positions (z_{12} = 1.5 Å) (indicated by *a* in Fig. 2-6A), with an additional, shallow energy well centered on the S_0-S_2 position (z_{12} = 3.5 Å) (indicated by *b* in Fig. 2-6A). In contrast, Ca^{2+} (Fig. 2-6A, Right) occupies a clearly defined energy well at z_3 = −7.5 Å, corresponding to the S_5 position with K^+ ions to the external end of the selectivity filter (z_{12} = 3.5 Å) (indicated by *b** in Fig. 2-6A, right). The PMF shows that the movement of Ca^{2+} from the S_{cav} to the S_5 position is most favorable after outward movement of K^+ ions. This idea is indicated by the relatively low energy pathway from *a* to *b* to *b** compared with a direct pathway from *a* to *b** without entering *b*.

Entry into the inactivated state in MthK is favored by depolarization (Fig. 2-10) (18, 23). To determine the impact of depolarization on movement of Mg^{2+}, Ca^{2+}, and K^+ in MthK, we performed additional 2D PMF calculations with a transmembrane voltage of 500 mV (Fig. 2-6B). Although this voltage is stronger than the depolarization typically applied in our electrophysiological experiments, our goal here was to identify the relative impact of voltage on energy wells corresponding to ion binding sites in the pore. In the presence of Mg^{2+}, depolarization drove K^+ ions to the extracellular end of the selectivity (on average), resulting in deeper energy well at position *b* relative to *a*, although movement of Mg^{2+} beyond the S_{cav} position was essentially unaffected. In contrast, depolarization resulted in outward displacement of K^+ ions with Ca^{2+} at either S_{cav} or S_5 (at positions *b* and *b**) and seemed to permit slight stabilization of Ca^{2+} at the S_5 position with K^+ ions centered on the S_1-S_3 positions (position *a**). However, the lowest energy pathway of a to *b* to *b** persists even with stronger depolarization, relative to the pathway of *a* to *a** to *b**. This result suggests that, in terms of MthK inactivation, the predominant effect of voltage is to drive K^+ outward. This outward K^+ movement is permissive for binding of Ca^{2+} at the S_5 position, which in turn, could attenuate access of K^+ from the cytoplasmic end of the pore and prevent replenishing of the pore with K^+.

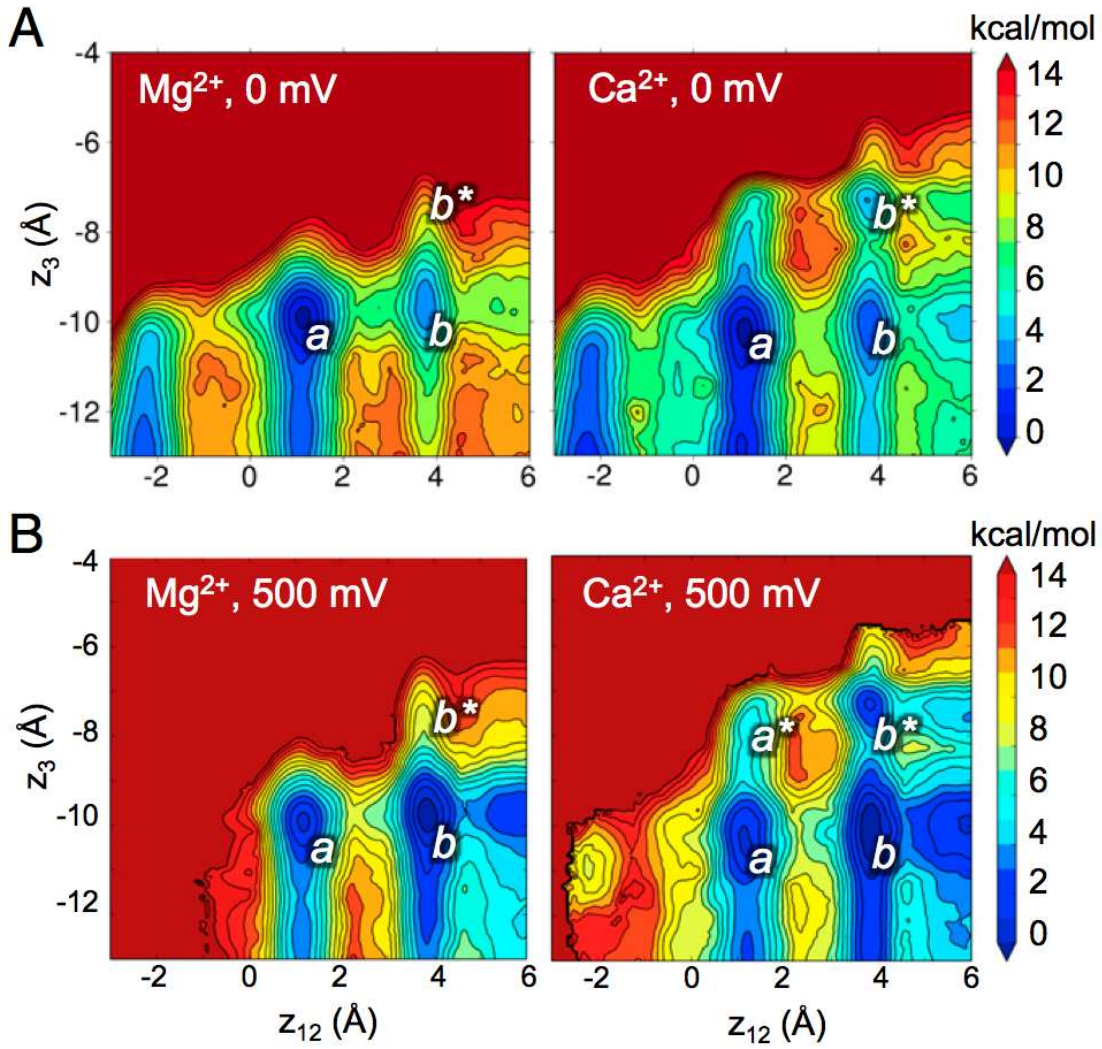

Fig. 2-5 **Energetic relations among ion binding configurations in the MthK pore**

(A) Free energy of ion configurations as a function of K^+ ion positions (z_{12}) and Ca^{2+} or Mg^{2+} (z_3) from simulations performed at 0 mV. Ca^{2+}, but not Mg^{2+}, occupies an energy well located at S_5 (z_3 = −7.5 Å; indicated by *b**), with K^+ ions driven to the extracellular end of the selectivity filter (z_{12} = 3.5 Å). Colors correspond to free energies (in kilocalories per mol) as indicated in the scale bar on the right. (B) Free energy of ion configurations from simulations performed with 500 mV depolarizing voltage. Depolarization drives K^+ ions to the extracellular end of the filter (z_{12} = 3.5 Å) and permits Ca^{2+} to bind more stably at S_5. In A and B, z_{12} corresponds to the center of mass of pairs of K^+ ions in the filter relative to the center of mass of the selectivity filter; z_3 represents the position of the Ca^{2+} or Mg^{2+} ion (as indicated) relative to the center of mass of the selectivity filter.

To further illustrate the impact of K^+, Mg^{2+}, and Ca^{2+} on the distribution of K^+ ions in the selectivity filter, we performed additional simulations by restraining these ions within their respective energy wells in the MthK pore (K^+ and Ca^{2+} in S_5 and Mg^{2+} in S_{cav} at 0 mV) (Fig. 2-11). We observe that occupancy of Mg^{2+} at the S_{cav} position leads to likely stabilization of K^+ ions centered on the S_1-S_3 positions (z_{12} = 1.5 Å), with additional shallow energy wells

centered on the S_2-S_4 and S_0-S_2 positions (z_{12} = −2 and 3.5 Å, respectively) (Fig. 2-11, green line). In contrast, a K^+ ion at S_5 leads to a bias of ions within the filter to the extracellular end, which is indicated by a shallower energy well at z_{12} = −2 Å (by ~4 kcal/mol) and a slightly deeper energy well at z_{12} = 3.5 Å (−2 kcal/mol compared with Mg^{2+}) (Fig. 2-11, black line). A Ca^{2+} ion at S_5, in turn, leads to an even stronger bias to the extracellular end, with the energy well at z_{12} = −2 Å replaced by an energy barrier of >10 kcal/mol, and an even deeper energy well at z_{12} = 3.5 Å (−6 kcal/mol compared with Mg^{2+}) (Fig. 2-11, blue line). Thus, both K^+ and Ca^{2+} have the effect of stabilizing K^+ ions to the extracellular end of the selectivity filter. However, whereas a K^+ ion can move beyond S_5 to drive K^+ permeation to the extracellular side, a Ca^{2+} ion is unlikely to move beyond S_5 deeper into the selectivity filter. Thus, Ca^{2+} occupancy at S_5 favors the outward movement of K^+, preceding its own dissociation from S_5 to the cytoplasmic side of the channel.

2.5.5 Geometry of the S_5 site favors access by Ca^{2+} over Mg^{2+}

To further understand the basis for selection of Ca^{2+} over Mg^{2+} at the S_5 site and coordination of these ions in the MthK pore, we quantified the number of oxygen ligands provided by water and protein atoms in our simulations as a function of Mg^{2+} or Ca^{2+} position in the pore. The results illustrate that Mg^{2+} remains hydrated with six water molecules while it resides in the pore and in contrast, that Ca^{2+} is hydrated with a maximum of seven water molecules at more shallow positions in the pore ($z < -10$ Å) and progressively dehydrates, exchanging three to four water molecules for protein oxygen atoms as it moves to the S_5 position (Fig. 2-4A).

Hydration and coordination of Mg^{2+} and Ca^{2+} near the selectivity filter are illustrated in a series of snapshots from our simulations (Fig. 2-4B). An Mg^{2+} ion at the S_{cav} position is fully hydrated by six water molecules (Fig. 2-4B, a and b). When an Mg^{2+} ion reaches the S_5 position, it is energetically very unfavorable for the ion to exchange its hydration shell waters for protein oxygen atoms, and occupancy of S_5 by the fully hydrated ion leads to distortion of the protein structure (Fig. 2-4B, c). In contrast, Ca^{2+} can shed up to three hydration shell water molecules as it moves from S_{cav} to S_5 (Fig. 2-4B, d–f) with a relatively small net energetic cost (the energetics corresponding to these ion configurations are illustrated in Fig. 2-5C, solid curve and D, solid curve). Together, these results suggest that Ca^{2+} likely gains access to the S_5 site owing to the favorable energetics of exchanging hydration shell water molecules in the context of the geometry of the S_5 site.

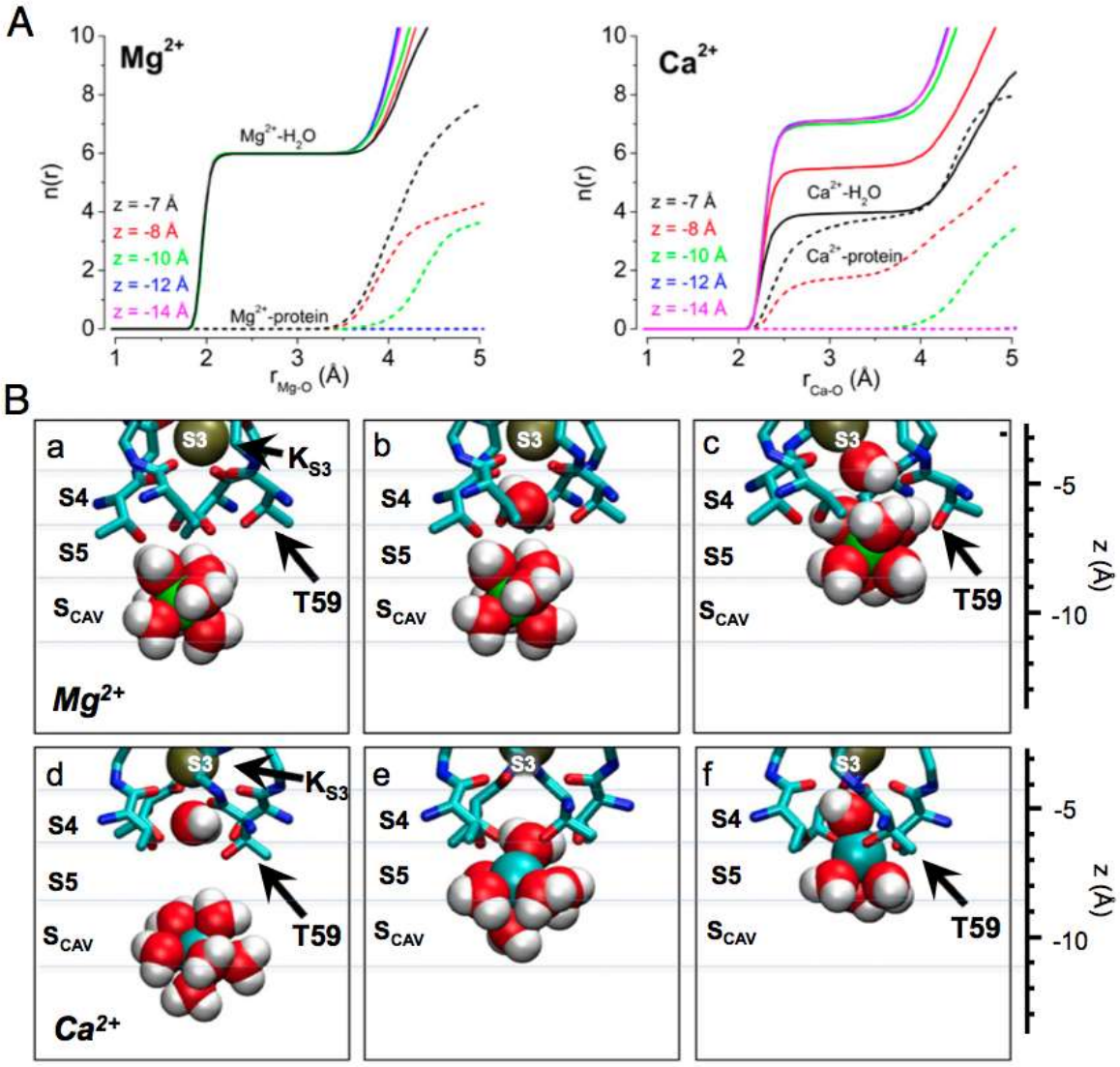

Fig. 2-6. **Structural basis for Ca^{2+} access and binding at the S_5 site**

(A) Number of oxygen atoms within radius *r* [*n*(*r*)] of (Left) Mg^{2+} and (Right) Ca^{2+}; *n*(*r*) is shown separately for water and protein oxygen (solid and dashed lines, respectively), and each curve represents the relative position of the ion along the central axis of the MthK pore (z). These data show that Mg^{2+} remains hydrated with up to six water molecules at these positions in the MthK pore (coordination distance between 2 and 3.5 Å), whereas Ca^{2+} can exchange three to four water molecules for protein oxygen as it approaches the S_5 site (z between −7 and −8 Å). (B) Representative snapshots from MthK pore simulations with (a–c) Mg^{2+} (green spheres) and (d–f) Ca^{2+} (cyan spheres) with nearby water molecules (red spheres, oxygen; white spheres, hydrogen) and selectivity filter atoms (shown as sticks with side chain of Thr-59 indicated by black arrows). These snapshots illustrate that the energy barrier impeding Mg^{2+} access to S_5 arises primarily from its strong interaction with hydration shell water molecules, which leads to overall steric hindrance by selectivity filter atoms (c), whereas Ca^{2+} exchanges its hydration shell water molecules in favor of the hydroxyl side chains of T59 (f).

2.5.6 Ion dissociation from the selectivity filter favors a conformational change that can break the permeation cycle

Our electrophysiological and in-silico results are consistent with the idea that Ca^{2+} can access the S_5 site at the threshold of the selectivity filter, where it drives K^+ ions to the extracellular side to potentially dissociate into the bulk extracellular solution (Fig. 2-10, Fig. 2-5, Fig. 2-6). In addition, transitions to the inactivated state are facilitated by strong depolarization in the nominal absence of Ca^{2+} as well as lowered external [K^+] (Fig. 2-2) (5, 6, 18). To determine the possible relation between ion movements and entry into the inactivated state, we analyzed the structure of the selectivity filter during simulations in different ionic conditions. We reasoned that conditions that mimic those conditions that favor inactivation could reveal structural changes that underlie interruptions in K^+ conduction or increased barriers to permeation.

In simulations initiated with K^+ ions at the S_2 and S_4 positions in the selectivity filter and 150 mM K^+ in the bulk solution, we observe that dihedral (Φ) angles for filter residues remain stable about their canonical positions (Fig. 2-4A). This result is not unexpected; in electrophysiological experiments with MthK in the presence of 200 mM external K^+, no apparent inactivation is observed without strong depolarization (Fig. 2-10) (18). Interestingly, in these simulations, a K^+ ion from the bulk external solution is observed to stably occupy a site at the external mouth of the selectivity filter, termed S_0 (29). Because lowering external [K^+] facilitates entry to the inactivated state, we designed additional simulations to mimic these electrophysiological experiments (termed 0 K^+_{bulk}) (Methods). The results (Fig. 2-7B) suggest that, under conditions in which the K^+ ion at the S_0 position rapidly dissociates to the external bulk solution, the peptide linkage between residues Val-60 and Gly-61 in one of four subunits is observed to rearrange between its canonical position and an alternative inverted (rotated) position (Fig. 2-7C). Histograms of Φ-angles determined from these simulations indicate a rotation of around 110° for the Φ-angle of Gly-61, corresponding to a rotation of the carbonyl oxygen of Val-60 away from the central axis of the selectivity filter. This distorted selectivity filter conformation, which was previously observed in simulations of the KcsA K^+ channel, is known to underlie a nonconducting state of the filter (30). Thus, dissociation of a K^+ ion from the extracellular end of the MthK selectivity filter is correlated with a conformational change in the filter that underlies a nonconducting state. Rotation of the Val-60 carbonyl oxygen is also observed in simulations with K^+ ions initially at the S_1 and S_3 sites (Fig. 2-12). The relation between the Val-60 carbonyl rotation and dissociation of ion from the selectivity filter led us to hypothesize that the canonical state of the selectivity filter is favored in conditions where three ions are associated with the selectivity filter, whereas the energy barrier preventing

carbonyl rotation is reduced in conditions where two ions are associated with the filter. Three-ion states correspond to the simulations in Fig. 2-7A (S_0-S_2-S_4) and Fig. 2-12A (S_1-S_3-S_5); two-ion states are reached in simulations using the 0 K^+_{bulk} constraint (Fig. 2-7B and Fig. 2-12B) and could be reached in electrophysiological experiments with low external [K^+] (Fig. 2-2A).

To determine the impact of ion occupancy on the energetics of Val-60 carbonyl rotation, we performed PMF calculations of the Φ-angle with the filter in three-(K^+_{S0} ; K^+_{S2} ; and Ca^{2+}_{S5}) or two-ion states (K^+_{S2} and Ca^{2+}_{S5} or K^+_{S3} and Ca^{2+}_{S5}). Fig. 2-1A illustrates that, in the three-ion state, the canonical state ($\Phi_{Gly\text{-}61} \sim 45°$) is favored by >5 kcal/mol over the rotated state ($\Phi_{Gly\text{-}61} \sim -75°$) and strongly favored by >10 kcal/mol over any additional rotations. In contrast, Fig. 2-1B shows that dissociation of K^+ from S_0 resulting in the two-ion state K^+_{S2}/Ca^{2+}_{S5} can potentially lower the energy barrier for rotation (by ~2 kcal/mol), and in the two-ion state, K^+_{S3}/Ca^{2+}_{S5} (Fig. 2-1C), the canonical and rotated states are effectively equivalent in terms of free energy. Potential impacts of K^+ ion dissociation on selectivity filter structure are further illustrated through plots of ion position and selectivity filter Φ-angles as a function of time in Fig. 2-3.

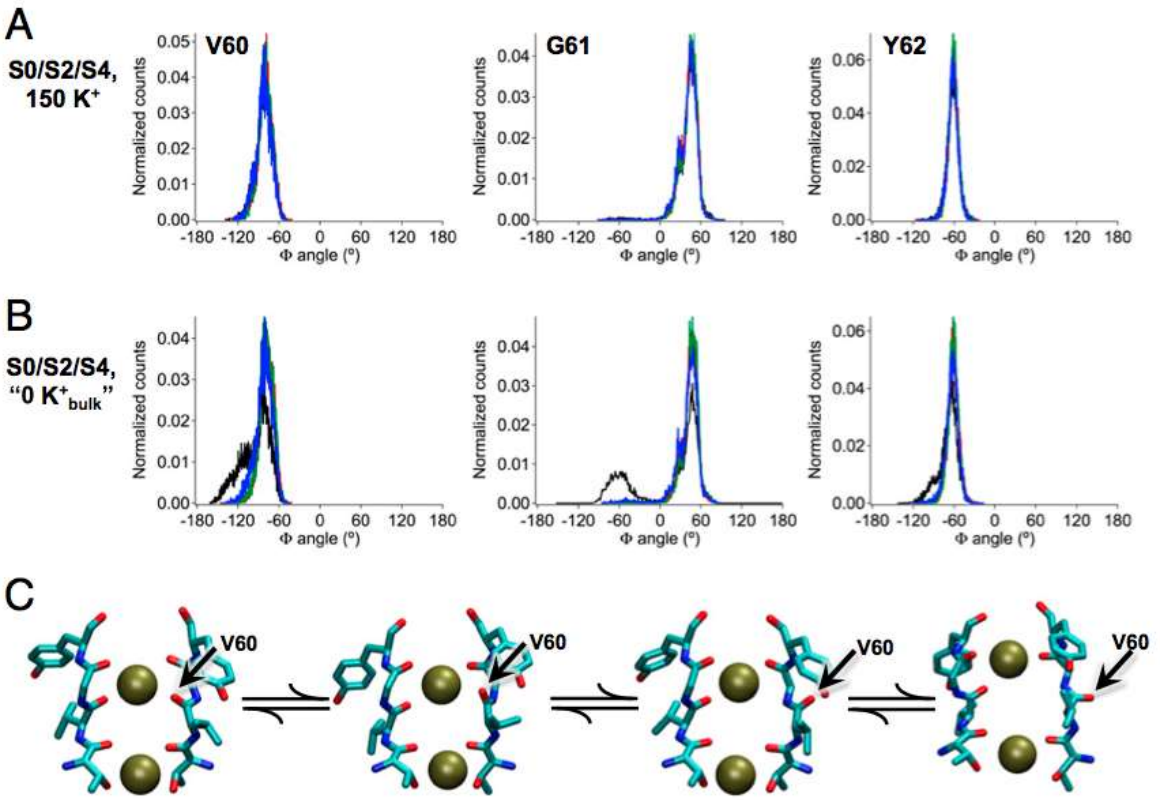

Fig. 2-7 **K^+ dissociation facilitates a conformational change in the MthK selectivity filter**

(A) Histograms of Φ-angles for the indicated residue sampled during molecular simulations. Each channel subunit is represented by a different color (black, red, green, and blue). With K^+ occupying the S_0-S_2-S_4 positions, all carbonyl oxygen atoms face the central axis of the pore (in canonical positions) over the entire simulation. Thus, the Φ-angles for each residue are centered around single peaks. (B) With K^+ ions initially occupying the S_0-S_2-S_4 positions but a force applied to repel binding of K^+ ions coming from the bulk (0 K^+_{bulk}) (Methods), the S_0 K^+ ion dissociates from the channel, and a conformational change occurs, leading primarily to a 110° rotation of the Val-60 carbonyl oxygen in one of four subunits (black). Thus, for one of the subunits, the Φ-angles determining the position of the Val-60 carbonyl oxygen and its adjacent residues are distributed bimodally, with one peak corresponding to the canonical position and one peak corresponding to the rotated (flipped) position (black lines). (C) Series of selectivity filter snapshots from simulations illustrating rotation of the Val-60 backbone carbonyl (indicated by arrows). Selectivity filter segments from two of four subunits are shown side by side, with K^+ ions at S_2 and S_4 shown as dark green spheres.

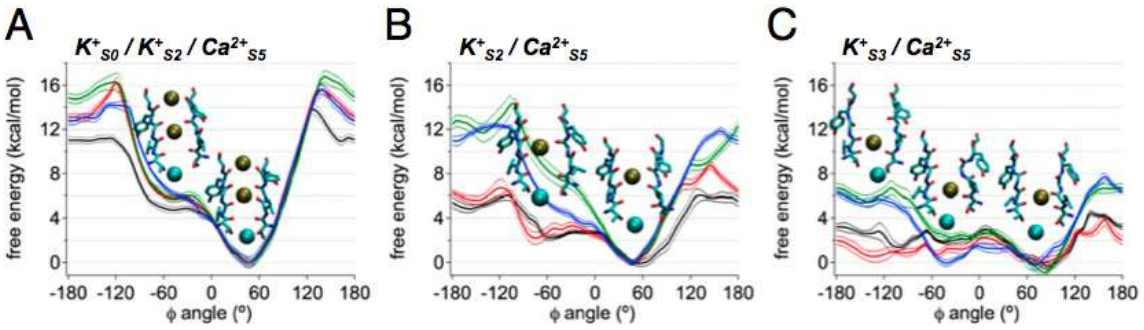

Fig. 2-8. **Free energy of a conformational change in the MthK selectivity filter with different ion configurations**

Free energy plotted as a function of the Φ-angle of Gly-61. Each curve is determined for a single MthK subunit in four independent simulations, in which three of four subunits in the pore are constrained to have the canonical Gly-61 Φ-angle (45°). Curves are shown as means ± SDs. (A) In the three-ion state, K^+_{S0}-K^+_{S2}-Ca^{2+}_{S5}, an energy barrier of ~5 kcal/mol hinders rotation of the Val-60 carbonyl much beyond the canonical position. This energy barrier is attenuated in the two-ion states (B) K^+_{S3}-Ca^{2+}_{S5} and (C) K^+_{S3} -Ca^{2+}_{S5}.

2.6 Discussion

Inactivation in MthK displays properties in common with C-type inactivation in Kv channels, notably modulation by external [K^+] and other permeant ions (3, 5, 6, 18). In Kv channels, impermeant ions, such as quaternary ammonium derivatives, as well as the poorly permeant ion Cs^+ applied to the cytoplasmic side of the channel were found to increase the rate of inactivation. This observation is consistent with a mechanism in which dissociation of K^+, coupled with impeded refilling of the pore, facilitates subsequent inactivation (5, 6). Although the energetics of pore blockade by divalent cations have been described using empirical models, in which the charged blocking ion competes with permeant K^+ (31, 32), the structural bases of interactions between specific blocking ions and the pores of K^+ channels have not been well-understood.

Whereas the MthK channel can apparently accommodate up to three K^+ ions in the vicinity of its selectivity filter (at positions S_0-S_2-S_4 or S_1-S_3-S_5), strong depolarization and low external [K^+] can contribute to outward movement of K^+ ions and limit rebinding of K^+ from the external side of the selectivity filter, respectively (Fig. 2-10, Fig. 2-5, Fig. 2-6 and Fig. 2-2) (18). This K^+ dissociation can result in a state with only two ions in the vicinity of the selectivity filter. We observe that this configuration is permissive for rotation of a filter lining carbonyl group (of Val-60) (Fig. 2-7 and Fig. 2-1), which in turn, can raise an energy barrier to prevent K^+ permeation (28–30). Our electrophysiological and computational results are consistent with a working hypothesis, in which Ca^{2+} (but not Mg^{2+}), by preventing refilling of the pore with K^+, can stabilize ion configurations in the selectivity filter that favor transitions to a nonconducting, inactivated state (Fig. 2-8).

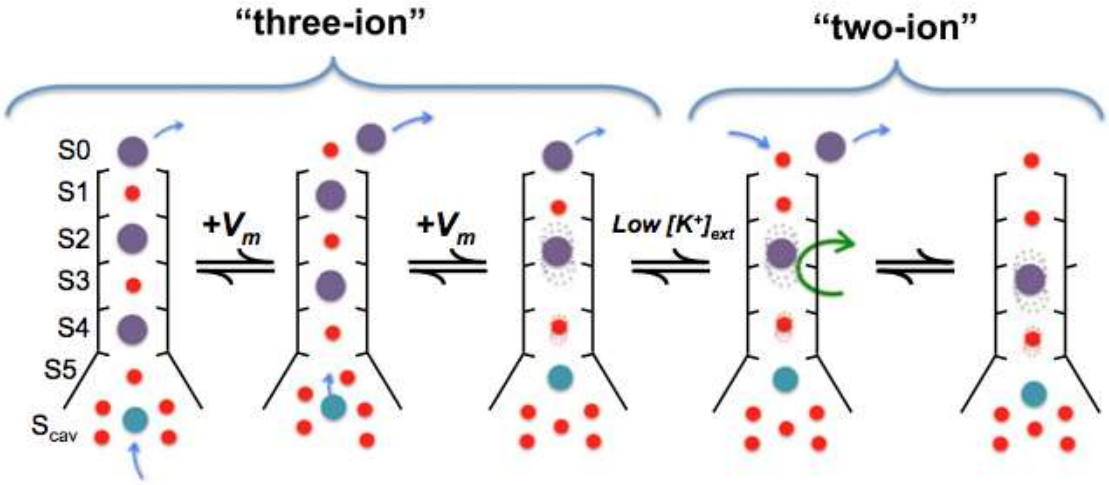

Fig. 2-9 **Working hypothesis of initial steps in MthK inactivation**

Schematic diagram of the MthK selectivity filter in a series of different ion occupancy states. From the state (far left) with K^+ ions occupying the S_0-S_2-S_4 positions (purple spheres), one Ca^{2+} (cyan sphere) occupies the S_{cav} position. Depolarization drives the K^+ ions outward in register as Ca^{2+} moves to the S_5 position. Lowered extracellular [K^+] drives the filter from the three-ion states to the two-ion states by lowering the probability of K^+ rebinding after its dissociation from S_0. In the final step (far right), carbonyl rotation occurs (indicated by the green arrow), leading to inactivation.

The distinct effects of Ca^{2+} and Mg^{2+} on MthK inactivation can be mainly attributed to differences in the interactions of these ions with their hydration shell water molecules. Ca^{2+}, which has a larger atomic radius than Mg^{2+} but identical charge, exchanges waters of hydration in favor of protein oxygen more readily than Mg^{2+} (33). It is the partial dehydration of Ca^{2+} that permits its access to the S_5 position, which in turn, impacts selectivity filter occupancy. Computational studies estimate the ion–water lifetime correlation function for Ca^{2+}-first hydration shell waters to be 18 ps, indicating an exchange rate ~10 times faster than that of Mg^{2+} (228 ps) (34). This slow exchange rate in the case of Mg^{2+} contributes to the high free energy barrier preventing binding to S_5. It is worth noting that divalent ions might induce important polarization of their ligands, which is likely not well-captured by classical force fields as used in our simulations (35). Nevertheless, we believe the calculated binding free energy difference between Ca^{2+} and Mg^{2+} remains meaningful, notably because the ions here interact mainly with water molecules (and the chemically similar hydroxyl group of threonine side chains), for which the polarization effects are implicitly included, at least partially, as ions were parameterized to reproduce properties in solution (36).

Crystallographic, electrophysiological, and in-silico studies of inactivation in the KcsA K^+ channel underscore the importance of pore helix side chains in the inactivation process (37–40). Specifically, hydrogen bond interactions involving the Glu-71 and Asp-80 side chains in KcsA provide a substantial driving force to promote inactivation, although other

factors are likely to contribute. Interestingly, whereas Glu-71 seems to be critical for inactivation in KcsA, the acidic side chain at this position is not highly conserved among other inactivating K^+ channels, including either Shaker or MthK. In its place, both Shaker and MthK contain Val (Val-55 in MthK and Val-438 in Shaker), which has a branched hydrophobic side chain that cannot form hydrogen bonds. Therefore, although Glu-71 clearly facilitates and stabilizes the inactivated state in KcsA, a model to account for C-type inactivation as observed in Shaker would need to incorporate additional or alternative driving forces. These driving forces might include the ion effects addressed above.

Both fast blockade and inactivation of MthK display voltage dependence, which must arise from movement of charged particles across the transmembrane electric field (Fig. 2-13 and Fig. 2-10). If fast blockade arises from a divalent ion (Mg^{2+} or Ca^{2+}) reaching the S_{cav} site, which appears to be substantially outside of the transmembrane electric field (41), then the observed zδ-value of ~0.42–0.45 e_0 observed with fast blockade by Mg^{2+}, Ca^{2+}, or Sr^{2+} must arise primarily from coupling between the movement of a divalent ion to the S_{cav} site with either net movement of one K^+ ion nearly halfway through the selectivity filter (e.g., from S_{cav} to S_3) or more likely, movement of two K^+ ions some shorter distance through the filter (e.g., from S_4-S_2 to S_3-S_1) (42, 43). These hypothetical coupled divalent/K^+ movements are consistent with the interactions between Mg^{2+} and K^+ in our PMF calculations (Fig. 2-5 and Fig. 2-6). Similarly, steady-state inactivation of MthK in either the presence or the nominal absence of Ca^{2+} or Sr^{2+} can be described by a Boltzmann equation with a zδ-value of ~1.3 e_0 (Fig. 2-10) (18, 23). Because the electrical distance between S_{cav} and S_5 also appears to be relatively small, then the voltage dependence of inactivation must, similarly, arise primarily from net movement of at least two K^+ ions through two positions in the selectivity filter (e.g., from S_4-S_2 to S_2-S_0). These hypothetical Ca^{2+}/K^+ movements are consistent with the interactions between Ca^{2+} and K^+ that were suggested in our PMF calculations (Fig. 2-5 and Fig. 2-6).

Although our results suggest that the coupling of ion movements within the pore and dissociation of K^+ within the selectivity filter of MthK are linked to changes in filter conformation, C-type inactivation is likely to be a complex process that is controlled by many chemical driving forces, including interactions among side chains that determine selectivity filter structure (30, 37, 38, 44). Clearly, a complete understanding of inactivation and other forms of gating at the K^+ channel selectivity filter will require additional determination of energetic relationships among these processes.

2.7 Methods

2.7.1 Channel purification and reconstitution

MthK was expressed, purified, and reconstituted into proteoliposomes as described previously (15, 17). Proteoliposomes were composed of *Escherichia coli* lipids (Avanti) that were rapidly frozen in liquid N_2 and stored at −80 °C until use. Protein concentrations in proteoliposomes ranged from 5 to 25 μg protein/mg lipid.

2.7.2 Electrophysiology

Recordings were obtained using planar lipid bilayers of 1- palmitoyl-2-oleoyl-sn-glycero-3-phosphoethanolamine:1-palmitoyl-2-oleoyl-sn-glycero-3-phospho-(1′-rac-glycerol) (POPE: POPG) (3:1) in a horizontal bilayer chamber. Unless otherwise specified, solution in the cis (top) chamber contained 200 mM KCl and 10 mM Hepes (pH 7.0). Solution in the trans (bottom) chamber contained 200 mM KCl, 10 mM Hepes (pH 8.1), 100 μM $Cd2^{+}$, and the specified concentration of different divalent cations. Within each bilayer, multiple solution changes were performed using a gravity-fed perfusion system. To ensure completeness of solution changes, the trans chamber was washed with a minimum of 10 mL (~10 chamber volumes) solution before recording under a given set of conditions.

Single channel currents were amplified using a Dagan PC-ONE patch clamp amplifier with low-pass filtering to give a final effective filtering of 333 Hz (dead time of 0.538 ms) and sampled by computer at a rate of 50 kHz. Currents were analyzed by measuring durations of channel openings and closings at each current level by 50% threshold analysis using pClamp 9.2. These measurements were used to calculate *NPo* as

$$NPo = \sum_{i=1}^{n} iPi \qquad [1]$$

in which *i* is the open level and *Pi* is probability of opening at that level. The mean single channel open probability (*Po*) is obtained by dividing *NPo* by *N*, which is the number of channels in the bilayer, determined by recording under conditions where the maximum level of channel opening can be observed. The voltage dependence of *Po* was described by the Boltzmann equation,

$$Po = Po\max / \left(1 + \exp\left(z\delta\left(V - V_{1/2}\right)/k_B T\right)\right) \qquad [2]$$

in which *Po*max is the maximal *Po*, zδ is the effective gating valence (in units of electronic charge, e_0), $V_{1/2}$ is the voltage at half-maximal *Po*, k_B is Boltzmann constant, and *T* is temperature. For data where *Po* at a given voltage was described as a function of divalent cation concentration (like with Ca^{2+} and Cd^{2+} in Fig. 2-9D), data were fitted with a Hill equation,

$$Po = Po\max / \left(1 + \left(EC_{50}/[\mathrm{X}^{2+}]\right)\right)^{\eta_H} \qquad [3]$$

in which $[X^{2+}]$ is the divalent cation concentration, EC_{50} is the $[X^{2+}]$ required to reach half-maximal *Po*, and n_H is the fitted Hill coefficient. Single channel current amplitudes were quantified by plotting all-points histograms of current levels for a given voltage and subtracting the mean closed level from the mean open level. Fast blockade of unitary current was quantified by first estimating the divalent ion concentration (i.e., Mg^{2+}, Ca^{2+}, or Sr^{2+}) yielding 50% current at several voltages, using

$$Po = Po\max/(1+(EC_{50}/[X^{2+}]))^{\eta_H} \quad [4]$$

in which [B] is the divalent (blocker) concentration, K_{app} is the blocker concentration required to reduce the unitary current to 50% of its amplitude in absence of blocker (at a given voltage), and I/I_0 is the fractional unitary current amplitude. Estimated K_{app} values at each voltage were used to estimate K_{app} at 0 mV and the voltage dependence (zδ) of K_{app} by fitting with the Woodhull equilibrium blockade model (22):

$$I/I_0 = 1/(1+(K_{app}/[B])) \quad [5]$$

in which *V* is the transmembrane voltage, *F* is Faraday's constant, *R* is the gas constant, and *T* is absolute temperature. Data points (e.g., *Po* and mean interval durations) are presented as means ± SEMs of three to five obser- vations for each data point, and collectively, they represent data from a total of 48 different bilayers.

2.7.3 Molecular dynamics simulations

Molecular dynamics simulations were performed using the MthK pore structure in high $[K^+]$ (Protein Data Bank ID code 3LDC) (13) using methods described previously (45). Briefly, molecular systems were assembled using the CHARMM-GUI web service (46) using a protocol developed by Woolf and Roux (47). The channel protein, with its symmetry axis aligned along the z axis, was embedded in a lipid bilayer of dipalmitoyl-phosphatidylcholine molecules. The number of ions in the bulk was adjusted to reproduce experimental ionic concentrations (150 mM KCl) and obtain electrical neutrality. The molecular system contained about 59,170 atoms total. All calculations were performed using the CHARMM software version c34 (48) using the all-atom potential energy function PARAM27 for protein and phospholipids and the TIP3P potential for water molecules (49, 50). Parameters for K^+, Ca^{2+}, and Mg^{2+} ions were as provided by PARAM27, with an additional NBFIX correction applied to K^+–carbonyl oxygen pair interactions (51). Periodic boundaries conditions were applied, and long-range electrostatic interactions were treated by the particle mesh Ewald algorithm (52). The molecular systems were equilibrated for about 300 ps with decreasing harmonic restraints applied to the protein atoms, the pore ions, and the water molecules localized in the P loop and the filter. All trajectories were generated with a time step of 2 fs at constant normal pressure (1 atm) controlled by an extended Lagrangian algorithm and constant temperature (323 K) using a Nosé–Hoover thermostat (53–55).

The 0 K^+_{bulk} condition (Fig. 2-7B and Fig. 2-12), mimicking a low concentration of external K^+, was created by applying to all K^+, except those K^+ already present in the filter, a repulsive potential to disfavor the ions from reaching S_0. Ions entering a sphere of 15-Å radius, centered 3 Å below the center of mass of the selectivity filter, were subjected to a harmonic potential with a force constant of 5 kcal/mol·Å^2. The transmembrane voltage was modeled by the application of a constant electric field along the z axis, with the potential difference of 500 mV taken between the extremities of the simulation cell (56).

2.7.4 PMF and radial distribution calculations

PMF calculations were performed according to the umbrella sampling approach using a self-learning adaptive scheme for the 2D PMFs (57). Reaction coordinates involving a single ion (z and z_3) were defined as the distance along the pore axis between the ion and the center of mass of the selectivity filter. The reaction coordinate z_{12}, used in Fig. 2-6 and Fig. 2-11, was defined as the distance along the pore axis between the center of the mass of pairs of K^+ ions in the selectivity filter and the center of the mass of the selectivity filter protein atoms. Independent simulations of 1 ns were performed every 0.5 Å along the reaction coordinates using a biasing harmonic potential with a force constant of 20 kcal/mol·Å^2. The PMF calculations on the Φ-angle of Gly-61 were performed for one subunit at a time. Windows separated by 15° were sampled for 1 ns with a harmonic restraint of 20 kcal/mol·rad^2. The corresponding dihedral angles of the three subunits not subjected to the PMF calculations were restrained to Φ = 45°, with a force constant of 5 kcal/mol·rad^2. The ions were restrained to their binding sites with a force constant of 20 kcal/mol·Å^2. All calculations were unbiased using the weighted histogram analysis method (58).

For each PMF calculation, the sampling was split into 10 intervals of 100 ps, and a PMF was calculated independently for each interval. After comparison of these 10:00 PMFs, only the last 500 ps of sampling were considered for the final PMF calculation, considering the first 500 ps as equilibration. The SE given in all 1D PMFs is the SD calculated using the independent PMFs of the last five intervals and the total PMF as the average. The relative free energy between each of five interval PMFs and the average PMF was beforehand adjusted to minimize the rmsd between the two PMFs.

The number of coordinating ligands, $n(r)$, was calculated by counting the number of coordinating atoms within concentric spherical shells with a thickness of 0.04 Å and radius r centered on the targeted ion as described previously (45).

2.8 Acknowledgements

The authors thank Victor Pau and Carol Deutsch for helpful discussions and critical reading of the manuscript. Computational resources were provided by the Basel Computational Biology Center. This work is supported by grants from the Swiss National Science Foundation (Professorship no. PP00P3-139205 to S.B.) and the US National Science Foundation (MCB-1243803 to B.S.R.).

2.9 References

1. Hille B (2001) Ion Channels of excitable membranes (Sinauer, Sunderland, MA), 3rd Ed, p 814.
2. Hoshi T, Zagotta WN, Aldrich RW (1991) Two types of inactivation in Shaker K+ channels: Effects of alterations in the carboxy-terminal region. Neuron 7(4):547–556.
3. López-Barneo J, Hoshi T, Heinemann SH, Aldrich RW (1993) Effects of external cations and mutations in the pore region on C-type inactivation of Shaker potassium channels. Receptors Channels 1(1):61–71.
4. Yellen G, Sodickson D, Chen TY, Jurman ME (1994) An engineered cysteine in the external mouth of a K+ channel allows inactivation to be modulated by metal binding. Biophys J 66(4):1068–1075.
5. Baukrowitz T, Yellen G (1995) Modulation of K+ current by frequency and external [K+]: A tale of two inactivation mechanisms. Neuron 15(4):951–960.
6. Baukrowitz T, Yellen G (1996) Use-dependent blockers and exit rate of the last ion from the multi-ion pore of a K+ channel. Science 271(5249):653–656.
7. Liu Y, Jurman ME, Yellen G (1996) Dynamic rearrangement of the outer mouth of a K+ channel during gating. Neuron 16(4):859–867.
8. Levy DI, Deutsch C (1996) A voltage-dependent role for K+ in recovery from C-type inactivation. Biophys J 71(6):3157–3166.
9. Levy DI, Deutsch C (1996) Recovery from C-type inactivation is modulated by extracellular potassium. Biophys J 70(2):798–805.
10. Ray EC, Deutsch C (2006) A trapped intracellular cation modulates K+ channel recovery from slow inactivation. J Gen Physiol 128(2):203–217.
11. Hoshi T, Armstrong CM (2013) C-type inactivation of voltage-gated K+ channels: Pore constriction or dilation? J Gen Physiol 141(2):151–160.
12. Jiang Y, et al. (2002) Crystal structure and mechanism of a calcium-gated potassium channel. Nature 417(6888):515–522.
13. Ye S, Li Y, Jiang Y (2010) Novel insights into K+ selectivity from high-resolution structures of an open K+ channel pore. Nat Struct Mol Biol 17(8):1019–1023.
14. Pau VP, et al. (2011) Structure and function of multiple Ca2+-binding sites in a K+ channel regulator of K+ conductance (RCK) domain. Proc Natl Acad Sci USA 108(43): 17684–17689.
15. Pau VP, Abarca-Heidemann K, Rothberg BS (2010) Allosteric mechanism of Ca2+ activation and H+-inhibited gating of the MthK K+ channel. J Gen Physiol 135(5): 509–526.
16. Li Y, Berke I, Chen L, Jiang Y (2007) Gating and inward rectifying properties of the MthK K+ channel with and without the gating ring. J Gen Physiol 129(2):109–120.
17. Parfenova LV, Crane BM, Rothberg BS (2006) Modulation of MthK potassium channel activity at the intracellular entrance to the pore. J Biol Chem 281(30):21131–21138.
18. Thomson AS, Rothberg BS (2010) Voltage-dependent inactivation gating at the selectivity filter of the MthK K+ channel. J Gen Physiol 136(5):569–579.

19. Smith FJ, Pau VP, Cingolani G, Rothberg BS (2012) Crystal structure of a Ba(2+)-bound gating ring reveals elementary steps in RCK domain activation. Structure 20(12): 2038–2047.
20. Kuo MM, Baker KA, Wong L, Choe S (2007) Dynamic oligomeric conversions of the cytoplasmic RCK domains mediate MthK potassium channel activity. Proc Natl Acad Sci USA 104(7):2151–2156.
21. Dvir H, Valera E, Choe S (2010) Structure of the MthK RCK in complex with cadmium. J Struct Biol 171(2):231–237.
22. Woodhull AM (1973) Ionic blockage of sodium channels in nerve. J Gen Physiol 61(6): 687–708.
23. Posson DJ, McCoy JG, Nimigean CM (2013) The voltage-dependent gate in MthK potassium channels is located at the selectivity filter. Nat Struct Mol Biol 20(2): 159–166.
24. Li W, Aldrich RW (2009) Activation of the SK potassium channel-calmodulin complex by nanomolar concentrations of terbium. Proc Natl Acad Sci USA 106(4):1075–1080.
25. Zeng XH, Xia XM, Lingle CJ (2005) Divalent cation sensitivity of BK channel activation supports the existence of three distinct binding sites. J Gen Physiol 125(3):273–286.
26. Oberhauser A, Alvarez O, Latorre R (1988) Activation by divalent cations of a Ca2+-activated K+ channel from skeletal muscle membrane. J Gen Physiol 92(1):67–86.
27. Heginbotham L, Lu Z, Abramson T, MacKinnon R (1994) Mutations in the K+ channel signature sequence. Biophys J 66(4):1061–1067.
28. Bernèche S, Roux B (2003) A microscopic view of ion conduction through the K+ channel. Proc Natl Acad Sci USA 100(15):8644–8648.
29. Bernèche S, Roux B (2001) Energetics of ion conduction through the K+ channel. Nature 414(6859):73–77.
30. . Bernèche S, Roux B (2005) A gate in the selectivity filter of potassium channels. Structure 13(4):591–600.
31. . Moscoso C, et al. (2012) K+ conduction and Mg2+ blockade in a shaker Kv-channel single point mutant with an unusually high conductance. Biophys J 103(6):1198–1207. 32.
32. Ferguson WB (1991) Competitive Mg2+ block of a large-conductance, Ca(2+)-activated K+ channel in rat skeletal muscle. Ca2+, Sr2+, and Ni2+ also block. J Gen Physiol 98(1): 163–181.
33. Dudev T, Lim C (2003) Principles governing Mg, Ca, and Zn binding and selectivity in proteins. Chem Rev 103(3):773–788.
34. Jiao D, King C, Grossfield A, Darden TA, Ren P (2006) Simulation of Ca2+ and Mg2+ solvation using polarizable atomic multipole potential. J Phys Chem B 110(37): 18553–18559.
35. Halgren TA, Damm W (2001) Polarizable force fields. Curr Opin Struct Biol 11(2): 236–242.
36. Beglov D, Roux B (1994) Finite representation of an infinite bulk system—solvent boundary potential for computer-simulations. J Chem Phys 100(12):9050–9063.
37. Cordero-Morales JF, et al. (2007) Molecular driving forces determining potassium channel slow inactivation. Nat Struct Mol Biol 14(11):1062–1069.
38. Cuello LG, Jogini V, Cortes DM, Perozo E (2010) Structural mechanism of C-type inactivation in K(+) channels. Nature 466(7303):203–208.
39. Cordero-Morales JF, Jogini V, Chakrapani S, Perozo E (2011) A multipoint hydrogenbond network underlying KcsA C-type inactivation. Biophys J 100(10):2387–2393.

40. Pan AC, Cuello LG, Perozo E, Roux B (2011) Thermodynamic coupling between activation and inactivation gating in potassium channels revealed by free energy molecular dynamics simulations. J Gen Physiol 138(6):571–580.
41. Jiang Y, et al. (2002) The open pore conformation of potassium channels. Nature 417(6888):523–526.
42. Shin HG, Lu Z (2005) Mechanism of the voltage sensitivity of IRK1 inward-rectifier K+ channel block by the polyamine spermine. J Gen Physiol 125(4):413–426.
43. Xu Y, Shin HG, Szép S, Lu Z (2009) Physical determinants of strong voltage sensitivity of K(+) channel block. Nat Struct Mol Biol 16(12):1252–1258.
44. Cordero-Morales JF, et al. (2006) Molecular determinants of gating at the potassium channel selectivity filter. Nat Struct Mol Biol 13(4):311–318.
45. Boiteux C, Bernèche S (2011) Absence of ion-binding affinity in the putatively inactivated low-[K+] structure of the KcsA potassium channel. Structure 19(1):70–79.
46. Jo S, Kim T, Iyer VG, Im W (2008) CHARMM-GUI: A web-based graphical user interface for CHARMM. J Comput Chem 29(11):1859–1865.
47. Woolf TB, Roux B (1994) Molecular dynamics simulation of the gramicidin channel in a phospholipid bilayer. Proc Natl Acad Sci USA 91(24):11631–11635.
48. Brooks BR, et al. (1983) Charmm—a program for macromolecular energy, minimization, and dynamics calculations. J Comput Chem 4(2):187–217.
49. Mackerell AD, Jr., Feig M, Brooks CL, 3rd (2004) Extending the treatment of backbone energetics in protein force fields: Limitations of gas-phase quantum mechanics in reproducing protein conformational distributions in molecular dynamics simulations. J Comput Chem 25(11):1400–1415.
50. Jorgensen WL, Chandrasekhar J, Madura JD, Impey RW, Klein ML (1983) Comparison of simple potential functions for simulating liquid water. J Chem Phys 79(2):926–935.
51. Roux B, Bernèche S (2002) On the potential functions used in molecular dynamics simulations of ion channels. Biophys J 82(3):1681–1684.
52. Essmann U, et al. (1995) A smooth particle mesh Ewald method. J Chem Phys 103(19): 8577–8593.
53. Feller SE, Zhang YH, Pastor RW, Brooks BR (1995) Constant-pressure molecular dynamics simulation—the Langevin piston method. J Chem Phys 103(11):4613–4621.
54. Nose S (1984) A unified formulation of the constant temperature molecular-dynamics methods. J Chem Phys 81(1):511–519.
55. Hoover WG (1985) Canonical dynamics: Equilibrium phase-space distributions. Phys Rev A 31(3):1695–1697. 56.
56. Roux B (2008) The membrane potential and its representation by a constant electric field in computer simulations. Biophys J 95(9):4205–4216.
57. Wojtas-Niziurski W, Meng Y, Roux B, Bernèche S (2013) Self-learning adaptive umbrella sampling method for the determination of free energy landscapes in multiple dimensions. J Chem Theory Comput 9(4):1885–1895.
58. Kumar S, Bouzida D, Swendsen RH, Kollman PA, Rosenberg JM (1992) The weighted histogram analysis method for free-energy calculations on biomolecules. 1. The method. J Comput Chem 13(8):1011–1021.

2.10 Supporting information

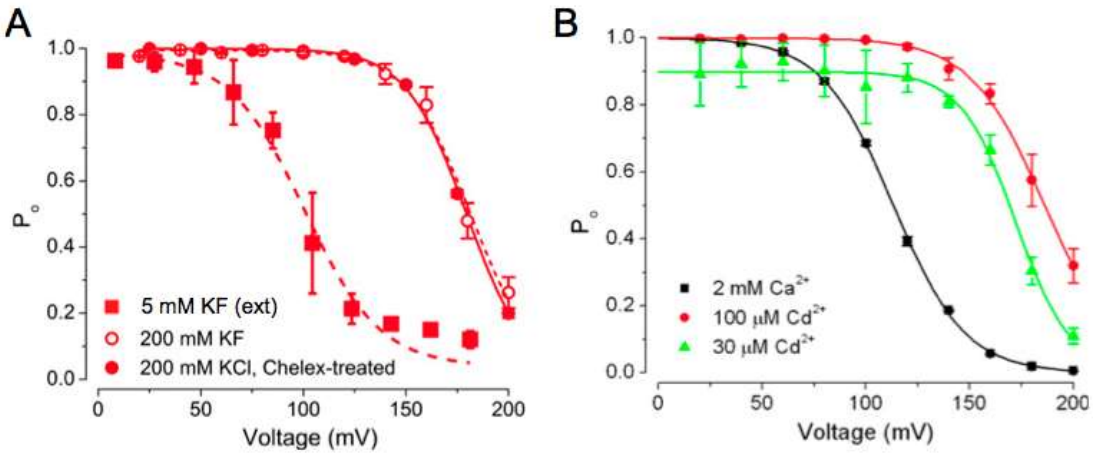

Fig. 2-10 **Intrinsic inactivation of MthK channels at depolarized voltages**

(A) Po vs. voltage for MthK channels recorded with either KF-based solutions or KCl- based solutions from which Ca^{2+} was sequestered using Chelex-100 resin. In each case, solutions at the cytoplasmic side of the channel contained 100 µM Cd^{2+} and 200 mM K^{+} (as either chloride or fluoride salt) as well as 10 mM Hepes (pH 8.1). Solutions at the extracellular side contained 5 mM KF, 195 mM N-methyl glucamine (red squares), 200 mM KF (red open circles), or 200 mM KCl (red filled circles). All extracellular solutions additionally contained 10 mM Hepes at pH 7.0. These results illustrate that gating into the inactivated state persists even after sequestration or buffering of free Ca^{2+} to low levels (<1 µM) and that inactivation was enhanced by lowering extracellular [K^{+}]. (B) Po vs. voltage for single MthK channels in the presence of 2 mM Ca^{2+} (black), 30 µM Cd^{2+} (green), and 100 µM Cd^{2+} (red). Gating into the nonconducting, inactivated state shifts $V_{1/2}$ values to less positive voltages (i.e., to the left) with 2 mM Ca^{2+}. If 100 µM Cd^{2+} also promoted gating into the inactivated state, then one would predict that lowering [Cd^{2+}] to 30 µM would shift the $V_{1/2}$ to more positive values, leading to higher Po at 200 mV compared with that observed with 100 µM Cd^{2+}. Instead, lowering the [Cd^{2+}] leads to overall lower levels of maximal activation but does not preferentially decrease entry to the inactivated state. Together, these results suggest that gating in the inactivated state does not arise from 100 µM Cd^{2+} or low levels of contaminant Ca^{2+}.

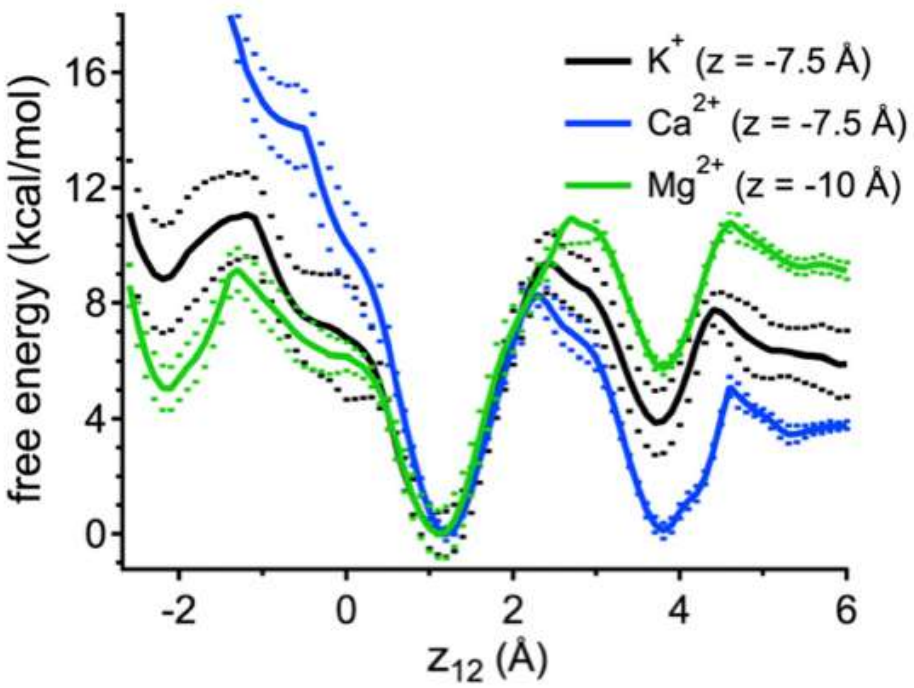

Fig. 2-11 **Free energies of K+ ions in the selectivity filter**

Free energies of K^+ ions in the selectivity filter with K^+, Mg^{2+}, or Ca^{2+} at their respective energy wells in the pore; z_{12} corresponds to the center of mass of the K^+ ions in the filter relative to the center of mass of the selectivity filter atoms. With a Ca^{2+} ion at S_5 (z = −7.5 Å), K^+ ions are driven to an energy well at the extracellular end of the selectivity filter compared with the effect of K^+ at S_5 (z = −7.5 Å) or Mg^{2+} at its energy well in S_{cav} (z = −10 Å). Dotted lines represent ± SD.

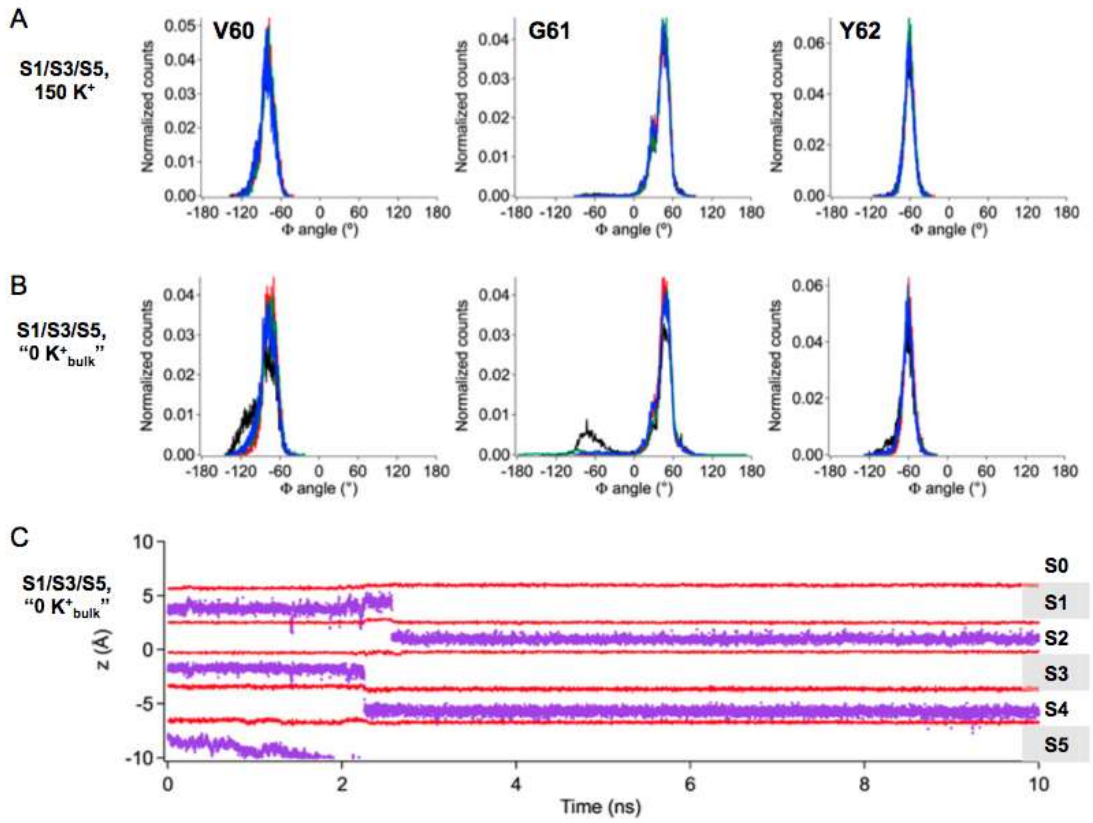

Fig. 2-12 **K^+ dissociation facilitates a conformational change in the MthK selectivity filter**

(A) Histogram of dihedral (Φ) angles for the indicated residue sampled during molecular simulations; each of four subunits is represented by a different color (black, red, green, and blue). With K^+ occupying the S_1-S_3-S_5 sites, all carbonyl oxygen atoms face the central axis of the pore (in canonical positions) during the course of simulation; thus, the Φ-angles for each residue are centered around single peaks. (B) With K^+ ions initially occupying the S_1-S_3-S_5 but with a force applied to repel binding of K^+ ions coming from the bulk (0 K^+_{bulk}) (Methods chapter 2.7.3), the S_1-S_3 ions redistribute to the S_2-S_4 sites, leading principally to a rotation of the V60 carbonyl oxygen (illustrated in Fig. 2-7). (C) K^+ ion (purple) and protein oxygen positions (red) as a function of time during a representative molecular simulation illustrating movement of K^+ ions from their initial positions in the S_1-S_3-S_5 sites. After the K^+ ion diffuses from its initial position in the S_5 site, the S_1 and S_3 K^+ ions move rapidly into the S_2 and S_4 sites.

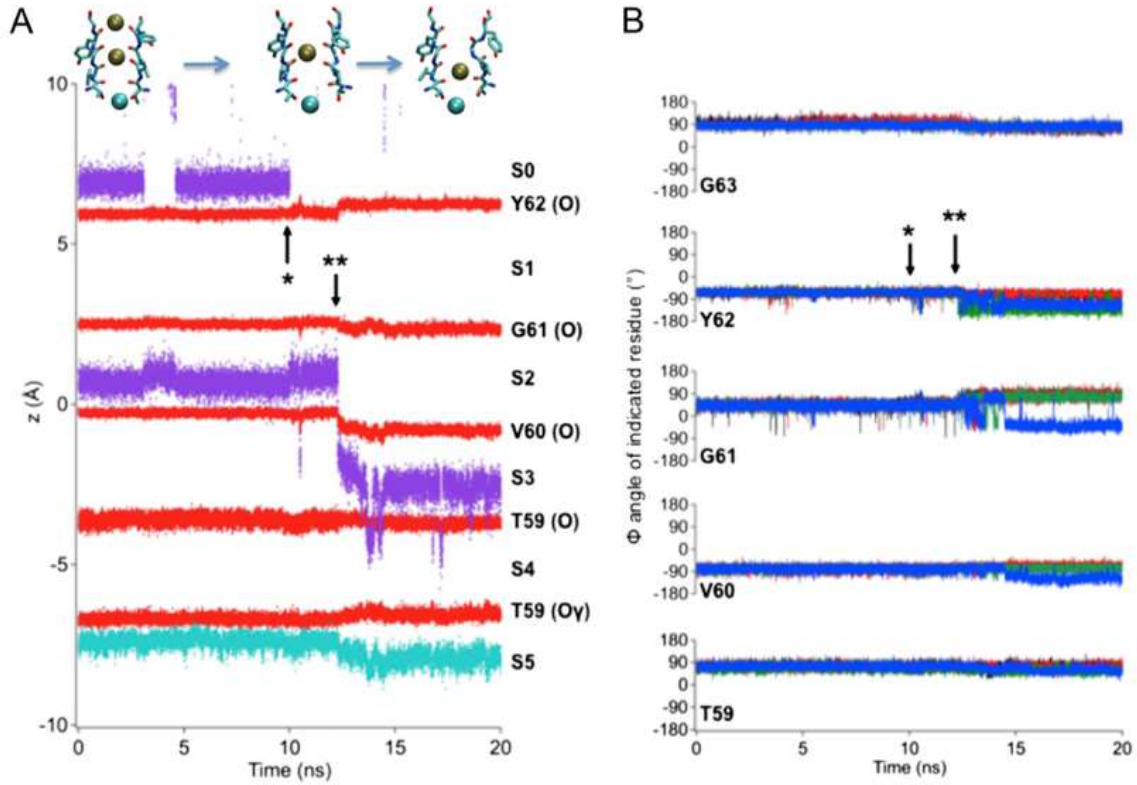

Fig. 2-13 **Ion dissociation from S_0 can facilitate a conformational change in the selectivity filter**

(A) Axial positions of ions and protein oxygen as a function of time during a representative molecular simulation. (O) indicates the carbonyl oxygen of the indicated residue, whereas (Oγ) indicates the side chain oxygen of residue T59. (B) Φ-Angles for selectivity filter residues during the same simulation plotted as a function of time. Initially, with Ca^{2+} at S_5 (cyan) and K^+ ions at S_2 and S_0 (purple), carbonyl oxygen atoms forming the selectivity filter (red) are in their canonical positions. *Dissociation of K^+ from S_0. **Movement of the remaining K^+ ion from S_2 to S_3 leads to transitions between the canonical and rotated conformations.

3 Mechanistic differences in MthK inactivation in WT and V55E mutant

Florian T. Heer[1], Andrew S. Thomson[2], Céline Boiteux[1$], Brad S. Rothberg[2*], Simon Bernèche[1*]

[1]SIB Swiss Institute of Bioinformatics and Biozentrum, University of Basel, Klingelbergstrasse 50/70, 4056 Basel, Switzerland

[2]Department of Medical Genetics and Molecular Biochemistry, Temple University School of Medicine, 3400 N. Broad St., Philadelphia, PA 19140

3.1 Abstract

K^+ permeation through activated channels can be modulated by C-type inactivation, which is a time dependent closing around the selectivity filter. Inactivation can be modulated by external K^+ concentration. The inactivation of MthK and a strong inactivating mutant were investigated using electrophysiology and molecular simulation data. Under inactivation promoting conditions the mutant looses ions from the selectivity filter and adopts a structure similar to the originally proposed (and recently challenged to be the true) inactivation state. This mechanism is not shared in the WT channel, due to its inability to loose ions from the center of the selectivity filter. Simulations starting after these inaccessible steps adopt the originally proposed structural rearrangement suggesting this conformation is shared under most K^+ channels but corresponds to a later, possibly deeper, inactivated state.

3.2 Statement of own contribution

I performed all simulations and analyses, which I co-designed with S. Bernèche. I wrote the manuscript. All data presented are from my experiments, except the data shown in Fig. 3-4. This figure, the data and the caption are provided by our collaborator Prof. Brad S. Rothberg from Temple University, Philadelphia USA.

This manuscript is in preparation for publication.

3.3 Introduction

Selective potassium ion channels are involved in many vital processes in cells such as nerve pulses, heart beat and their disfunction can result in diseases like epileptic seizure, vascular diseases and tinnitus (Balut et al., 2012).

The conductance of potassium channels is regulated by different gating mechanisms. The inner gate, often called the main gate, is a constriction formed near the cytoplasmic end of the channel (Perozo et al., 1999). A conserved glycine acts as a gating hinge in prokaryotic channels (Gly83 in MthK) (Jiang et al., 2002). The inner gate is functionally coupled to a regulatory domain and responds to a number of different signals like transmembrane voltage and ligands, such as divalent ions.

Channels can inactivate even in presence of an activation signal in a time dependent manner. Two main mechanisms are known to underlie inactivation. N-type inactivation (fast inactivation) involves a positively charged N-terminal moiety, the N-ball, acting as a plug and blocking ion flow. C-type inactivation, originally identified by different C-terminal domain splicing variants in Shaker (Hoshi et al., 1991), involves conformational changes in or around the selectivity filter (Baukrowitz and Yellen, 1996, 1995; Hoshi and Armstrong, 2013; Levy and Deutsch, 1996a, 1996b; Liu et al., 2015, 1996; López-Barneo et al., 1993; Ray and Deutsch, 2006; Yellen et al., 1994) (see. Fig. 3-1).

It was shown that inactivation is dependent on external potassium concentration, intracellular presence of some divalent ions and small charged molecules as well as voltage (Fedida et al., 1999; Hoshi et al., 1990; López-Barneo et al., 1993; Rasmusson et al., 1995; Thomson et al., 2014; Thomson and Rothberg, 2010).

In 2001, a structure representing a collapsed selectivity filter was solved for the channel KcsA from *Streptomyces lividans (Zhou et al., 2001)* (see also Fig. 3-3). The protein crystal was soaked in a low K^+ concentration solution. Later, this structure was associated with the C-type inactivated state, induced by the loss of ions from the conductive state. (Cordero-Morales et al., 2007; Yellen, 2001) (see also Fig. 3-1A).

It is not clear whether this inactivation mechanism is universally shared among selective ion channels. Devaraneni et al. constructed a semisynthetic K^+ channel which sterically hinders the channel to adopt the collapsed state without changing the C-type inactivation behavior of the channel (Devaraneni et al., 2013).

The MthK channel from *Methanobacterium thermoautotrophicum (Zeikus and Wolfe, 1972)*, a model channel for human Kv channels, did not change conformation in the selectivity filter under low K^+ ion concentration crystallization conditions (Ye et al., 2010), resembling the conditions used in the crystallization of the inactivated KcsA channel structure. Nevertheless, MthK does inactivate, although at a lower rate than KcsA WT.

It is notable that mutation of a glutamic acid at position 71 to an alanine in KcsA lead to a decrease in inactivation (Cordero-Morales et al., 2006) and crystal structures did not show the conformational change observed in the WT low K^+ structure. Instead either the same structure as in the conductive state (Cordero-Morales et al., 2006) or a flip of the valine carbonyl in the TVGYG signature sequence (Cheng et al., 2011) was observed. At this key residue, MthK (position 55 for MthK) has a valine. A mutation to a glutamic acid did increase inactivation rate.

We describe conductance of both WT and the mutant MthK channel over a range of voltages, and show that only the mutant reaches the collapsed state mentioned above. Further analysis of the WT shows that the collapsed state could be reached in the absence of K^+ ions, suggesting that the collapsed state could be a later, deeper inactivated state.

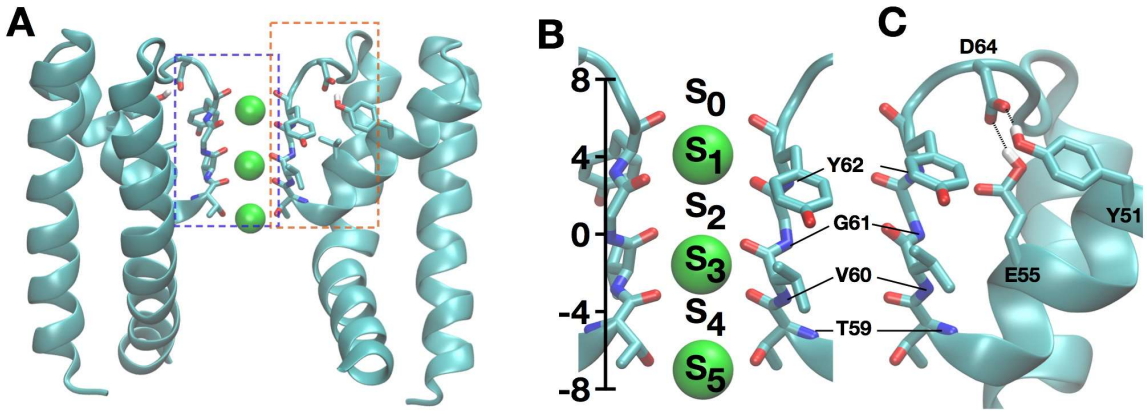

Fig. 3-1 **Structural view of MthK**

Representation of the pore of MthK (based on PDB ID code 3LDC). (A) Side view of the pore of the MthK channel. The amino acids forming the selectivity filter, Thr59 to Tyr62, as well as the side-chains of Tyr51,Val/Glu55 and Asp64 are shown in licorice. For clarity, the front and back subunit as well as all hydrogens, which do not interact with Asp64, were removed. Potassium ions are represented as green spheres. Note that the bottom K^+ ion interacting directly with the selectivity filter, moved into this position from the cavity during equilibration of the system (see Methods chapter 3.6.1). (B) View into the selectivity filter, marked in a blue box in (A). The potassium binding sites in the selectivity filter are labeled from extracellular to intracellular S_1 to S_4. The extracellular binding site is S_0 and the intracellular binding site is S_5. The bar in the left shows the relative positions of the ions used in the simulations. (C) Mutant MthK V55E (corresponds to orange box in (A)). Note the protonation of the glutamic acid.

3.4 Results

3.4.1 Molecular dynamic simulations reveal a highly attractive selectivity filter in WT

A molecular system of MthK was set up and molecular dynamic (MD) simulations were run with 150 mM KCl bulk ion concentration. Under such ion concentration the ions in the channel are stable (Fig. 3-2A) with no significant change in the conformation of the selectivity filter during the simulation (Fig. 3-2D-E). A third ion was recruited to S_5 within 100 ps of simulation.

MthK inactivation can be promoted by lowering the external K^+ concentration (Thomson and Rothberg, 2010). The simulation was repeated applying a constrain to keep ions away from the selectivity filter mimicking a low ion concentration (see Methods chapter 3.4.1). In this simulation, the ion in S_3 dropped to S_4 in 2.5 ns, followed by the ion in S_1 dropping to S_2 250 ps later (Fig. 3-2B). After these events, the ions remained stable at their positions for the rest of the simulation. The selectivity filter did not change its overall conformation, but one Val60 carbonyl tilted out of its original position. Fluctuations of the selectivity filter were larger in this subunit than the other three, in which carbonyls were all interacting with the ions (Fig. 3-2J-L).

In neither case did the selectivity filter adopt a conformation similar to the collapsed state seen in KcsA (Zhou et al., 2001). It was shown that, in KcsA, this state is quickly (within 5 ns of simulation) reached in MD simulations in the absence of ion (Boiteux and Bernèche, 2011). To investigate the existence of this state in MthK, this computer experiment was repeated replacing the ions in the filter with water molecules. As expected, the Val60 carbonyls tilted away from the ion permeation pathway, narrowing the diameter of the pore around the S_2 binding site. Within the first 20 ns of the simulation the selectivity filter was fluctuating but, in combination with an additional water molecule in the p-loop, adopted the expected collapsed state (starting structure as shown in Fig. 3-3A to the final structure Fig. 3-3B).

Overall, the flexibility of the selectivity filter was increased compared to the ion bound states. Thus, in absence of ions, the MthK channel could adopt an inactivated structure similar to the collapsed state of KcsA (Fig. 3-3D), though showing more flexibility in the filter region compared to the ion bound states.

3.4.2 Strong inactivating mutant MthK V55E

The mutant V55E was used to investigate strong inactivation (see Fig. 3-2C). The original MD simulation at 150 mM external KCl concentration was repeated with this mutation. Again, starting with ions in S_1 and S_3 a third ion is recruited to S_5 at the bottom of the selectivity filter. The selectivity filter is fluctuating more than in WT, even with ions bound (Fig. 3-2L). After temporary loosing the ion from S_5, the middle ion in S_3 drops to S_4 and

within 500 ps to S_5. Immediately following the drop of the bottom ion to S_4, the top ion starts to occupy a position between S_1 and S_2 for 750 ps and then leaves the channel outwards, leaving an empty channel, which adopts, within 1 ns, a structure similar to the collapsed state described for KcsA (final state is shown in Fig. 3-3C). The fluctuations of the filter are similar to those observed in simulations of the WT channel without any ions.

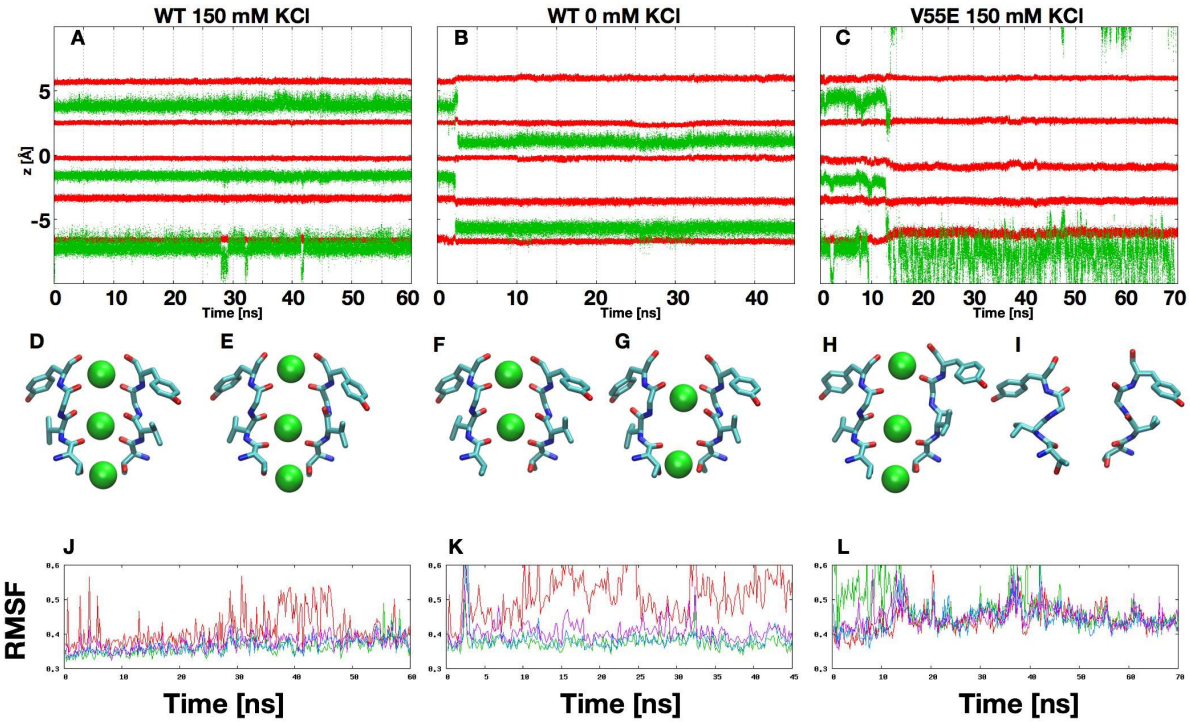

Fig. 3-2 **MD simulations, ion trajectory in the selectivity filter of MthK**

(A-C) Time series analysis of the position of K^+ ions along the permeation pathway. The oxygen atoms of the selectivity filter are shown in red, potassium ions in green. The trajectories are centered around the center of mass of the backbone of residues 59 to 62. In all simulations the bottom ion moves from S_{cav} to S_5, exchanging four water molecules of the first solvation shell with threonine side-chains at the beginning of the simulation. Three different systems were analyzed: MthK WT (A), Trajectory of MthK WT excluding bulk ions from the filter (B) (see Methods chapter 3.6.1) and Trajectory of MthK V55E mutant (C). (D-I) First frame after equilibration and last frame of the simulations. (J-K) RMSF calculation for the backbone of residues T59 to Y62. The four subunits were analyzed separately for WT with ions in S_1-S_3-S_5 (J), WT with ions in S_2-S_4(K) and V55E starting with ions in S_1-S_3 (L).

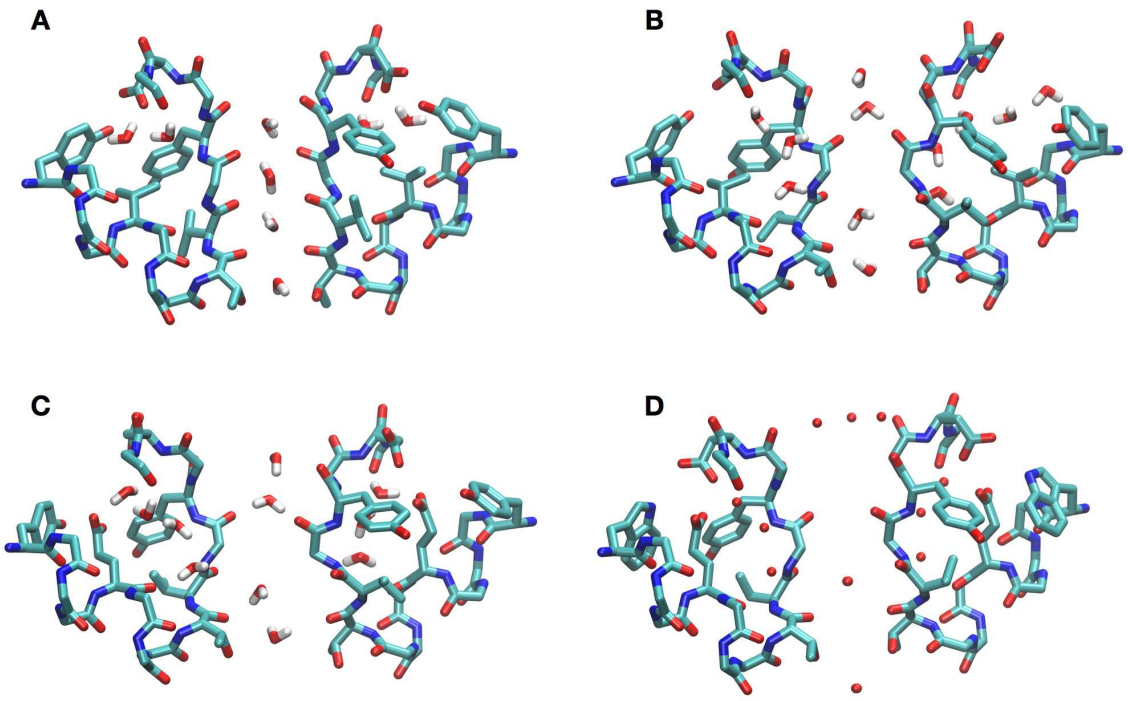

Fig. 3-3 **Comparison between different states of the selectivity filter**

(A) MthK WT crystal (PDB id 3LDC) structure with water molecules in S_1 to S_4. The two water molecules in the P-loop are solved in the crystal structure. This structure correspond to the initial conformation of the computer experiments. (B) Structure after 30 ns of simulation of empty MthK WT channel under low K^+ conditions. (C) Structure of MthK V55E after 50 ns of MD simulation under high K^+ concentrations. (D) KcsA crystal structure (PDB id 1K4D) solved under low K^+ concentrations. Two adjacent subunits of MthK (KcsA) are shown from residue 51 to 65 (67 to 81). For clarity reasons no hydrogens are shown and only the side chains of the selectivity filter 59-62 as well as the residues 51 55 and 64 (67 71 and 80).

3.4.3 Modulation of inactivation by variation of ion concentration and applied voltage

Inactivation of MthK channels were investigated further with electrophysiological single channel recordings over a range of voltages. In presence of 200 mM symmetric K^+ concentration, MthK WT shows a high open probability over a wide range of voltages, but above 160 mV the open probability decreases drastically (Fig. 3-4A,C). Fig. 3-4B shows that lowering external concentration of K^+ to 5 mM reduces the open probably. The channel is still mostly open up to 60 mV, but the open probability decreases at higher voltages.

The V55E mutant has a maximal open probability of about 0.8 at -120 mV. At ±20 mV the open probability is around 0.6 versus almost 1 in WT. Above 100 mV the open probability between V55E mutant and WT at low external K^+ concentration is similar (Fig. 3-4C).

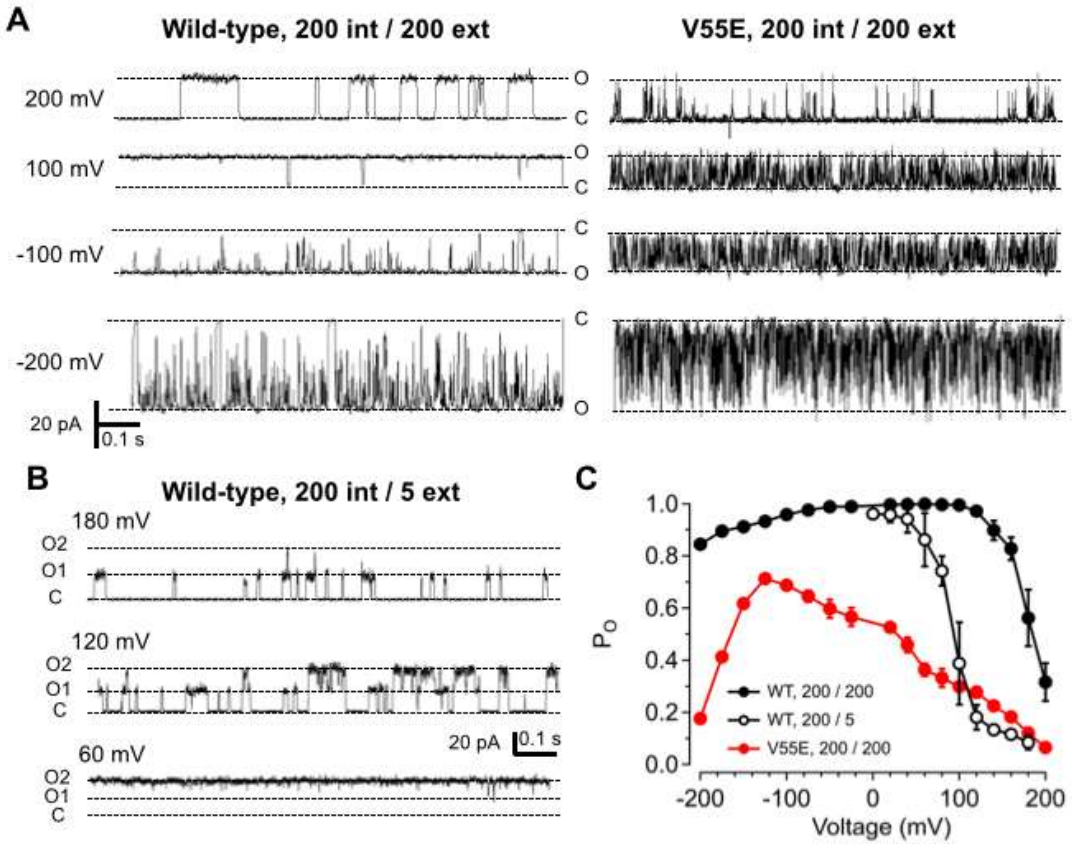

Fig. 3-4 **Effects of V55E mutation on MthK channel gating**

(A) Representative single-channel current through MthK wild-type and V55E channels over a range of voltages. For these recordings, solutions at both sides of the membrane contained 200 mM KCl. “O” and “C” indicates open and closed channel current levels, respectively. Strong depolarization (200 mV) leads to decreased open probability (Po) for wild-type channels, and V55E channels consistently display briefer openings than wild-type at all tested voltages. “O” and “C” indicates open and closed channel current levels, respectively. (B), Current through MthK wild-type channels with 5 mM external K^+. This bilayer contained two active channels, indicated by open levels “O1” and “O2”. Lower external [K^+] enhances inactivation at mildly depolarized voltages. (C), Po vs. voltage for wild-type (WT) channels with 200 mM (black circles, n=5 bilayers) or 5 mM external K^+ (open circles, n=3 bilayers), compared with V55E with 200 mM external K^+ (n=5 bilayers).

3.4.4 Ion dissociation is only energetically favorable in the mutant

Our MD simulations showed that a collapsed state could be reached if ions leave the selectivity filter. Electrophysiological measurements show that open probability is decreased under applied voltages and lowered external potassium concentrations. To investigate the binding affinity of ions to the selectivity filter, potential of mean force (PMF) calculations initiated with ions in S_1 and S_3 under low potassium conditions were performed for both WT and V55E at -500 mV, -200 mV, 0 mV, 200 mV and 500 mV.

In the WT calculations, the most favorable ion positions are S_1-S_3 and S_2-S_4 (Fig. 3-5A, top). The S_2-S_4 state is 3 kcal/mol more favorable than S_1-S_3 at 0 mV. Negative voltage favor the S_2-S_4 state further by another 2 kcal/mol while positive voltage has the opposite effect. The intermediate state S_1-S_4 is reachable, but overall unfavorable. The energy barrier between the states are more than 9 kcal/mol. In each PMF calculation, the most favorable states include two ions in the selectivity filter.

On the other hand, ions occupying the SF in the V55E mutant are more likely to be found in states S_2-S_4 followed by S_1-S_4, S_1-S_3 and S_0-S_4 (Fig. 3-5A, bottom). The free energy barriers between all the states are generally smaller than those observed in WT. At negative voltage, ions are released toward the intracellular side (ion Z_2 moves toward the cavity and the states in the lower part of the plot are accessible). In absence of voltage, these states are less favorable and ion Z_1 is more likely to be released toward the extracellular side. This is enhanced by the application of positive voltages. This is in vast contrast to the WT where loss of an ion is energetically unfavorable.

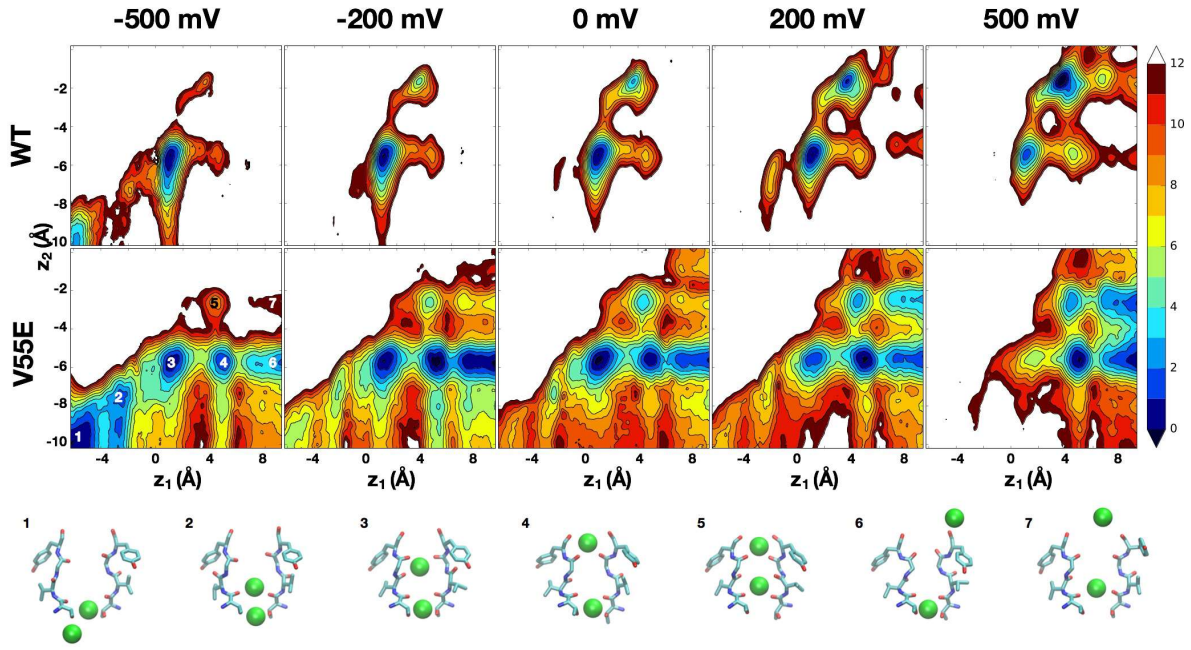

Fig. 3-5 **Free energy relations between two-ion states in the selectivity filter of MthK**

The free energy, measured by PMF calculations, is compared between WT and V55E mutant at different applied voltages. Top row: WT, middle row: V55E. From left to right: -500 mV, -200 mV, 0 mV, 200 mV, 500 mV. The scale bar is 1 kcal/mol per color and the lowest energy state is defined as zero free energy. The axis are the ion position along the z-axis (normal to the membrane), relative to the center of mass of the selectivity filter backbone (residue 59 to 62) (see Fig. 3-1B).
x-axis (Z_1) is the top ion, y-axis(Z_2) bottom ion.
Bottom: structural snapshots displaying the filter region of two opposite subunits and top ion (Z_1) and bottom ion (Z_2). The different states are numbered as in V55E at -500 mV.

3.4.5 Analysis of solvation states of ions in the selectivity filter

From the PMF calculations, the states with both ions within the filter (S_1-S_3, S_1-S_4, S_2-S_4) were analyzed further by investigating the coordination of ions (representations shown in Fig. 3-6A-C). Hydration of K^+ in water is 6.3-7.8 (4-8 for individual K^+ ions) (Bounds, 1985; Clementi and Barsotti, 1978; Impey et al., 1983; Marchese and Beveridge, 1984; Mezei and Beveridge, 1981; Migliore et al., 1986; Nguyen and Adelman, 1984).

To solvate the potassium ions in the selectivity filter, the protein has to reproduce bulk hydration. Fig. 3-6D-F show the number of oxygen atoms (carbonyl group from the backbone or the threonine side-chain) coordinating the ions. S_2-S_4 was the most favored binding state in the absence of voltage. The bottom ion in S_4 is coordinated by 8 oxygens at 3.5 Å in WT and 7.8 in V55E mutant while the top ion in S_2 is solvated by 7 in WT and only 6 in V55E mutant. If the top ion moves to S_1 the coordination is similar between WT and V55E in S_1-S_4, with a top ion coordination number around 6. Finally the S_1-S_3 state has ions coordinated by about 7 oxygens in WT, but only 6 in V55E.

Fig. 3-3G-I shows the histogram of phi61 angles. The WT channel shows only one peak around +50º if the ions are in S_2-S_4 or S_1-S_3 but a second peak around -75º if the ions are in S_1-S_4. This second peak occurs if the carbonyl oxygen of Val60 rotates out, away from the conducting pore. The small peak occurring around -150º is a single subunit briefly pointing the carbonyl oxygen directly out of the selectivity filter, similar as seen for KcsA in (Cheng et al., 2011).

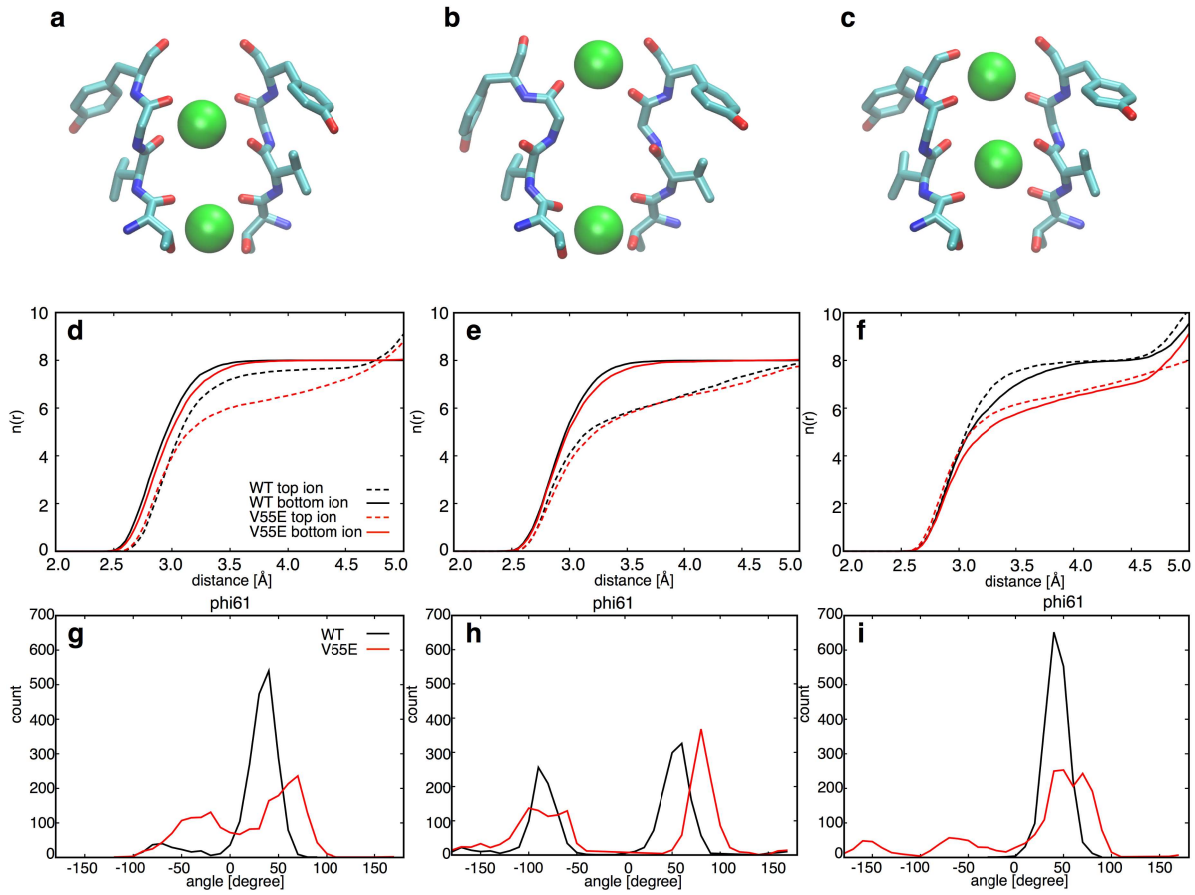

Fig. 3-6 **Coordination of ions in the selectivity filter**

The coordination of the ions in the three states (left to right) S_2-S_4, S_1-S_4, and S_1-S_3 from the PMF calculations are analyzed. The states correspond to the windows created at [1.0, -5.5],[4.5, -5.5], and [4.0, -2.0] without applied voltage. Top: molecular representation of the states. Middle: Average number of water molecules or carbonyl oxygen solvating the ion in dependence of distance in [Å]. WT is shown in black, V55E mutant in red. Solid line corresponds to the bottom (z_2) ions, dotted lines to the top (z_1) ions. Bottom: Histogram of the Psi61 angles. WT is shown in black, V55E mutant in red.

3.5 Discussion

MD simulations revealed a selectivity filter, which is often occupied by two ions at 150 mM K^+ concentration and an additional ion directly associated to the selectivity filter. Reducing the external ion concentration did not lead to a loss of the two ions originally bound in the selectivity filter.

Ions in the selectivity filter are coordinated by 7-8 carbonyl oxygens, as expected from crystallographic data and in agreement with the inner solvation shell of potassium ions in water.

Electrophysiological measurements revealed an almost non inactivating channel at low applied voltages. This explains well the stable selectivity filter with bound ions and fits well with the fact that no change in conformation was observed when the channel was crystallized under low potassium concentration.

Under symmetric ion condition, the channel showed strong inactivation at high positive voltages, but not at high negative voltages. Given the architecture of potassium channels, it is possible that inactivation at positive voltages is facilitated by reduced recruitment of ions towards the bottom of the selectivity filter, explaining the increasing inactivation at positive voltages. On the other hand the external binding site S_0 is easy to reach because it is next to the bulk solution. However, the comparison between 200 mM and 5 mM external K^+ concentration shows that ion occupancy on the extracellular side is a major driving force in inactivation and shows that replenishment of ions from the intracellular side can not be a major contributor to inactivation at voltages below +160 mV.

Different to the WT, the mutant V55E did loose ions in MD simulations even at high K^+ concentrations, leaving the selectivity filter in a collapsed state, well in agreement with the proposed inactivation mechanism.

To investigate, whether MthK inactivation is driven by the loss of ions in WT, one has to compare the stability of ions in the selectivity filter at voltages above 160 mV to ensure that the channel is favoring an inactivated state.

In PMF simulations, ions can leave the selectivity filter in the V55E mutants without significant ion barriers. This is well in agreement with the MD simulations, where the ions in the channel left the selectivity filter and the filter collapsed. In stark contrast, the ions are “trapped” by high energy barriers in the WT simulations. With a high positive voltages applied (where both WT and mutant show strong inactivation), the top ion Z_1 was able to leave the channel. But the release of the ion is only possible via the S_1-S_3 state in WT at positive voltages. Our previous work (Thomson et al., 2014) showed however that this position is prone to recruiting intracellular ions. Additionally the states reached were less stable than the states within the selectivity filter. These observation are in stark contrast

with a model where inactivation occurs via the loss of ions. It is possible that more than one inactivation state exists, as proposed in (Kiss et al., 1999). However, the first initial step must occur with still two ions bound to the filter. It does not exclude the loss of ions in a later stage of inactivation.

One interesting finding is that potassium ions bind favorably in the two states S_1-S_3 and S_2-S_4, which are states most likely involved in permeation. The state S_1-S_4, which is reachable but not favorable, did show some conformational changes reminiscent of the originally described inactivated state, or collapsed state.

The external binding site S_0 can only be reached, if ions are in the S_2-S_4 state. S_0-S_2-S_4 state, favored by increasing external K^+ concentration, is stabilizing the filter in its conducting state.

Combining the results from electrophysiological measurements and PMF calculations, we suggest that the V55E mutant inactivates via the loss of ions as described previously in KcsA and is a property directly linked to the glutamic acid. MthK WT channel however does not (initiate) inactivation via the loss of ions, further supporting the existence of different unknown inactivation mechanisms.

3.6 Methods

3.6.1 Molecular systems

Molecular systems of MthK WT and V55E mutant were built based on the MthK crystal structure (PDB entry 3LDC) (Ye et al., 2010). All residues were assigned their standard protonation state at pH7 except Glu55, which was protonated in the V55E construct. The systems were assembled using the CHARMM-GUI web service (Brooks et al., 2009; Jo et al., 2008).

The protein alignment with the membrane was taken from OPM (Lomize et al., 2006). The channel is embedded in a lipid bilayer consisting of 149 1,2-dimyristoyl-sn-glycero-3-phosphocholine (DMPC) molecules and the protein symmetry axis is aligned normal to the membrane. The number of ions were adjusted to reproduce a 150mM KCl concentration in a neutral system (29 potassium and 17 chloride ions). Water molecules are represented using the TIP3P water model (Jorgensen et al., 1983). Each system contains about 50'500 atoms.

3.6.2 Molecular dynamic simulations

Simulations were conducted using the CHARMM software version c36 (Brooks et al., 2009) with the PARAM36 force field (Best et al., 2012). A correction term was used for the potassium – carbonyl oxygen interaction (Roux and Bernèche, 2002). The system was minimized using steepest decent and adopted basis Newton-Raphson minimization followed by 450 ps of equilibration with decreasing harmonic restraints in the system. The MD simulation were run under periodic boundary conditions, using the Particle Mesh Ewald algorithm for long range electrostatics (Essmann et al., 1995) The NPT ensemble with the extended Langevin algorithm (Feller et al., 1995) and the Nose-Hoover thermostat (Hoover, 1985; Nosé, 1984) were applied to keep temperature at 323.15K and the pressure at 1 atm. A Time step of 2 fs was used and bonds involving hydrogen atoms were constrained using the SHAKE algorithm (Ryckaert et al., 1977).

Simulations mimicking a low external K^+ concentrations use a repulsive force restricting ions from the bulk solution to reach the selectivity filter. A spherical potential centered between S_2 and S_3 with a radius of 20 Å and a force constant of 5 kcal/mol/Å^2 was applied. Ions originally placed in the selectivity filter are not subject to this potential.

Molecular representations were prepared with VMD software (Humphrey et al., 1996).

3.6.3 Potential of mean force (PMF) calculations

The PMF were calculated using the self learning adapted umbrella sampling method (Wojtas-Niziurski et al., 2013). Reaction coordinates are the distance along the ion permeation path, normal to the membrane. The reference point is the center of mass of the backbone of the selectivity filter, defined as residues 59 to 62. For all calculations, ions were initially positioned at sites S_1 and S_3. The relative position of the top ion is shown on the x-axis and the relative position of the bottom ion is shown on the y-axis. The lowest free energy point in the system is attributed a value of 0 kcal/mol. Independent simulations of 500 ps were performed every 0.5 Å along the reaction coordinates using a biasing harmonic potential of 20 kcal/mol/Å^2. The first 50 ps of every independent window was considered as equilibration and thus excluded from the analysis. The independent simulations were combined and unbiased using the weighted histogram analysis method (WHAM) (Kumar et al., 1992) Bulk ions are restraint from interacting with the filter, mimicking a 0 K^+ bulk concentration. Voltage was applied as a constant electric field over the length of the entire simulation box (Roux, 2008). The individual plots in Figure 4 were made with the python library matplotlib (Hunter, 2007).

3.6.4 Calculation of radial distribution functions

The coordination number function n(r) of protein oxygen atoms around the ions was calculated. Every 2 ps of the simulations the coordinating carbonyl oxygens around the ion were counted in 0.04 Å thick concentric shells with r centered on the targeted ion. The data presented in the figure are from the PMF windows calculated without applied voltage (0 mV in Fig. 3-5). The configuration states S_2-S_4 S_1-S_4 and S_1-S_3 correspond to windows $[Z_1,Z_2]$= [1.0, -5.5], [4.5, -5.5] and [4.0, -2.0].

3.7 References

Balut, C.M., Hamilton, K.L., Devor, D.C., 2012. Trafficking of intermediate (KCa3.1) and small (KCa2.x) conductance, Ca(2+)-activated K(+) channels: a novel target for medicinal chemistry efforts? ChemMedChem 7, 1741–1755. doi:10.1002/cmdc.201200226

Baukrowitz, T., Yellen, G., 1996. Use-dependent blockers and exit rate of the last ion from the multi-ion pore of a K+ channel. Science 271, 653–656.

Baukrowitz, T., Yellen, G., 1995. Modulation of K+ current by frequency and external [K+]: a tale of two inactivation mechanisms. Neuron 15, 951–960.

Best, R.B., Zhu, X., Shim, J., Lopes, P.E.M., Mittal, J., Feig, M., Mackerell, A.D., 2012. Optimization of the additive CHARMM all-atom protein force field targeting improved sampling of the backbone φ, ψ and side-chain χ(1) and χ(2) dihedral angles. J. Chem. Theory Comput. 8, 3257–3273. doi:10.1021/ct300400x

Boiteux, C., Bernèche, S., 2011. Absence of ion-binding affinity in the putatively inactivated low-[K+] structure of the KcsA potassium channel. Struct. Lond. Engl. 1993 19, 70–79. doi:10.1016/j.str.2010.10.008

Bounds, D.G., 1985. A molecular dynamics study of the structure of water around the ions Li+, Na+, K+, Ca++, Ni++ and Cl-. Mol. Phys. 54, 1335–1355. doi:10.1080/00268978500101041

Brooks, B.R., Brooks, C.L., Mackerell, A.D., Nilsson, L., Petrella, R.J., Roux, B., Won, Y., Archontis, G., Bartels, C., Boresch, S., Caflisch, A., Caves, L., Cui, Q., Dinner, A.R., Feig, M., Fischer, S., Gao, J., Hodoscek, M., Im, W., Kuczera, K., Lazaridis, T., Ma, J., Ovchinnikov, V., Paci, E., Pastor, R.W., Post, C.B., Pu, J.Z., Schaefer, M., Tidor, B., Venable, R.M., Woodcock, H.L., Wu, X., Yang, W., York, D.M., Karplus, M., 2009. CHARMM: the biomolecular simulation program. J. Comput. Chem. 30, 1545–1614. doi:10.1002/jcc.21287

Cheng, W.W.L., McCoy, J.G., Thompson, A.N., Nichols, C.G., Nimigean, C.M., 2011. Mechanism for selectivity-inactivation coupling in KcsA potassium channels. Proc. Natl. Acad. Sci. U. S. A. 108, 5272–5277. doi:10.1073/pnas.1014186108

Clementi, E., Barsotti, R., 1978. Study of the structure of molecular complexes. Coordination numbers for Li+, Na+, K+, F− and Cl− in water. Chem. Phys. Lett. 59, 21–25. doi:10.1016/0009-2614(78)85605-X

Cordero-Morales, J.F., Cuello, L.G., Zhao, Y., Jogini, V., Cortes, D.M., Roux, B., Perozo, E., 2006. Molecular determinants of gating at the potassium-channel selectivity filter. Nat. Struct. Mol. Biol. 13, 311–318. doi:10.1038/nsmb1069

Cordero-Morales, J.F., Jogini, V., Lewis, A., Vásquez, V., Cortes, D.M., Roux, B., Perozo, E., 2007. Molecular driving forces determining potassium channel slow inactivation. Nat. Struct. Mol. Biol. 14, 1062–1069. doi:10.1038/nsmb1309

Devaraneni, P.K., Komarov, A.G., Costantino, C.A., Devereaux, J.J., Matulef, K., Valiyaveetil, F.I., 2013. Semisynthetic K+ channels show that the constricted conformation of the selectivity filter is not the C-type inactivated state. Proc. Natl. Acad. Sci. U. S. A. 110, 15698–15703. doi:10.1073/pnas.1308699110

Essmann, U., Perera, L., Berkowitz, M.L., Darden, T., Lee, H., Pedersen, L.G., 1995. A smooth particle mesh Ewald method. J. Chem. Phys. 103, 8577–8593. doi:10.1063/1.470117

Fedida, D., Maruoka, N.D., Lin, S., 1999. Modulation of slow inactivation in human cardiac Kv1.5 channels by extra- and intracellular permeant cations. J. Physiol. 515 (Pt 2), 315–329.

Feller, S.E., Zhang, Y., Pastor, R.W., Brooks, B.R., 1995. Constant pressure molecular dynamics simulation: The Langevin piston method. J. Chem. Phys. 103, 4613–4621. doi:10.1063/1.470648

Hoover, null, 1985. Canonical dynamics: Equilibrium phase-space distributions. Phys. Rev. A 31, 1695–1697.

Hoshi, T., Armstrong, C.M., 2013. C-type inactivation of voltage-gated K+ channels: pore constriction or dilation? J. Gen. Physiol. 141, 151–160. doi:10.1085/jgp.201210888

Hoshi, T., Zagotta, W.N., Aldrich, R.W., 1991. Two types of inactivation in Shaker K+ channels: Effects of alterations in the carboxy-terminal region. Neuron 7, 547–556. doi:10.1016/0896-6273(91)90367-9

Hoshi, T., Zagotta, W.N., Aldrich, R.W., 1990. Biophysical and molecular mechanisms of Shaker potassium channel inactivation. Science 250, 533–538.

Humphrey, W., Dalke, A., Schulten, K., 1996. VMD: visual molecular dynamics. J. Mol. Graph. 14, 33–38, 27–28.

Hunter, J.D., 2007. Matplotlib: A 2D Graphics Environment. Comput. Sci. Eng. 9, 90–95. doi:10.1109/MCSE.2007.55

Impey, R.W., Madden, P.A., McDonald, I.R., 1983. Hydration and mobility of ions in solution. J. Phys. Chem. 87, 5071–5083. doi:10.1021/j150643a008

Jiang, Y., Lee, A., Chen, J., Cadene, M., Chait, B.T., MacKinnon, R., 2002. The open pore conformation of potassium channels. Nature 417, 523–526. doi:10.1038/417523a

Jorgensen, W.L., Chandrasekhar, J., Madura, J.D., Impey, R.W., Klein, M.L., 1983. Comparison of simple potential functions for simulating liquid water. J. Chem. Phys. 79, 926–935. doi:10.1063/1.445869

Jo, S., Kim, T., Iyer, V.G., Im, W., 2008. CHARMM-GUI: a web-based graphical user interface for CHARMM. J. Comput. Chem. 29, 1859–1865. doi:10.1002/jcc.20945

Kiss, L., LoTurco, J., Korn, S.J., 1999. Contribution of the selectivity filter to inactivation in potassium channels. Biophys. J. 76, 253–263. doi:10.1016/S0006-3495(99)77194-8

Kumar, S., Rosenberg, J.M., Bouzida, D., Swendsen, R.H., Kollman, P.A., 1992. The weighted histogram analysis method for free-energy calculations on biomolecules. I. The method. J. Comput. Chem. 13, 1011–1021. doi:10.1002/jcc.540130812

Levy, D.I., Deutsch, C., 1996a. A voltage-dependent role for K+ in recovery from C-type inactivation. Biophys. J. 71, 3157–3166. doi:10.1016/S0006-3495(96)79509-7

Levy, D.I., Deutsch, C., 1996b. Recovery from C-type inactivation is modulated by extracellular potassium. Biophys. J. 70, 798–805. doi:10.1016/S0006-3495(96)79619-4

Liu, S., Focke, P.J., Matulef, K., Bian, X., Moënne-Loccoz, P., Valiyaveetil, F.I., Lockless, S.W., 2015. Ion-binding properties of a K+ channel selectivity filter in different conformations. Proc. Natl. Acad. Sci. U. S. A. 112, 15096–15100. doi:10.1073/pnas.1510526112

Liu, Y., Jurman, M.E., Yellen, G., 1996. Dynamic rearrangement of the outer mouth of a K+ channel during gating. Neuron 16, 859–867.

Lomize, M.A., Lomize, A.L., Pogozheva, I.D., Mosberg, H.I., 2006. OPM: orientations of proteins in membranes database. Bioinforma. Oxf. Engl. 22, 623–625. doi:10.1093/bioinformatics/btk023

López-Barneo, J., Hoshi, T., Heinemann, S.H., Aldrich, R.W., 1993. Effects of external cations and mutations in the pore region on C-type inactivation of Shaker potassium channels. Receptors Channels 1, 61–71.

Marchese, F.T., Beveridge, D.L., 1984. Pattern recognition approach to the analysis of geometrical features of solvation: application to the aqueous hydration of lithium(1+), sodium(1+), potassium(1+), fluoride(1-), and chloride(1-) ions. J. Am. Chem. Soc. 106, 3713–3720. doi:10.1021/ja00325a001

Mezei, M., Beveridge, D.L., 1981. Monte Carlo studies of the structure of dilute aqueous sclutions of Li+, Na+, K+, F−, and Cl−. J. Chem. Phys. 74, 6902–6910. doi:10.1063/1.441101

Migliore, M., Fornili, S.L., Spohr, E., Pálinkás, G., Heinginger, K., 1986. A molecular dynamics study of the structure of an aqueous KC1 solution. Z.Naturforsch. A41, 826–834.

Nguyen, H.L., Adelman, S.A., 1984. Studies of solvated ion motion: Molecular dynamics results for dilute aqueous solutions of alkali and halide ions. J. Chem. Phys. 81, 4564–4573. doi:10.1063/1.447430

Nosé, S., 1984. A unified formulation of the constant temperature molecular dynamics methods. J. Chem. Phys. 81, 511–519. doi:10.1063/1.447334

Perozo, E., Cortes, D.M., Cuello, L.G., 1999. Structural rearrangements underlying K+-channel activation gating. Science 285, 73–78.

Rasmusson, R.L., Morales, M.J., Castellino, R.C., Zhang, Y., Campbell, D.L., Strauss, H.C., 1995. C-type inactivation controls recovery in a fast inactivating cardiac K+ channel (Kv1.4) expressed in Xenopus oocytes. J. Physiol. 489 (Pt 3), 709–721.

Ray, E.C., Deutsch, C., 2006. A trapped intracellular cation modulates K+ channel recovery from slow inactivation. J. Gen. Physiol. 128, 203–217. doi:10.1085/jgp.200609561

Roux, B., 2008. The membrane potential and its representation by a constant electric field in computer simulations. Biophys. J. 95, 4205–4216. doi:10.1529/biophysj.108.136499

Roux, B., Bernèche, S., 2002. On the potential functions used in molecular dynamics simulations of ion channels. Biophys. J. 82, 1681–1684. doi:10.1016/S0006-3495(02)75520-3

Ryckaert, J.-P., Ciccotti, G., Berendsen, H.J.C., 1977. Numerical integration of the cartesian equations of motion of a system with constraints: molecular dynamics of n-alkanes. J. Comput. Phys. 23, 327–341. doi:10.1016/0021-9991(77)90098-5

Thomson, A.S., Heer, F.T., Smith, F.J., Hendron, E., Bernèche, S., Rothberg, B.S., 2014. Initial steps of inactivation at the K+ channel selectivity filter. Proc. Natl. Acad. Sci. U. S. A. 111, E1713–1722. doi:10.1073/pnas.1317573111

Thomson, A.S., Rothberg, B.S., 2010. Voltage-dependent inactivation gating at the selectivity filter of the MthK K+ channel. J. Gen. Physiol. 136, 569–579. doi:10.1085/jgp.201010507

Wojtas-Niziurski, W., Meng, Y., Roux, B., Bernèche, S., 2013. Self-learning adaptive umbrella sampling method for the determination of free energy landscapes in multiple dimensions. J. Chem. Theory Comput. 9, 1885–1895. doi:10.1021/ct300978b

Yellen, G., 2001. Keeping K+ completely comfortable. Nat. Struct. Biol. 8, 1011–1013. doi:10.1038/nsb1201-1011

Yellen, G., Sodickson, D., Chen, T.Y., Jurman, M.E., 1994. An engineered cysteine in the external mouth of a K+ channel allows inactivation to be modulated by metal binding. Biophys. J. 66, 1068–1075. doi:10.1016/S0006-3495(94)80888-4

Ye, S., Li, Y., Jiang, Y., 2010. Novel insights into K+ selectivity from high-resolution structures of an open K+ channel pore. Nat. Struct. Mol. Biol. 17, 1019–1023. doi:10.1038/nsmb.1865

Zeikus, J.G., Wolfe, R.S., 1972. Methanobacterium thermoautotrophicus sp. n., an anaerobic, autotrophic, extreme thermophile. J. Bacteriol. 109, 707–715.

Zhou, Y., Morais-Cabral, J.H., Kaufman, A., MacKinnon, R., 2001. Chemistry of ion coordination and hydration revealed by a K+ channel-Fab complex at 2.0 A resolution. Nature 414, 43–48. doi:10.1038/35102009

4 Mechanism of activation at the selectivity filter of a K^+ channel

Florian Heer[1], Wojciech Wojtas-Niziurski[1],David Posson[2], Crina Nimigean[2], Simon Bernèche[1*]

[1]SIB Swiss Institute of Bioinformatics

Biozentrum, University of Basel

Klingelbergstrasse 50/70, 4056 Basel, Switzerland

[2]Department of Physiology and Biophysics

Weill Cornell Medical College

1300 York Ave, New York, NY 10065

*Corresponding author:

simon.berneche@isb-sib.ch

Tel: +41 61 267 2003

Contributions

F.H. and W.W.-N. performed the simulations, free energy calculations, and the analyses. F.H. and S.B. designed the molecular mechanics simulations. D.P and C.N. designed and performed the functional experiments. S.B., F.H. and C.N. wrote the paper.

4.1 Statement of own contribution

My own data is presented in Fig. 4-2, Fig. 4-7, Fig. 4-8 and Fig. 4-9. I performed all simulations and analyses (represented in the figures mentioned above), which I co-designed with S. Bernèche. Additionally data presented in Fig. 4-1B and extended Fig. 4-2 are based on my structural models, described in chapter 4.6.1.

This manuscript is in preparation for publication.

4.2 Abstract

Ion efflux through potassium channels is regulated by a main gate activated by ligands and/or membrane potential. The opening of the main gate let K^+ ions flow down their gradient, diffusing through the selectivity filter of the channel, which can also contribute to the regulation of the ionic current by changing its conformation. Functional and structural data have brought evidence of interaction between the inner gate and the selectivity filter of potassium channels (Cuello et al., 2010). Here we show, using molecular dynamics simulation, potential of mean force calculations and electrophysiological measurements, that the selectivity filter of the KcsA channel constitutes a central element of the activation mechanism. With the inner gate in the closed state, the canonical conformation of the selectivity filter, in which K^+ ions are optimally coordinated by backbone carbonyls as shown by X-ray crystallography (Zhou et al., 2001), does not allow for the diffusion of ions at a rate compatible with experimental data. However, our calculations reveal that the opening of the main gate removes steric restraints at the level of the selectivity filter, which increases structural fluctuations and reduces ion binding affinity, thus favoring ion diffusion. Electrophysiology measurements show that a mutation that reduces steric contacts in the vicinity of the selectivity filter of the KcsA channel facilitates activation. The transmembrane helices forming the pore of K^+ channels are thus shown to regulate the conductance of the selectivity filter by varying their conformation and/or orientation. These findings support the idea that the inner gate of K^+ channels does not necessarily close completely in the resting state (Kowal et al., 2014) and provide a new perspective on K^+ channel gating that notably calls for a reassessment of voltage-dependent activation.

4.3 Introduction

To understand how ion permeation is regulated in K^+ channels, it is essential to fully understand the factors that define the conductance at their selectivity filter. Ion permeation through the selectivity filter of K^+ channels has been described based on X-ray crystallography data (Doyle et al., 1998; Zhou et al., 2001) and molecular mechanics simulations (Bernèche and Roux, 2001). The generally accepted model of permeation involves alternating states with two or three ions separated by water molecules, low ion de-solvation free energy at the entrance of the filter, and the occurrence of a knock-on transitional state in which two K^+ ions come in close contact in the lower part of the filter (in sites S_3 and S_4, see Fig. 4-1) (Bernèche and Roux, 2001). The molecular mechanics study mentioned here was performed based on the 3.2 Å structure of the KcsA channel (PDB id 1BL8) (Doyle et al., 1998) using a previous generation of the CHARMM molecular dynamics force field (v22) (Jorgensen et al., 1983; MacKerell et al., 1998). Since then, higher resolution structures were obtained (Zhou et al., 2001) and major improvement in molecular mechanics force fields took place (Best et al., 2012). Notably, corrections were made to backbone dihedrals, resulting in higher energy barriers between the different favorable states (Best et al., 2012). Parameters for lipids were also greatly improved, allowing for simulation at constant membrane tension (the previous generation of lipid force field was in practice imposing a fix membrane area) (Klauda et al., 2010).

4.4 Results

We have repeated the potential of mean force (PMF) calculation using the latest generation of force field (CHARMM36) and the canonical structure of the KcsA channel solved at a resolution of 2.0 Å (PDB id 1K4C) (Zhou et al., 2001). This structure, like the original one, is characterized by a closed main gate, which is formed by the crossing of transmembrane helices on the intracellular side of the channel and thought to stabilize the selectivity filter in its conductive conformation. Unexpectedly, the new 2D PMF reveals a high free energy barrier of at least 6 kcal/mol, impeding ion permeation (Fig. 4-1A). The knock-on state is notably not observed. PMF calculation performed with a different initial occupancy state (S_1-S_3-S_{Cav} instead of S_0-S_2-S_4) has shown the formation of such knock-on state, but with the loss of the water molecule between the 2nd and 3rd ions and a relatively high free energy barrier (Fig. 4-5). Similar results were obtained by other groups, who proposed alternative permeation schemes in which ions are most often not separated by water molecules (Köpfer et al., 2014). Others have concluded that molecular mechanics force field might not be accurate enough to properly describe ion permeation in ion channels (Jensen et al., 2013).

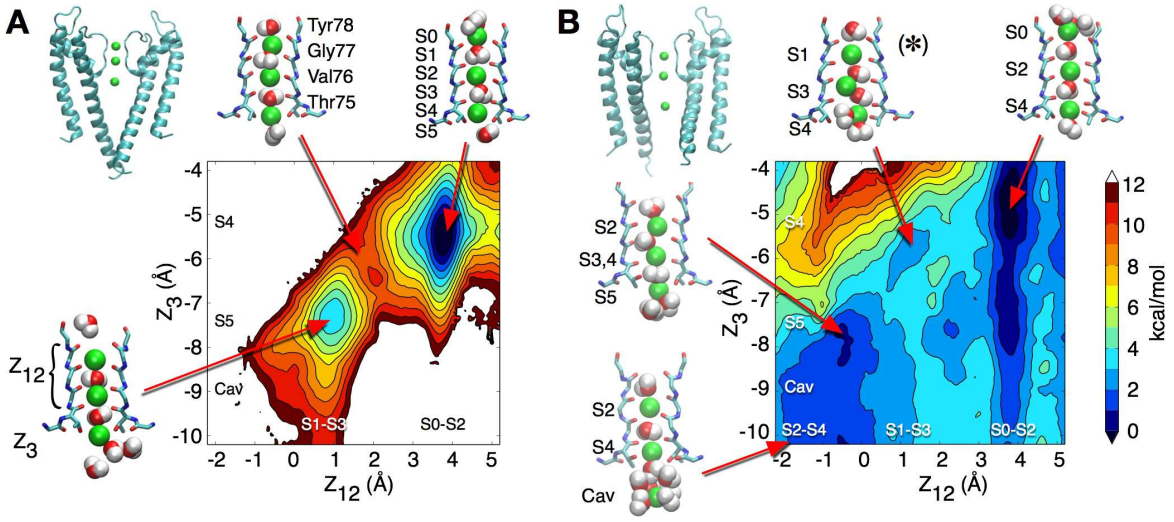

Fig. 4-1 **Potential of mean force calculations describing ion permeation for different channel conformations**

(A) In the closed state (based on structure PDB id 1K4C), ions are tightly bound to the selectivity filter in states S_1-S_3-S_5 or S_0-S_2-S_4, and can hardly diffuse. (B) In the open state (based on a model built from structure PDB id 3F5W), ion diffusion takes place by overcoming free energy barriers of 2-3 kcal/mol. A knock-on transition state (S_1-S_3-S_4) is observed (identified by ✻). The reaction coordinates Z_{12} corresponds to the centre-of-mass of the two outermost ions, and Z_3 to the lower ion. Ion positions are defined relative to the centre-of-mass of the backbone atoms of the selectivity filter core residues (Thr75-Val76-Gly77-Tyr78). Molecular structures are shown for the key states. Ions are represented by green sphere. The backbone of residue 74 to 79 is shown as well as nearby water molecules.

The previous series of simulations mentioned above suggests that the knock-on transition involves a widening of site S_4, which can then accommodate an ion and a water molecule almost side by side. Interestingly, the experimental electronic density for Rb^+ in the pore of the 1BL8 structure suggests a wider filter than that seen in 1K4C. We thought that the antibodies found in the 1K4C crystal but not in 1BL8 could maybe impact on the conformation of the selectivity filter. Repeating the PMF calculation on the 1BL8 structure using the latest force field yielded essentially the same results as those obtained for 1K4C (data not shown). We then considered possible limitations of the force field, especially in its description of the structure and dynamics of the conserved Thr75, which defines the S_4 binding site (see Fig. 4-1). Returning to the previous generation of force field (CHARMM 22) for residues 74 to 76, which implies a more flexible backbone for these residues, decreased the free energy barriers substantially. While such ad hoc decision cannot be justified given the known limitations of this previous generation of force fields (Best et al., 2012), and the overall excellent results obtained with the latest generation, the computer experiment nevertheless illustrates the impact of more flexibility at the bottom of the selectivity filter.

All of the above calculations were based on the premise that a closed main gate stabilizes the conductive state of the selectivity filter. We then reasoned that the most natural system to study ion permeation in the selectivity filter should nevertheless be constructed based on an open channel. Given the low open probability of KcsA, one would expect to find its selectivity filter in the inactivated state when under steady open conditions. A series of structures solved by Perozo et al. showed that an opening of the main gate with a diameter of 23 Å or 32 Å captures the selectivity filter in its inactivated state (PDB id 3F7V and 3F5W) (Cuello et al., 2010). Thus, these open structures most probably represent the scaffold of the open conducting channel. The inactivated conformation of the selectivity filter represents a slight reorientation of the amide plane of residues Val76 and Gly77, which are stabilized by water molecules intercalated between the subunits. Removing these water molecules allows for the reorientation of the amide plane and ion coordination by backbone carbonyl groups (Ostmeyer et al., 2013). We built such a model based on the 3F5W structure and repeated the PMF calculations after equilibration of the system. The PMF presented in Fig. 4-1B reveals small free energy barriers, and is in all points similar to the PMF obtained previously based on the initial KcsA structure with a previous generation of force field (Bernèche and Roux, 2001). The complete PMF describing the entrance and release of a K^+ ion is shown in Fig. 4-6.

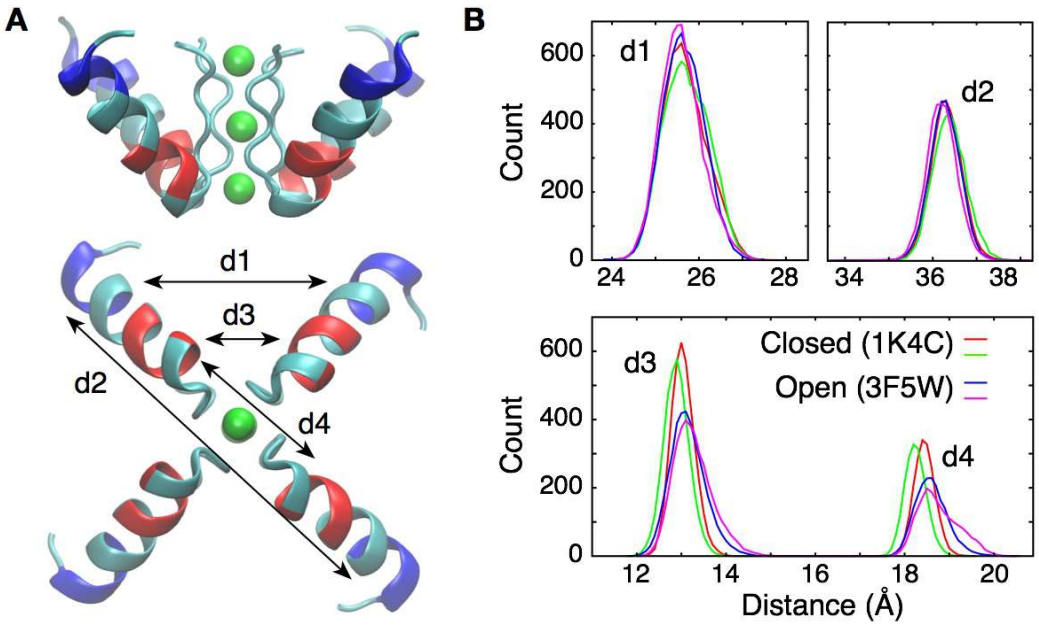

Fig. 4-2 **Fluctuations at the level of the pore helix following the opening of the intracellular gate**

(A) The molecular graphics depict side and bottom views of the selectivity filter and the pore helix of the four channel subunits. Arrows d1 and d2 indicate the distances between the centre-of-mass of backbone atoms of residues 62 to 65 (colored in blue) of adjacent and opposite subunits, respectively. Arrows d3 and d4 indicate corresponding distances between the helix turn formed by residues 70 to 73 (colored in red). (B) The histograms show how the distances defined in (A) fluctuate through simulations of the closed and open channels. Distances d1 and d2 between helix turn at the top of the pore helix show little fluctuations. Distances d3 and d4, between the helix turns at the bottom of the pore helix, show more fluctuations, with an increase of up to 1 Å.

The most favorable permeation pathway involves a knock-on transition state in which K^+ ions are found in both the S_3 and S_4 binding sites (state identified by (✽) in Fig. 4-1B). In comparison to the closed structure, this knock-on pathway is made accessible by a slight enlargement of the selectivity filter at the level of S_3 and S_4, providing the required volume to hold two ions and adjacent water molecules. This is illustrated by the distance histograms presented in Fig. 4-2. Comparison of simulations based on the open (PDB id 3F5W) and closed (PDB id 1K4C) structures reveals that the upper part of the pore helix maintains the same inter-subunit distance in the open and closed states (distances *d1* and *d2*). Distances *d3* and *d4* respectively describe the distance between the lower part of the pore helix in adjacent and opposite subunits. In comparison to the simulations performed with the closed structure, the open structure simulations reveal a broadening of the *d3* and *d4* distributions, involving that the bottom part of the pore helix moves slightly outward. This implies that the lower part of the pore helix is less constrained in the open channel than in the closed channel, allowing the lower part of the selectivity filter to expand.

The activation of K^+ channels is generally associated with conformational changes involving the inner helix of the pore domain, labelled TM2 in KcsA or S6 in Kv channels. Comparison between the open and closed structures studied here suggests that the outer transmembrane helix (TM1) also moves outward by up to 2-3 Å (see also Fig. 4-7). The main contact between TM1 and the pore helix is at the level of residue L40 (Fig. 4-3A). Our analysis suggests that the outward movement of L40 would give the pore helix and the selectivity filter the required space to expand, favoring ion permeation. According to this mechanism, one would expect that reducing the volume of the leucine residue would also favor ion permeation.

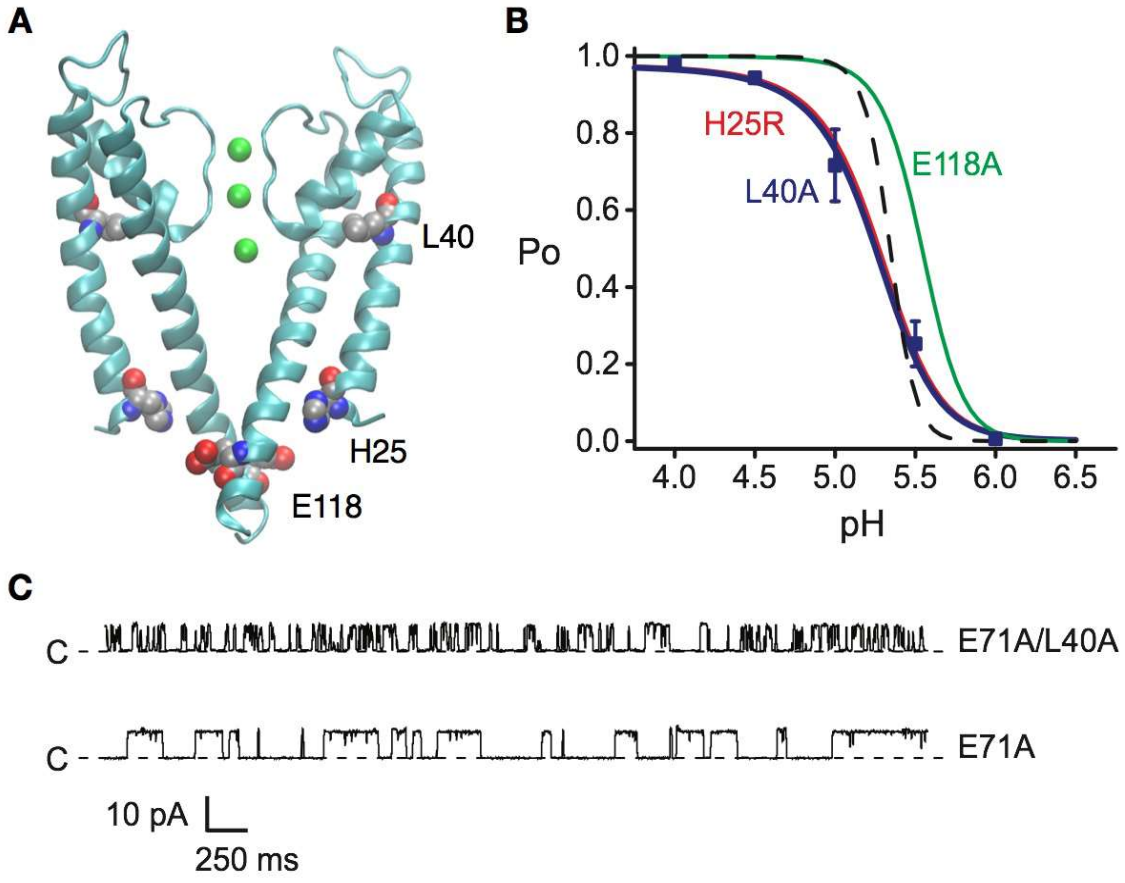

Fig. 4-3 **Coupling of the selectivity filter to the intracellular gate via residue L40**

(A) The pH sensor residues, H25 and E118, are found on the intracellular side of the channel. Residues H25 and L40 both lie on the transmembrane helix TM1. (B) pH response curves of WT (dashed line) and different mutants were obtained from single channel recordings. The L40A and H25R mutants behave quite similarly. (C) Single channel traces for the E71A/L40A (top) and E71A (bottom).

To verify this hypothesis we used single channel recordings to evaluate the pH dependent activation of the L40A mutant, following a methodology used in a recent study (Posson et al., 2013). To maximize the open probability of the channels, these experiments were performed on the background of the E71A mutant, which reduces C-type inactivation (Cordero-Morales et al., 2006). Fig. 4-3B shows that the pH response of L40A is similar to that of H25R, which was previously analyzed [(Posson et al., 2013)]. Two models were used to fit the electrophysiology data (see Methods, equations 1 and 2). In both cases, the model parameters for L40A are within errors from those for H25R, as shown in Fig. 4-10. Notably, the intrinsic gating equilibrium between the open and closed states in absence of protons, L_0, is 8 order of magnitude higher than the reference channel, implying that the L40A and H25R mutants facilitate the transition toward the open state of the channel. Residue H25 was identified as the strongest pH sensor, displaying a large shift in pKa between the closed and open states of the channel, which would imply an important energetic contribution to the activation process. Interestingly, for the L40A mutant, there is no difference between the pK_a^{open} and pK_a^{closed} values of H25, suggesting a small energetic contribution from this residue. This implies that, to some extent, L40A supersedes the work of the pH dependent H25.

To verify the impact of the L40A mutation on ion permeation along the transition from the closed to open state, we performed simulations of this mutant based on the 1K4C structure in which the main gate is closed, and the 3F7V structure in which the main gate is slightly less open than in 3F5W. The PMFs presented in Fig. 4-8 show that, in the closed conformation, the impact of the L40A mutation is minor since ion permeation is still largely impeded. However, in the partially open conformation (3F7V), the L40A/E71A mutant clearly favors ion permeation in comparison to E71A, with the main free energy barrier decreasing from 7 to 2 kcal/mol. The PMF for L40A/E71A in the partially open conformation is similar to that obtained for E71A in the fully open conformation (3F5W). These results support the idea that the L40A mutation facilitates the activation of the channel by reducing the required conformational change and associated energy to reach the maximal open probability.

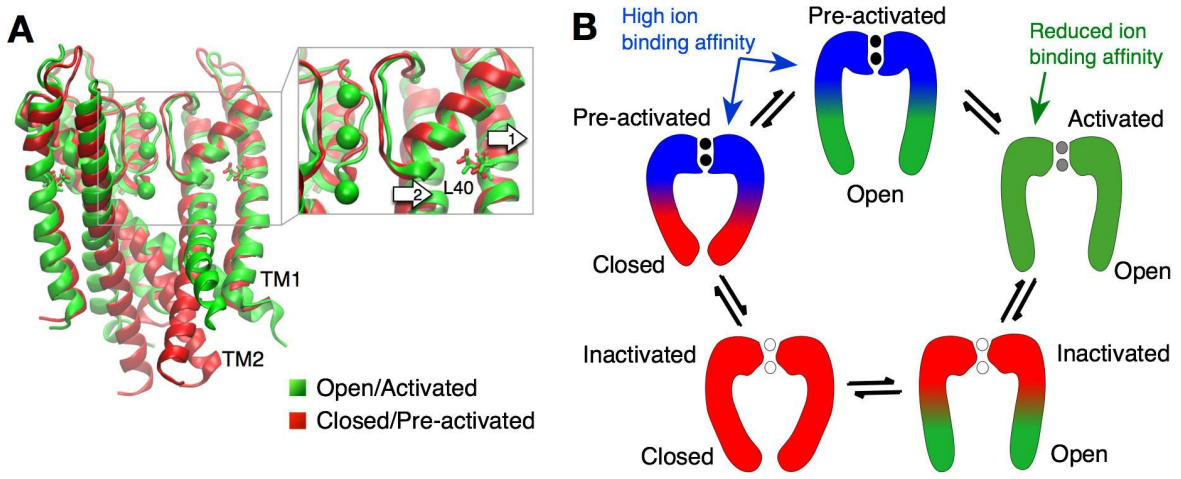

Fig. 4-4 **The selectivity filter at the centre of the activation mechanism**

(A) The superimposition of the open and closed channel illustrates how the movement of the TM1 helices (arrow 1) allows for the displacement of the pore helix and slight expansion of the selectivity filter (arrow 2). (B) The kinetic model describes the main functional states of K^+ channels. The intracellular gate is found in two states, open or closed. The filter is found in pre-activated, activated and inactivated states. The open/pre-activated state is transient as the selectivity filter will spontaneously reach its activated state following the opening of the intracellular gate.

4.5 Conclusion

We propose that the high ion binding affinity state of the selectivity filter, observed when the main gate is closed, corresponds to a pre-activated (resting) state in which the selectivity filter is stabilized and made ready to conduct (Fig. 4-4). Such stabilization of the selectivity filter is likely to play a key role in recovery from inactivation. The mutagenesis experiments and simulations suggest that activation involves the release of steric restraints at the outer vestibule, compatible with the increased structural dynamics observed in EPR experiments. Such changes in the structural dynamics of the selectivity filter through activation could explain the sub-conductance levels with altered selectivity detected by electrophysiology measurements in Shaker.

Functional experiments using pore blockers (del Camino et al., 2005; Nimigean and Allen, 2011), and electron microscopy data (Kowal et al., 2014) suggest that the inner gate of some channels remain open in the resting state. Our work provides a mechanism explaining how the selectivity filter might on its own determine the different functional states of the channel [resting (closed), conducting (open) and inactivated]. The main role of the inner gate might thus be to modulate the state of the selectivity filter through an allosteric mechanism, though this does not exclude that it may form a physical barrier to permeation and form a second activation gate. The activation of the selectivity filter mainly depends on the movement of the outer helix (TM1), potentially explaining why residue H25 of KcsA, found at the intra-cellular end of TM1, was identified as the strongest pH sensor (Posson et al., 2013). The corresponding helix in voltage-dependent channel is S_5, which is directly

connected to the voltage-sensor through a linker. While S_5 is generally thought to play little role in activation gating, it is plausible that the voltage-sensor exerts force on S_5 and by doing so regulates the conductance of the selectivity filter. More generally, our work shows how fluctuations at the selectivity filter have direct impact on its conductance and gating properties, and could potentially be affected by other signaling factors, e.g. temperature and membrane tension (Rusinova et al., 2014).

4.6 Methods

4.6.1 Molecular simulation systems

The molecular membrane systems were built based on the X-ray structure of the KcsA channel in its high-[K^+] closed conformation (PDB id 1K4C) (Zhou et al., 2001) and the open inactivated structures (PDB id 3F7V and 3F5W) (Cuello et al., 2010). Helical turns were added to the transmembrane helices of the two open structures so that these helices have the same length in all constructs, each subunit containing residues 22 to 124. The selectivity filter of the open inactivated conformation was modeled in its putative conducting conformation by maintaining K^+ ions in sites S_1 and S_3, with no water molecule in the P-loop. All residues were assigned their standard protonation state at pH 7, except Glu71, which was protonated. The E71A and L40A mutations were applied to the X-ray structures and a new system was built for each independent case. The systems were assembled using the CHARMM-GUI web-service (Jo et al., 2008) following a protocol developed by Woolf and Roux (Woolf and Roux, 1996). The protein channel, with its symmetry axis aligned along the Z axis, was embedded in a lipid bilayer of about 130 dipalmitoyl-phosphatidylcholine (DPPC) molecules in the case of WT, or dioleoylphosphocholine (DOPC) for E71A constructs. The number of ions in the bulk was adjusted to reproduce an ionic concentration of about 150 mM KCl and to obtain neutral systems, which typically yields a total of 19 cations and 31 anions. The resulting molecular systems each contained about 48’000 atoms.

All calculations were performed using the CHARMM software version c36 (Brooks et al., 2009). The all-atom potential energy function PARAM36 (Best et al., 2012) was used for protein and phospholipids, and water molecules were modeled using the TIP3P potential (Jorgensen et al., 1983). The Lennard-Jones parameters for the K^+-carbonyl oxygen pair interactions were refined to correctly reproduce the solvation free energy of potassium in liquid N-methylacetamide (NMA), a model of the main chain of amino acids (Allen et al., 2006; Bernèche and Roux, 2001). The Lennard-Jones parameters were adjusted to match both the solvation free energies for potassium in water (-79.6 kcal*mol^{-1}) and in liquid NMA (-83.2 kcal*mol^{-1}) (Noskov et al., 2004). Periodic boundaries conditions were applied and long-range electrostatic interactions were calculated using the Particle Mesh Ewald algorithm (Essmann et al., 1995). The molecular systems were equilibrated for about 300 ps with decreasing harmonic restraints applied to the protein atoms, the ions and the water

molecules localized in the P-loop and the filter. All trajectories were generated with a time step of 2 fs at constant normal pressure (1 Atm) controlled by an extended Lagrangian algorithm (Feller et al., 1995) and constant temperature (323,25 K) using a Nose-Hoover thermostat (Hoover, 1985; Nosé, 1984). In the simulations of the open E71A constructs, the conformation of the intracellular gate was maintained by a harmonic root-mean-square-deviation (RMSD) restraints (force constant of 10 kcal/mol•Å with an offset of 0.1 Å) applied to residues 22 to 38 and 100 to 124. Trajectories of 20 ns were produced for each system (some in two replicas), and were used for the distance analyses.

4.6.2 Potential of mean force calculations

The 2D potential of mean force (PMF) calculations were performed using the self-learning adaptive umbrella sampling method (Wojtas-Niziurski et al., 2013). Starting from a single initial configuration, this self-learning approach automatically constructs simulation windows following the valleys of lower energy. PMF calculations were initiated from the occupancy state S_1-S_3-S_{Cav}, except those presented in Fig. 4-1, which were initiated from the state S_0-S_2-S_4 to assure that water molecules were present between ions in the case of the closed channel. The upper free energy limit for the creation of new windows was set to 12 kcal/mol. The reaction coordinates were defined as the distance along the pore axis (which is align with the Z axis) between the ion, or the center-of-mass of two ions, and the center of mass of the selectivity filter backbone (defined as residues 75 to 79). Independent simulations of 600 ps were performed every 0.5 Å along these reaction coordinates using a biasing harmonic potential with a force constant of 20 kcal/(mol*Å^2) and were unbiased using the weighted histogram analysis method (WHAM) (Kumar et al., 1992). The first 100 ps of all simulations were considered as an equilibration period and thus not used for the WHAM analysis. For each PMF, the reference free energy value was set to zero at the free energy minimum. The statistical error on the PMF calculations is illustrated by subdividing the sampling in slices of 50 ps (see Fig. 4-9).

4.6.3 Protein purification and reconstitution

The L40A mutation was made in a construct of the non-inactivating (Cordero-Morales et al., 2006) KcsA-E71A pQE60 by QuikChange mutagenesis (Agilent Technologies) and verified with sequencing. KcsA protein was expressed and purified as described previously (Heginbotham et al., 1999; Posson et al., 2013; Thompson et al., 2008). Briefly, KcsA protein expression was induced in BL21 (DE3, Invitrogen) *E. coli* cells at 37°C in Luria-Bertani media with 500 µM IPTG. Cells were sonicated (Fisher Scientific) in a suspension (100 mM KCl, 50 mM Tris, pH 7.5) and KcsA was extracted with 25 mM n-decyl maltoside (DM, Affymetrix) and then purified from the clarified, soluble fraction in 100 mM KCl, 20 mM Tris, and 5 mM DM, pH 7.5 buffer using a Ni^{2+}-affinity column (Novagen) and gel filtration (Superdex 200, GE Healthcare).

KcsA was reconstituted into liposomes using protein to lipid ratios of 0.1-2.5 µg protein per mg of lipid (3:1 POPE: POPG, Avanti Polar Lipids). Detergent was removed from protein-lipid mixtures using a gel filtration column (G50 fine, GE Healthcare) in buffer (400 mM KCl, 5 mM NMG, 20 mM Tris, pH 7.5). Liposome aliquots were flash-frozen in liquid nitrogen and stored at -80°C.

4.6.4 Single-channel recording and analysis

KcsA L40A/E71A channels were recorded and analyzed as described previously (Posson et al., 2013; Thompson et al., 2008). Briefly, channel liposomes were fused to horizontal planar lipid bilayers (3:1 POPE :POPG in decane) and single channel currents were obtained using 70 mM KCl, 30 mM KOH, 10 mM MOPS, 10 mM succinate, and 10 mM Tris, pH adjusted using HCl to pH 7 for the *cis* (extracellular side) and pH 4-6 for the *trans* (cytoplasmic side). KcsA L40A/E71A channels were initially observed using pH 4 and behaved similar to E71A control channels. Subsequent perfusion of the cytoplasmic side to higher pH values was used to determine the pH-dependent gating.

Bilayers were voltage-clamped using an Axopatch 200B amplifier (Molecular Devices) and current recordings were filtered at 2 kHz using a 4-pole Bessel filter, digitized at 25 kHz using a Digidata 1440A (Molecular Devices), and recorded in Clampex 10. Single channel open probabilities (Po) were calculated using Clampfit 10 (Molecular Devices) and Po vs. pH data were fit in Origin (Microcal) with the Hill equation (Equation 1):

$$P_O = \frac{P_O^{max}}{1+\left(\frac{EC_{50}}{[\mathrm{H}^+]}\right)^{nH}} = \frac{P_O^{max}}{1+\left(10^{(pH-pH_{1/2})}\right)^{nH}} \quad (1)$$

P_o^{max} is the maximal open probability, EC_{50} is the proton concentration of half-activation (also represented by $pH_{½}$), $[H^+]$ is the proton concentration (also represented by pH), and n_H is the Hill coefficient.

The Po vs. pH data were also fit to a two proton-binding sites MWC model (Equation 2) (Posson et al., 2013):

$$P_O = \frac{L_O\left(\frac{[\mathrm{H}^+]}{K_{a1}^{open}}\right)^4\left(\frac{[\mathrm{H}^+]}{K_{a2}^{open}}\right)^4}{L_O\left(\frac{[\mathrm{H}^+]}{K_{a1}^{open}}\right)^4\left(\frac{[\mathrm{H}^+]}{K_{a2}^{open}}\right)^4+\left(\frac{[\mathrm{H}^+]}{K_{a1}^{closed}}\right)^4\left(\frac{[\mathrm{H}^+]}{K_{a2}^{closed}}\right)^4} = \frac{L_O\left(1+10^{(pK_{a1}^{open}-pH)}\right)^4\left(1+10^{(pK_{a2}^{open}-pH)}\right)^4}{L_O\left(1+10^{(pK_{a1}^{open}-pH)}\right)^4\left(1+10^{(pK_{a2}^{open}-pH)}\right)^4+\left(1+10^{(pK_{a1}^{closed}-pH)}\right)^4\left(1+10^{(pK_{a2}^{closed}-pH)}\right)^4} \quad (2)$$

Lo is the intrinsic gating equilibrium between open and closed in the absence of protons, $[H^+]$ is the proton concentration (also represented by pH), K_a^{open} and K_a^{closed} are the acid dissociation constants for a proton sensor in the open and closed states, respectively (also represented by pK_a^{open} and pK_a^{closed}). Equation 2 contains two proton sensors that are labeled with subscripts 1 and 2. For the analysis of L40A/E71A, independent adjustment of Lo or pH-sensor pK_a values were not sufficient to adequately describe the data. Since the mutant dose response was very similar to that observed in the H25R mutant (Posson et al., 2013) (Fig. 4-3), we assumed that L40A altered both Lo and pK_a^{closed}. Using these two free parameters, the best fit resulted in an increased Lo value and a loss of the H25 pH sensor because the pK_a^{closed} value climbed to a constrained maximum value equal to pK_a^{open}. Subsequently constraining pK_a^{closed} resulted in a fit for Lo, the single free parameter. Model parameters for L40A and relevant pH-sensor mutants (Posson et al., 2013) are summarized in Fig. 4-10.

4.7 Acknowledgements

S.B. acknowledges support by the Swiss Foundation for Excellence and Talent in Biomedical Research, the Swiss National Science Foundation (SNF Professorship No PP00P3_139205) and the FP 7 European Union Human Brain Project (grant No 604102). Calculations were performed at sciCORE (http://scicore.unibas.ch/) scientific computing core facility at University of Basel and at the Swiss National Supercomputing Centre (CSCS) under project ID s421.

4.8 References

Allen, T.W., Andersen, O.S., Roux, B., 2006. Ion permeation through a narrow channel: using gramicidin to ascertain all-atom molecular dynamics potential of mean force methodology and biomolecular force fields. Biophys. J. 90, 3447–3468. doi:10.1529/biophysj.105.077073

Bernèche, S., Roux, B., 2001. Energetics of ion conduction through the K+ channel. Nature 414, 73–77. doi:10.1038/35102067

Best, R.B., Zhu, X., Shim, J., Lopes, P.E.M., Mittal, J., Feig, M., Mackerell, A.D., 2012. Optimization of the additive CHARMM all-atom protein force field targeting improved sampling of the backbone φ, ψ and side-chain χ(1) and χ(2) dihedral angles. J. Chem. Theory Comput. 8, 3257–3273. doi:10.1021/ct300400x

Brooks, B.R., Brooks, C.L., Mackerell, A.D., Nilsson, L., Petrella, R.J., Roux, B., Won, Y., Archontis, G., Bartels, C., Boresch, S., Caflisch, A., Caves, L., Cui, Q., Dinner, A.R., Feig, M., Fischer, S., Gao, J., Hodoscek, M., Im, W., Kuczera, K., Lazaridis, T., Ma, J., Ovchinnikov, V., Paci, E., Pastor, R.W., Post, C.B., Pu, J.Z., Schaefer, M., Tidor, B., Venable, R.M., Woodcock, H.L., Wu, X., Yang, W., York, D.M., Karplus, M., 2009. CHARMM: the biomolecular simulation program. J. Comput. Chem. 30, 1545–1614. doi:10.1002/jcc.21287

Cordero-Morales, J.F., Cuello, L.G., Zhao, Y., Jogini, V., Cortes, D.M., Roux, B., Perozo, E., 2006. Molecular determinants of gating at the potassium-channel selectivity filter. Nat. Struct. Mol. Biol. 13, 311–318. doi:10.1038/nsmb1069

Cuello, L.G., Jogini, V., Cortes, D.M., Pan, A.C., Gagnon, D.G., Dalmas, O., Cordero-Morales, J.F., Chakrapani, S., Roux, B., Perozo, E., 2010. Structural basis for the coupling between activation and inactivation gates in K(+) channels. Nature 466, 272–275. doi:10.1038/nature09136

del Camino, D., Kanevsky, M., Yellen, G., 2005. Status of the intracellular gate in the activated-not-open state of shaker K+ channels. J. Gen. Physiol. 126, 419–428. doi:10.1085/jgp.200509385

Doyle, D.A., Morais Cabral, J., Pfuetzner, R.A., Kuo, A., Gulbis, J.M., Cohen, S.L., Chait, B.T., MacKinnon, R., 1998. The structure of the potassium channel: molecular basis of K+ conduction and selectivity. Science 280, 69–77.

Essmann, U., Perera, L., Berkowitz, M.L., Darden, T., Lee, H., Pedersen, L.G., 1995. A smooth particle mesh Ewald method. J. Chem. Phys. 103, 8577–8593. doi:10.1063/1.470117

Feller, S.E., Zhang, Y., Pastor, R.W., Brooks, B.R., 1995. Constant pressure molecular dynamics simulation: The Langevin piston method. J. Chem. Phys. 103, 4613–4621. doi:10.1063/1.470648

Heginbotham, L., LeMasurier, M., Kolmakova-Partensky, L., Miller, C., 1999. Single streptomyces lividans K(+) channels: functional asymmetries and sidedness of proton activation. J. Gen. Physiol. 114, 551–560.

Hille, B., Armstrong, C.M., MacKinnon, R., 1999. Ion channels: from idea to reality. Nat. Med. 5, 1105–1109. doi:10.1038/13415

Hoover, null, 1985. Canonical dynamics: Equilibrium phase-space distributions. Phys. Rev. A 31, 1695–1697.

Jegla, T.J., Zmasek, C.M., Batalov, S., Nayak, S.K., 2009. Evolution of the human ion channel set. Comb. Chem. High Throughput Screen. 12, 2–23.

Jensen, M.Ø., Jogini, V., Eastwood, M.P., Shaw, D.E., 2013. Atomic-level simulation of current-voltage relationships in single-file ion channels. J. Gen. Physiol. 141, 619–632. doi:10.1085/jgp.201210820

Jorgensen, W.L., Chandrasekhar, J., Madura, J.D., Impey, R.W., Klein, M.L., 1983. Comparison of simple potential functions for simulating liquid water. J. Chem. Phys. 79, 926–935. doi:10.1063/1.445869

Jo, S., Kim, T., Iyer, V.G., Im, W., 2008. CHARMM-GUI: a web-based graphical user interface for CHARMM. J. Comput. Chem. 29, 1859–1865. doi:10.1002/jcc.20945

Klauda, J.B., Venable, R.M., Freites, J.A., O'Connor, J.W., Tobias, D.J., Mondragon-Ramirez, C., Vorobyov, I., MacKerell, A.D., Pastor, R.W., 2010. Update of the CHARMM all-atom additive force field for lipids: validation on six lipid types. J. Phys. Chem. B 114, 7830–7843. doi:10.1021/jp101759q

Köpfer, D.A., Song, C., Gruene, T., Sheldrick, G.M., Zachariae, U., de Groot, B.L., 2014. Ion permeation in K^+ channels occurs by direct Coulomb knock-on. Science 346, 352–355. doi:10.1126/science.1254840

Kowal, J., Chami, M., Baumgartner, P., Arheit, M., Chiu, P.-L., Rangl, M., Scheuring, S., Schröder, G.F., Nimigean, C.M., Stahlberg, H., 2014. Ligand-induced structural changes in the cyclic nucleotide-modulated potassium channel MloK1. Nat. Commun. 5, 3106. doi:10.1038/ncomms4106

Kumar, S., Rosenberg, J.M., Bouzida, D., Swendsen, R.H., Kollman, P.A., 1992. The weighted histogram analysis method for free-energy calculations on biomolecules. I. The method. J. Comput. Chem. 13, 1011–1021. doi:10.1002/jcc.540130812

Kuo, M.M.-C., Haynes, W.J., Loukin, S.H., Kung, C., Saimi, Y., 2005. Prokaryotic K(+) channels: from crystal structures to diversity. FEMS Microbiol. Rev. 29, 961–985. doi:10.1016/j.femsre.2005.03.003

Lang, F., Föller, M., Lang, K., Lang, P., Ritter, M., Vereninov, A., Szabo, I., Huber, S.M., Gulbins, E., 2007. Cell volume regulatory ion channels in cell proliferation and cell death. Methods Enzymol. 428, 209–225. doi:10.1016/S0076-6879(07)28011-5

MacKerell, A.D., Bashford, D., Bellott, M., Dunbrack, R.L., Evanseck, J.D., Field, M.J., Fischer, S., Gao, J., Guo, H., Ha, S., Joseph-McCarthy, D., Kuchnir, L., Kuczera, K., Lau, F.T., Mattos, C., Michnick, S., Ngo, T., Nguyen, D.T., Prodhom, B., Reiher, W.E., Roux, B., Schlenkrich, M., Smith, J.C., Stote, R., Straub, J., Watanabe, M., Wiórkiewicz-Kuczera, J., Yin, D., Karplus, M., 1998. All-atom empirical potential for molecular modeling and dynamics studies of proteins. J. Phys. Chem. B 102, 3586–3616. doi:10.1021/jp973084f

Nimigean, C.M., Allen, T.W., 2011. Origins of ion selectivity in potassium channels from the perspective of channel block. J. Gen. Physiol. 137, 405–413. doi:10.1085/jgp.201010551

Nosé, S., 1984. A unified formulation of the constant temperature molecular dynamics methods. J. Chem. Phys. 81, 511–519. doi:10.1063/1.447334

Noskov, S.Y., Bernèche, S., Roux, B., 2004. Control of ion selectivity in potassium channels by electrostatic and dynamic properties of carbonyl ligands. Nature 431, 830–834. doi:10.1038/nature02943

Ostmeyer, J., Chakrapani, S., Pan, A.C., Perozo, E., Roux, B., 2013. Recovery from slow inactivation in K+ channels is controlled by water molecules. Nature 501, 121–124. doi:10.1038/nature12395

Posson, D.J., Thompson, A.N., McCoy, J.G., Nimigean, C.M., 2013. Molecular interactions involved in proton-dependent gating in KcsA potassium channels. J. Gen. Physiol. 142, 613–624. doi:10.1085/jgp.201311057

Rusinova, R., Kim, D.M., Nimigean, C.M., Andersen, O.S., 2014. Regulation of ion channel function by the host lipid bilayer examined by a stopped-flow spectrofluorometric assay. Biophys. J. 106, 1070–1078. doi:10.1016/j.bpj.2014.01.027

Thompson, A.N., Posson, D.J., Parsa, P.V., Nimigean, C.M., 2008. Molecular mechanism of pH sensing in KcsA potassium channels. Proc. Natl. Acad. Sci. U. S. A. 105, 6900–6905. doi:10.1073/pnas.0800873105

Wojtas-Niziurski, W., Meng, Y., Roux, B., Bernèche, S., 2013. Self-learning adaptive umbrella sampling method for the determination of free energy landscapes in multiple dimensions. J. Chem. Theory Comput. 9, 1885–1895. doi:10.1021/ct300978b

Woolf, T.B., Roux, B., 1996. Structure, energetics, and dynamics of lipid-protein interactions: A molecular dynamics study of the gramicidin A channel in a DMPC bilayer. Proteins 24, 92–114. doi:10.1002/(SICI)1097-0134(199601)24:1<92::AID-PROT7>3.0.CO;2-Q

Zhou, Y., Morais-Cabral, J.H., Kaufman, A., MacKinnon, R., 2001. Chemistry of ion coordination and hydration revealed by a K+ channel-Fab complex at 2.0 A resolution. Nature 414, 43–48. doi:10.1038/35102009

4.9 Supporting information

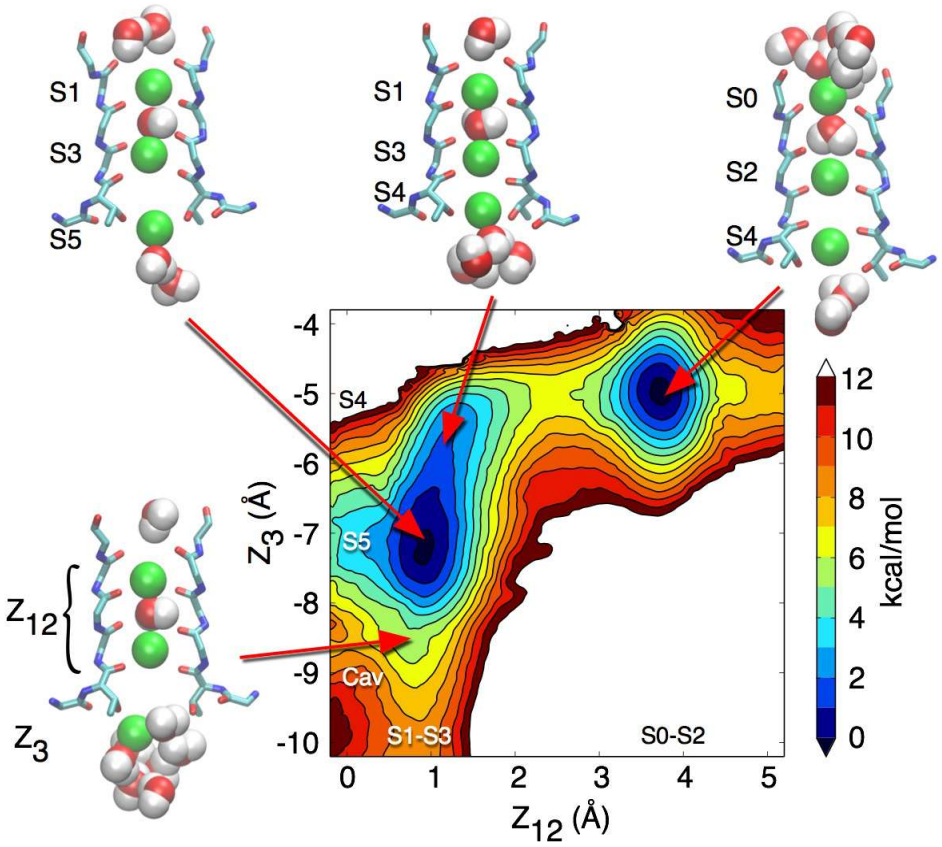

Fig. 4-5 **Potential of mean force describing ion permeation in the selectivity filter of the closed KcsA channel starting from the S_1-S_3-S_{Cav} occupancy state**

When an ion moves from the cavity to the S_4 binding site, no water molecule is seen between this ion and the one in S_3. The volume of the S_4 binding site seems to be too small and not flexible enough to hold both an ion and a water molecule, which is observed in the open structure.

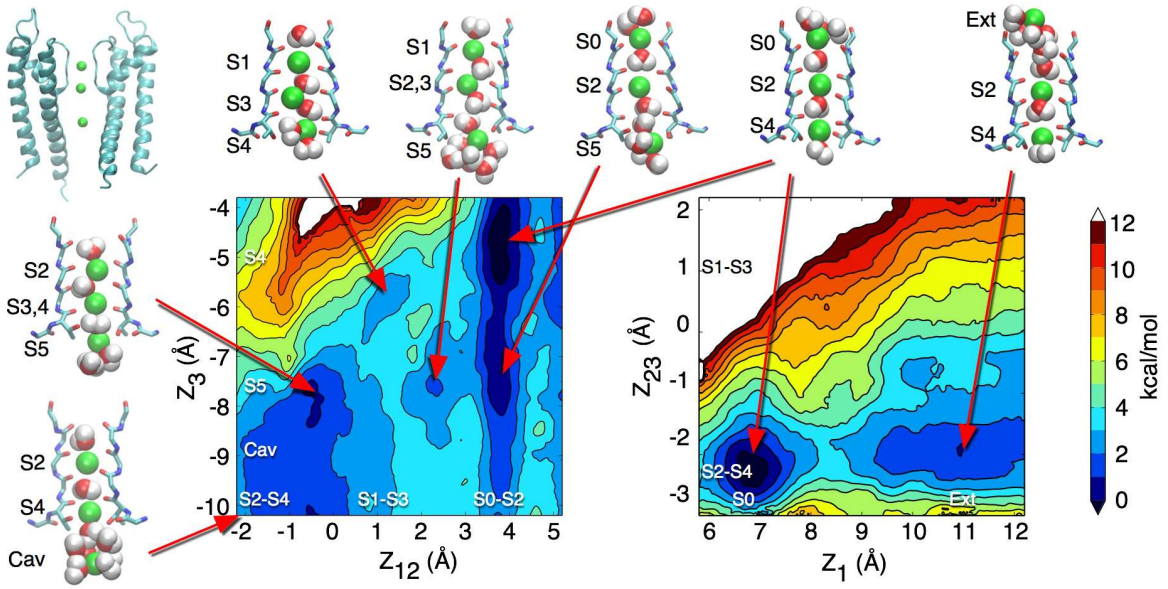

Fig. 4-6 **Potential of mean force describing ion permeation in the open channel**

The free energy map on the left is identical to the one presented in Fig. 4-1B and describes the recruitment by the selectivity filter of an ion coming from the cavity. The map on the right describes the release of an ion from the selectivity filter to the external bulk. The reaction coordinates for this second PMF are Z_1, the position along the channel axis of the outermost ion, and Z_{23}, the position of the centre-of-mass of the lower two ions, both in reference to the centre-of-mass of the selectivity filter (residues 75 to 78). Note that when only two ions remain in the selectivity filter, state S_2-S_4 is favored. The entrance of a third ion allows the transition to the S_1-S_3 state.

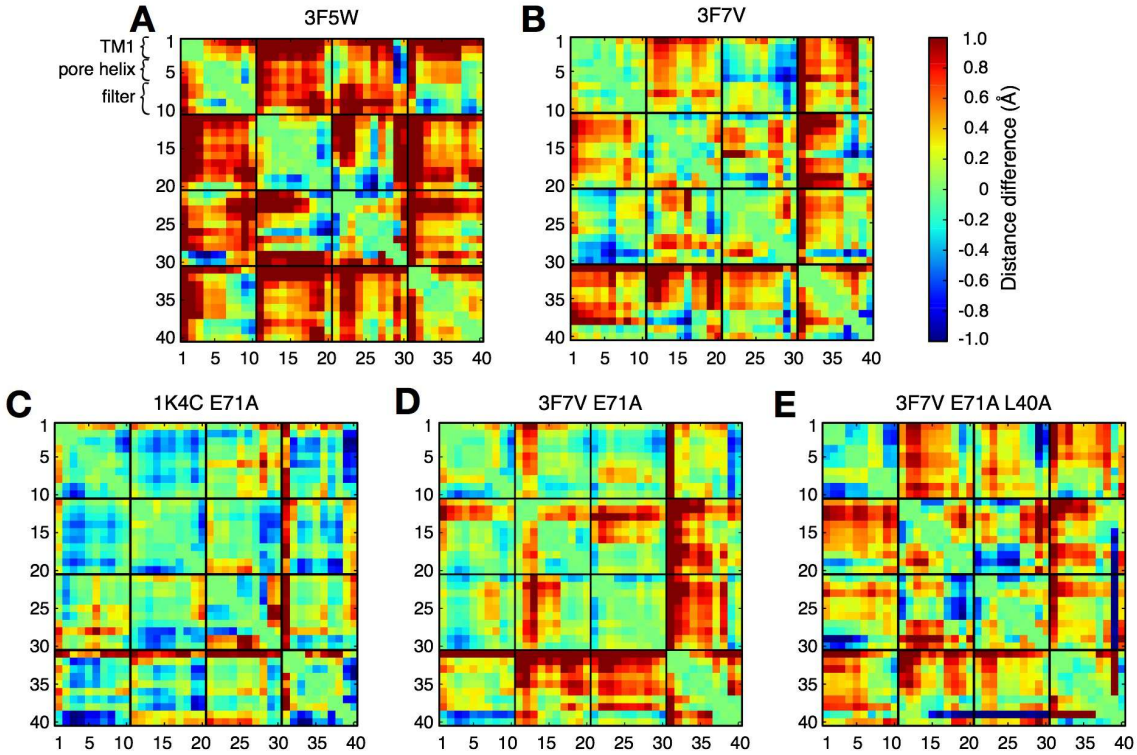

Fig. 4-7 **Distance difference matrixes of model channels**

Comparison of average distance difference between MD simulations run based on structure PDB id 1K4C and 3F5W (A), 3F7V (B), 1K4C with a E71A mutant (C), 3F7V with a E71A mutant (D) or E71A and L40A mutant (E). The subunits (from left to right and top to bottom) are the same as the distances defined in Fig. 4-2. TM1 marks the residues 35-41, pore helix are residues 69-71 and the filter 75-78. A Distance difference bigger than zero indicates that the average distance between the residue is bigger than in 1K4C.

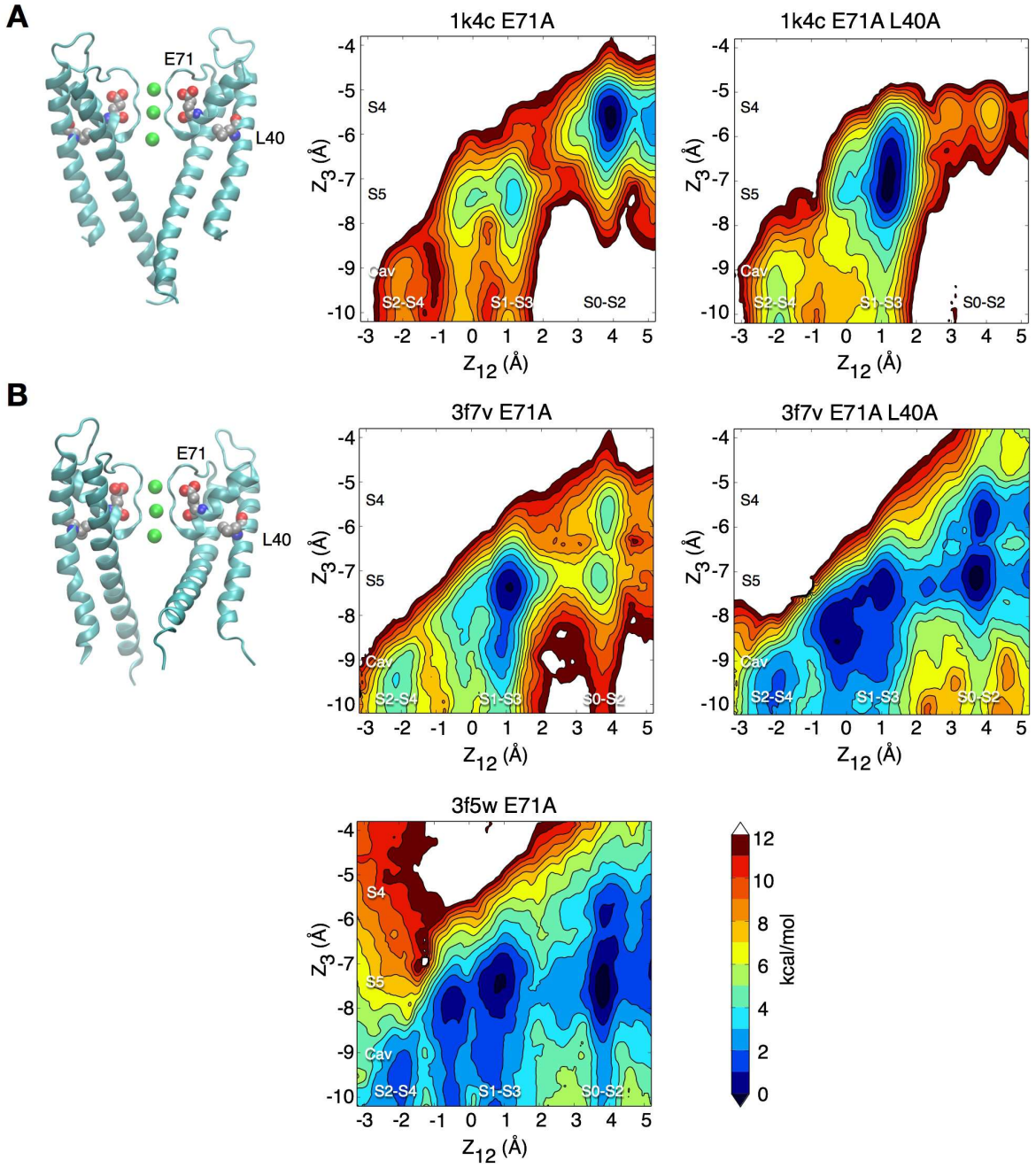

Fig. 4-8 **Ion permeation for different channel conformations with activating mutants**

PMF calculations of channels with closed (A) or (partially) open (B) inner gate. All models have the non inactivating mutation E71A (middle). On the right site are models with the addition of the activating mutant L40A. For labeling of the figure see Fig. 4-1.

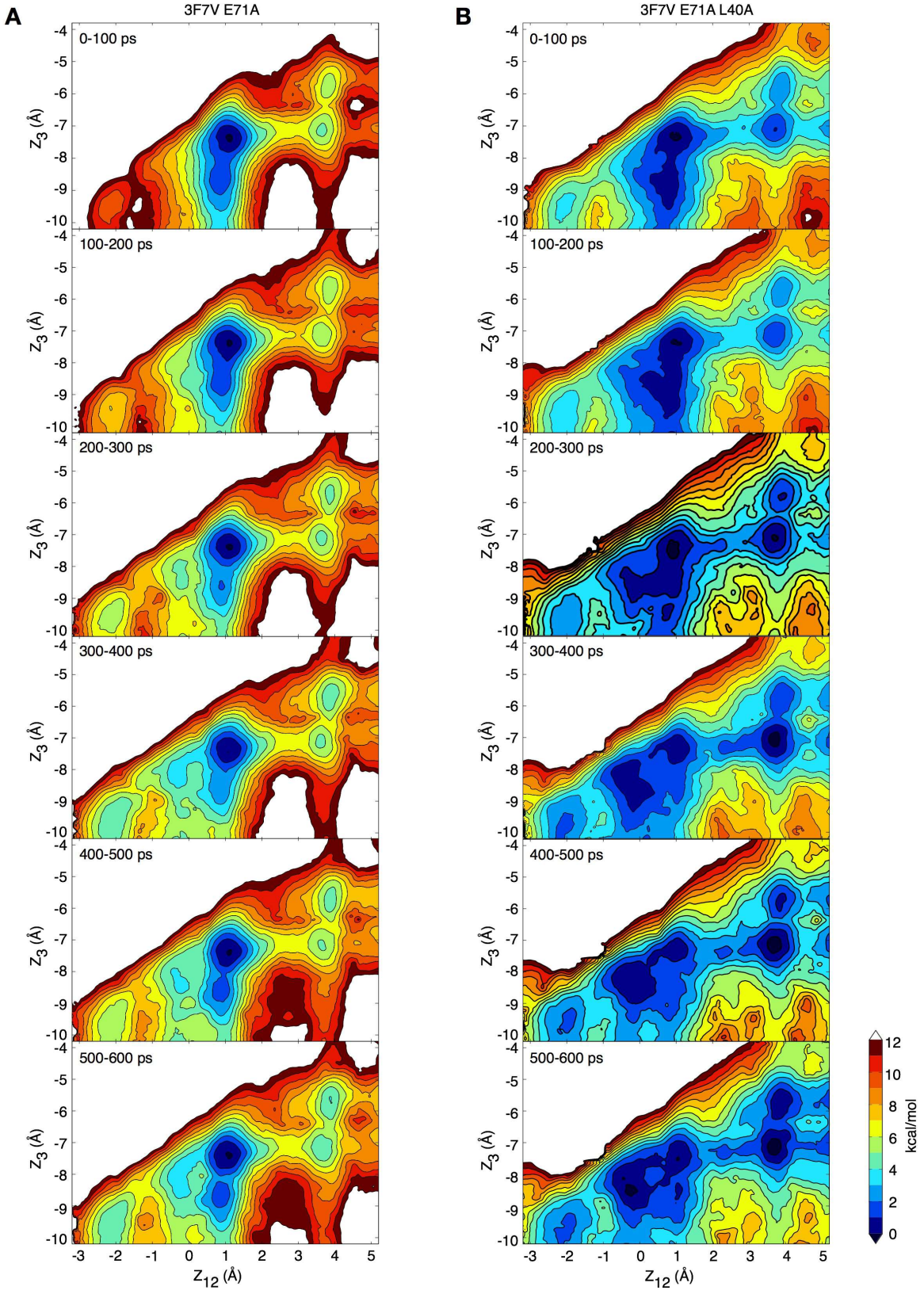

Fig. 4-9 **Convergence of the potential of mean force calculations**

(A,B) The sampling for two of the PMF presented in Fig. 4-8 has been split in interval of 100 ps. The PMF calculated for such intervals are shown for 3F7V E71A (A) and 3F7V E71A L40A (B).

Fig. 4-10 **Model parameters**

Mutant[a]	Hill fit		pH sensor 1 (H25)		pH sensor 2 (E188)		Intrinsic gating
	$PH_{1/2}$ (±)	n_H (±)	pK_{a1}^{closed} (±)	pK_{a1}^{open} (±)	pK_{a2}^{closed} (±)	pK_{a2}^{open} (±)	Lo (±)
E71A[b] (control channel)	5.3 (0.01)	4.4 (0.1)	4.8 (N/A)	7.6	5.0	6.2	2.50E-012 (0.3E-12)
L40A	5.2 (0.02)	1.9 (0.2)	7.6[d]	7.6	5.0	6.2	6.20E-004 (0.7E-4)
H25R[b]	5.3 (0.02)	1.9 (0.2)	-	-	5.0 (0.1)	6.2 (0.1)	7E-4 (4E-4)
E118A[b]	5.5 (0.03)	4.5 (2.8)	4.8	7.6	-	-	1.1E-8 (0.1E-8)
H25R/E118A[b]	-	-	-	-	-	-	52 (11)

[a]All mutants on the background of E71A.

[b]Data and fits from Thompson et al. (2008) and Posson et al. (2013).

[c]Not applicable; no error given when the parameters were constrained (see Materials and Methods).

[d]The data were fit by abolishing the H25 pKa state-dependence, similar to the H25R mutant.

5 General conclusion and outlook

Activation and inactivation mechanisms in selective potassium channels are very complex processes. It is clear, however, that many key events are dependent on each other (inner gate influences the selectivity filter and vice versa, ion concentration, type of ions, binding of ligands etc), making it very difficult to investigate a single event and put it into relation to experimental data. However, these cross interactions allowed us to identify extreme cases, in which we were able to distinguish functional differences between the states.

The inactivated state of MthK is still unknown, but we were able to show possible initial steps of inactivation. Experimentally, we showed that internal Ca^{2+}, but not Mg^{2+}, favors inactivation. The key difference is that Ca^{2+} is able to bind to the selectivity filter and promotes a change in occupancy of K^+ ions in the filter.

We were able to show that the inactivation mechanism in MthK must be different from that of KcsA, and therefore that the mechanism proposed for KcsA is not transferable to all channels. However, we also showed that the collapsed state found in crystallization experiments with KcsA can be reached in MthK, but only in the absence of ions. This fits well with a working hypothesis that the collapsed state in KcsA represents a later state of inactivation in other channels.

In the last chapter, we focused on several seemingly contradictory findings in channel conductance over the past decade. Originally, it seemed as if newer and better force fields lead to computational results, which were less consistent with experimental data. These unexpected findings arose from the originally neglected cooperativity between the selectivity filter and the inner gate, which is only observable with methodological improvements of the last years.

We were able to show that the closing of the inner gate decreases the flexibility of the selectivity filter and thus favor ion binding, which was not observed in older MD simulations, in which the force field allowed more flexibility in the backbone of proteins. This effect was described using several structures with different opening states of the inner gate. Additionally, we identified a mutation that favors channel activation by increasing the flexibility of the selectivity filter without modifying the opening properties of the inner gate. This clearly shows that the selectivity filter plays a major role in channel activation, not just in inactivation.

To further investigate inactivation in MthK WT (and K^+ ion channels in general), two key aspects have to be investigated further. On one hand, the computational experiments were performed in neutral lipids. It is clear that negatively charged lipids have an impact on function of the channel (Poveda et al., 2014). It will be a great challenge to investigate the local interaction of these lipids with the channel. The main obstacles are the unknown distribution of the different lipids around the protein to start with and the slow diffusion of lipids in the membrane, making it difficult to find a good lipid distribution around the channel

by simulations. On the other hand, we clearly showed the importance of the inner gate in modulation the permeation of ions and the inactivation at the selectivity filter. With more and more crystal structures of channels solved, it could be very beneficial to further investigate the opening of the inner gate in the new structures and it's effect on the selectivity filter. For instance the MthK channel structure used in our studies (PDB id 3DLC) is presumed to be in the open activated state. In our free energy calculations, however, we observed energy barriers between ion occupancy states that were higher than what one would expect, considering the experimentally observed conductance of the channel. Our findings on the activation of the KcsA channel suggest that MthK channel might not be in its open conductive state, but rather still (partly) trapped in a pre-activated state.

5.1 Reference

Poveda, J.A., Giudici, A.M., Renart, M.L., Molina, M.L., Montoya, E., Fernández-Carvajal, A., Fernández-Ballester, G., Encinar, J.A., González-Ros, J.M., 2014. Lipid modulation of ion channels through specific binding sites. Biochim. Biophys. Acta 1838, 1560–1567. doi:10.1016/j.bbamem.2013.10.023